Politecnico di Milano

SCUOLA DI INGEGNERIA INDUSTRIALE E DELL'INFORMAZIONE
Corso di Laurea Magistrale in Ingegneria dell'Automazione

Tesi di Laurea Magistrale

Modeling and multi-layer optimal control of a mixed AC-DC grid

Relatore
Prof. Riccardo Scattolini

Correlatori
Ing. Alessio La Bella
Ing. Carlo Sandroni
Ing. Riccardo Lazzari

Candidato
Fabio Bonassi
Matricola 874204

Anno Accademico 2017–2018

Datemi un punto d'appoggio e vi solleverò la Terra.

Archimede

Sommario

Pur essendo l'integrazione delle risorse rinnovabili nella rete elettrica il primo passo per la lotta al surriscaldamento globale, la sua effettiva attuazione è ostacolata da molteplici problematiche. La transizione verso unità di generazione distribuite sul territorio è infatti difficilmente conciliabile con lo schema che ha sorretto la rete elettrica nell'ultimo secolo e lo rende, di fatto, obsoleto. Questo trend, insieme alla progressiva diffusione di dispositivi domestici ad alto consumo come le auto elettriche, impone la necessità di introdurre un sistema di controllo che compensi le incertezze introdotte nella rete, così da consentire una miglior pianificazione dello stadio di generazione.

Recentemente la ricerca si è concentrata sulle cosiddette *microreti*, ovvero reti elettriche in piccola scala coordinate da schemi di controllo spesso molto avanzati, che consentono di bilanciare i carichi massimizzando l'efficienza complessiva. Le microreti possono inoltre offrire all'Operatore di Distribuzione alcuni *servizi ancillari*, quali ad esempio la regolazione di potenza attiva e reattiva.

L'obiettivo di questa Tesi è quello di sfruttare tali servizi ancillari per mitigare l'incertezza della rete, assicurando così un assorbimento di potenza dallo stadio di trasmissione prossimo a quello dichiarato il giorno antecedente. Questo proposito è stato perseguito tramite il partizionamento della rete in *cluster*, ciascuno dei quali controllato da un sistema di controllo predittivo che, utilizzando il minimo numero di misure, compensa localmente le variazioni di potenza attiva rispetto ai valori previsti richiedendo servizi ancillari alle microreti ivi contenute. I cluster, oltre che dai tradizionali collegamenti trifase, sono considerati collegati da una rete di trasmissione a media tensione continua (MVDC), una soluzione di recente molto investigata dalle principali aziende operanti nel settore, grazie alla sua elevata efficienza e alla controllabilità dei flussi di potenza.

Questi collegamenti MVDC vengono sfruttati non solo per ottimizzare i flussi di potenza e per de-saturare lo scheletro della rete di distribuzione, ma anche per sostenere le aree della rete maggiormente in difficoltà in maniera controllata: questo è possibile grazie ad un supervisore centralizzato adibito all'attuazione dei flussi di potenza lungo la trasmissione a corrente continua.

Nella soluzione proposta è altresì eseguito un periodico aggiustamento delle tensioni, in modo da garantire che rispettino i limiti regolamentari della rete, minimizzando contestualmente le perdite di potenza. Il sistema di controllo è infine validato, dando prova di soddisfare i sopraelencati obiettivi.

Abstract

Despite the integration of renewable energy sources into the power grid is the first big step against the climate change, its accomplishment is hindered by several obstacles. The transition towards Distributed Energy Resources (DER) can hardly be reconciled with the traditional model onto which the electric grid has been based for decades, de facto making it obsolete. The progressive diffusion of DER, as well as high-demand consumer devices such as Electric Vehicles, calls for a control system capable of attenuating the uncertainty injected in the grid, thus improving resources' planning at the generation stage.

In the latest years, researchers has been focusing on the so-called *microgrids*, i.e. small-scale grids coordinated by advanced control systems maximizing the overall efficiency while satisfying the power demand. Microgrids can furthermore provide some *ancillary services* to the Distribution System Operator, such as active and reactive power regulation.

The goal of this Thesis is to exploit these ancillary services to mitigate the grid's uncertainty, hence attaining a power absorption from the transmission stage adequately close to the day-ahead declared profile. This can be achieved partitioning the grid into *clusters*, each controlled by a decentralized predictive control system which, based on as few measurements as possible, compensates the power deviations from expected profiles by requesting ancillary services to the microgrids therein included. Moreover, in addition to the traditional three-phase transmission lines, clusters are supposed to be connected by means of a Medium-Voltage Direct Current grid, which technology has been subject to an increasing interest by the main companies operating in the field of power distribution, owing to its high efficiency and to the controllability of power transfers.

These DC links are indeed exploited not only to optimize the power flows and to de-saturate the AC backbone of the grid, but also to sustain - in a controlled fashion - the most hindered regions: a clusters supervisor, in fact, is designed to adjust and actuate the power flows through the MVDCs transmission.

In the proposed solution, a periodic voltage adjustment is further executed to ensure the compliance of nodal voltages to the regulatory limits and to minimize the power losses. The designed control system is eventually tested, proving to attain the desired performances.

Contents

List of Figures

List of Tables

List of Acronyms

AC Alternating Current

BMI Binary Mixed Integer

BQP Binary Quadratic Programming

C-MPC Cluster Model Predictive Control

C-SCMPC Cluster Scenario-based Model Predictive Control

CS Clusters Supervisor

DAM Day-Ahead Market

DC Direct Current

DER Distributed Energy Resource

DR Demand Response

DSM Demand Side Management

DSO Distribution Service Operator

EHV Extra High Voltage

FACTS Flexible AC Transmission System

FRH Flexible Receding Horizon

GAN Generative Adversarial Networks

HV High Voltage

HVDC High Voltage Direct Current

KPI Key Performances Index

LA Load Aggregates

LM Load Management

LV Low Voltage

MG Microgrid

MPC Model Predictive Control

MV Medium Voltage

MVDC Medium Voltage Direct Current

OLTC On-Load Tap Changer

OPF Optimal Power Flow

ORPF Optimal Reactive Power Flow

PCC Point of Common Coupling

PF Power Flow

PV Photo Voltaic

QP Quadratic Programming

RES Renewable Energy Sources

RMS Root Mean Square

SA Scenario Approach

SCMPC Scenario-based Model Predictive Control

SOC State Of Charge

V2G Vehicle To Grid

VPP Virtual Power Plant

VSC Voltage Source Converter

WTG Wind Turbine Generator

Chapter 1

Introduction

1.1 Motivations

In the last decades the climate change has been progressively acknowledged to be the greatest threat for the mankind, leading to the *COP21* agreement, where almost all the nations of the world accepted to reduce the usage of fossil fuels in favor of renewable energy sources. As a matter of fact, pollution does not only make the environment unhealthy and harmful, but also implies a slow yet unstoppable increase of the temperature, leading to a vicious circle.

Meanwhile, the electric power system has been facing dramatic changes to accomplish a more reliable and efficient power distribution. Indeed, in order to shrink the environmental footprint associated to the electric power generation, it is mandatory to reduce the usage of the fossil-fuel generators, exploiting as much as possible the Renewable Energy Sources (RES) to generate green electric power. In the last years we have assisted to the proliferation of renewable-based power plants, thanks to the strong incentives dispensed, the visionary long-term energetic plans submitted and the CO_2 reduction agreement signed by most of the governments.

This transition, however, is not painless and requires a lot of adaptations to the electric systems: first and foremost, the RES are non-dispatchable and unpredictable, i.e. they cannot further sustain the grid during demand peaks and the production forecasts are subject to uncertainty, complicating the power distribution planning; second, replacing big dispatchable fossil-fuel generators with RES can significantly affect the grid stability, since the big inertia of the rotating generators allows to maintain the electric frequency to its nominal value (i.e. 50/60 Hz depending on the region), rejecting sudden and unexpected load variations. Such a stability preservation mechanism can be obtained with Distributed Energy Resources (DER) based on renewables only by means of large energy storages and requires a tailored control system in order to properly work. Small and heterogeneous DER can be aggregated into Virtual Power Plants (VPP), equivalent dispatchable power plants exploiting RES as much as possible and mitigating their intermittence by means of controllable generators.

A trending research topic concerns the definition and use of microgrids (MG), small-scale grids designed to locally manage aggregates of loads, energy storages

and both dispatchable and non-dispatchable generators, operating in either grid-connected or island mode (i.e. detached from the main grid), usually equipped with a hierarchical control system able to minimize the internal losses and to optimally supply internal loads subject to uncertainty. Microgrids operate as intermediates between DERs and the *Distribution Service Operator* (DSO)[1], providing remunerated ancillary services to the grid, like active and reactive power generation - for example to compensate for grid frequency or power unbalancing - and energy storage. The coordination of these local distributed entities is of paramount interest in the evolution from the classical grid, based onto big dispatchable power plants, to the future *smart grid*, in which power should be instead provided by properly coordinated DER.

Nevertheless, not only how power is being generated is undergoing significant changes, but also the way in which it is being consumed. The diffusion of electric vehicles (EV) providing ancillary storage services to the grid and, in general, the spread of demand-side management (DSM) controllable loads, represent an opportunity to improve grid stability, reliability and efficiency, but also rise the necessity for a powerful control system.

Unfortunately, however, the current infrastructure is mostly inadequate to cope with these future challenges. The grid was in fact designed for unidirectional power flows (from the generators to distribution, through the transmission stage), while in presence of DER the power flow direction can be any. In countries like Italy, there are areas very weakly tied to the main grid because of their geographic position, that is, the transmission lines connecting those areas to the national grid could be almost saturated; high investments would be required in order to enlarge the transmission capacity. For this purposes in latest years the Medium Voltage DC (MVDC) transmission lines have been subject to an increasing research interest by universities and power companies, mainly owed to their high efficiency - even for long distances - and to the possibility to transmit both active and reactive power in a controlled fashion.

This Thesis focuses on the problem of compensating the uncertainty introduced by loads and RES exploiting the ancillary services provided by microgrids, assuming the electric frequency to be imposed by the power grid inertia. More specifically, owing to the introduction of MVDC transmission lines, a mixed AC-DC distribution grid is considered.

In the remainder of this chapter, after a brief overview of the main topics mentioned above, the proposed solution is introduced.

[1]DSO is the entity in charge of managing the grid and distributing electric power to the consumers

1.2 Grid

The transfer of electric power from the producers to the consumers is operated by the electric grid, or simply *grid*, historically driven by three-phase *Alternating Current* (AC). Indeed, before the development of power electronics devices, AC had several advantages over *Direct Current* (DC):

- It is possible to step up voltages, thus reducing power losses, simply by means of transformers, which instead do not work with DC.
- It is easier to open a circuit with a switch, as AC current crosses 0 at each period, while DC current is constant.
- It is possible to drive motors without the need of driving circuits.

The grid can be decomposed in three stages: *generation*, *transmission* and *distribution*.

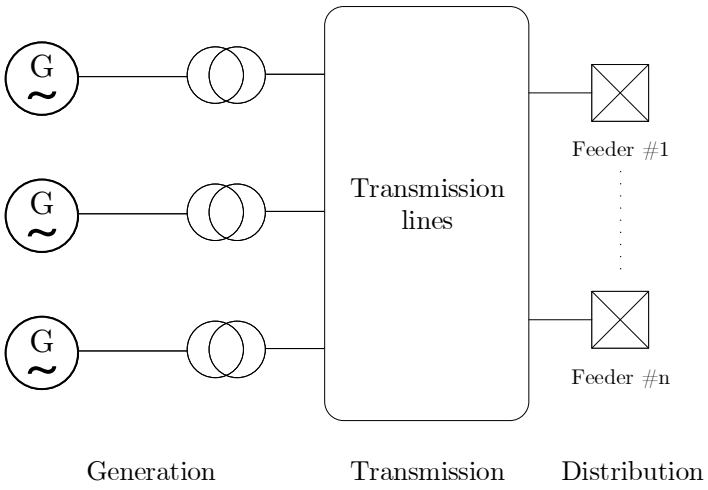

Figure 1.1: Electric Grid stages

Generation stage Electric power is generated by power plants from natural energy sources, typically at medium voltages (few kV). In order to maximize the power which can be transferred with acceptable losses, the voltage is increased by means of step-up transformers to High Voltages (HV, $60 \div 380$ kV) or Extra High Voltages (EHV $380 \div 750$ kV). Generators can either be dispatchable or non-dispatchable. The former, typically fossil-fuel, nuclear, hydroelectric and geothermal generators, can produce a controllable amount of power; the latter, typically *Photo Voltaic* (PV) and *Wind Turbine Generators* (WTG), produce an uncontrollable amount of power, depending on environmental factors. As aforementioned, generators' dispatchability is essential for load matching and frequency regulation.

Transmission stage Once the generated power is stepped-up to HV/EHV, it is transferred towards the consumers via transmission lines, which are generally divided into multiple segments connected by *stations*. Each segment is either underground or overhead and it is characterized by a voltage that is depending on the

amount of flowing power: backbone segments work at extra high voltages, while terminating transmission segments work at high voltages. Stations can be shunting stations if they connect two or more lines at the same voltage or interconnecting stations if they step down the voltage by means of a transformer. High power industrial loads, like furnaces, may be connected directly to transmission lines.

Distribution stage Also known as *feeder* network, distribution stage corresponds to a tree - traditionally acyclic, except for backup links - in charge of feeding the loads. Feeders draw power from the transmission network through the HV to MV station. Distribution stage is composed of the Primary Distribution, in charge of supplying industrial loads and scattering power towards minor loads at Medium Voltage (MV), and the Secondary Distribution, in charge of supplying residential and small industrial loads at 220/380 V, directly connected to the Primary Distribution through a MV to LV substation.

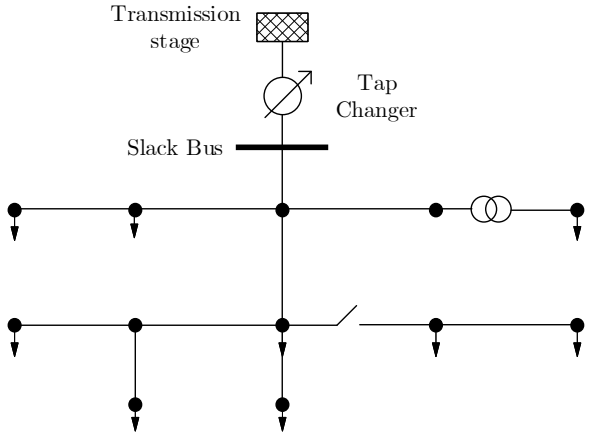

Figure 1.2: IEEE 13-bus feeder

In figure 1.2 the IEEE 13-bus feeder has been reported. The feeder is connected to the transmission through the *slack bus*. A so-called tap changer, that is a transformer whose voltage ratio can be changed within a discrete set, allows to adjust the voltage of the buses, i.e. the nodes of the tree. Each node is interconnected by links - or branches - through which active and reactive powers flow. Eventually, loads attached to nodes are represented with triangles: those are both industrial loads directly connected to the MV buses and aggregated loads connected to LV sub-network. In normal steady-state conditions, the grid must meet some regulatory requirement:

- The AC frequency must be close enough to the nominal frequency (e.g. 50 Hz in Europe and 60 Hz in U.S.), within narrow limits, typically of 1%.
- The voltage applied to the loads must be relatively close to the nominal one, with a tolerance of $5 - 10\%$
- Voltages and currents must be sinusoidal.
- Continuity and safety of the service must be guaranteed to avoid economic losses.

1.3 MVDC transmission

The advent of power electronics devices unlocked the possibility to perform an AC to DC conversion with high efficiencies, even for powers as high as some GW. High voltages can also be achieved, thus minimizing the joule losses due to line impedance. Undoubtedly the inclusion of such DC transmission lines in the electric grid has several advantages:

- For long distances, e.g. more than 20 km, the joule losses are significantly lower, since no reactive power is transferred by the link.
- The DC/AC power converters can exchange an arbitrary amount of reactive power with the AC grid.
- Less cables are required, leading to a relevant economic saving.
- Since the power converters are controllable devices, the power flow through the DC link can be regulated changing the DC voltage.

It is worth noting that, depending on the DC voltage - which is, in turn, chosen in view of the required power transfers - we may speak of Medium Voltage DC, *MVDC*, or High Voltage DC, *HVDC*.

HVDC links are widely used to transfer high powers between different countries or to areas so remote that using AC transmission lines would imply unacceptable power losses due to the reactive power component. For example, HVDC is used to connect Sardinia to Italy's mainland electric grid (working at ± 200 kV) and Greece to Italy (working at ± 400 kV). Another typical implementation is to connect regions with a different nominal frequency.

MVDC is instead adopted to transmit medium powers - ranging from few to tens of MW - usually to small regions not directly connected to the AC grid, where a three-phase connection is economically inconvenient, or to reinforce almost-saturated AC backbone lines, see [1].

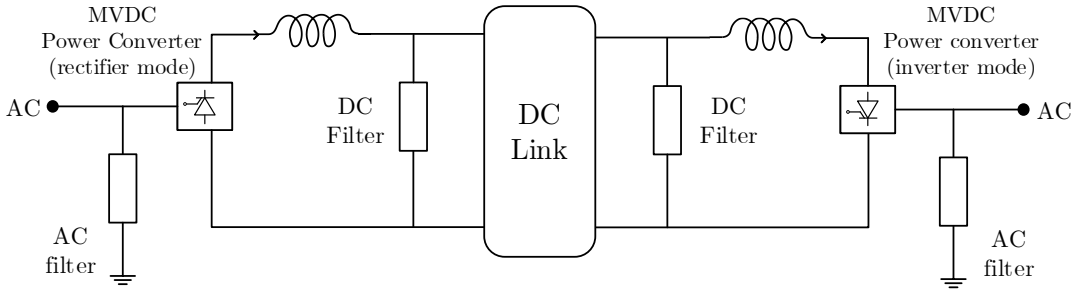

Figure 1.3: MVDC transmission scheme, powered by two reversible rectifiers.

The DC link configuration depends on the power converter adopted, but it is usually based onto XLPE cables, characterized by a very high voltage insulation (up to 750 kV) and a low resistivity.

Of course, along with their relevant advantages, DC transmission lines also show some drawback:

- The power converters are expensive and may require periodic maintenance, thus DC transmission is generally not worth for small distances.
- Since redundant equipment generally make the investment unprofitable, their reliability is lower.
- The maximum voltage is limited by the converter rated voltage.
- Depending on the power converter, the power flow may be unidirectional, from *rectifier* to *inverter*.

For more details on the topic, the interested reader is addressed to [1]–[3].

1.3.1 Power converters

As mentioned, before the invention of semiconductor power electronic devices, AC was preferred over DC because of the possibility to use voltage step-up transformers in order to reduce joule losses.

$$P = \Re(V \cdot I) \tag{1.3.1}$$

As evident from (1.3.1), increasing the voltage *Root Mean Square* (RMS) one can transfer the same amount of real power with a lower current, i.e. with lower losses, since joule losses are proportional to the current squared. Once silicon valves were invented AC/DC power converters started to be developed, becoming more and more efficient, owing to the increasing nominal voltage. Nowadays two main families of high-power AC/DC converters exist: thyristor-based rectifiers and Voltage Source Converters (VSC), represented respectively in figure 1.4 and 1.5.

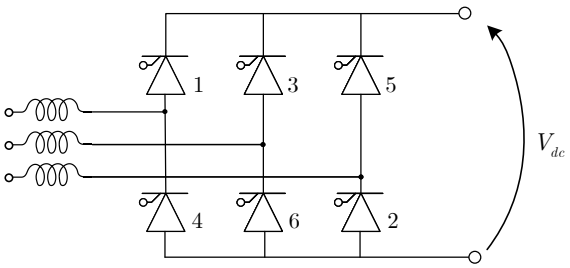

Figure 1.4: Three-phase one-level thyristor-based rectifier simplified scheme.

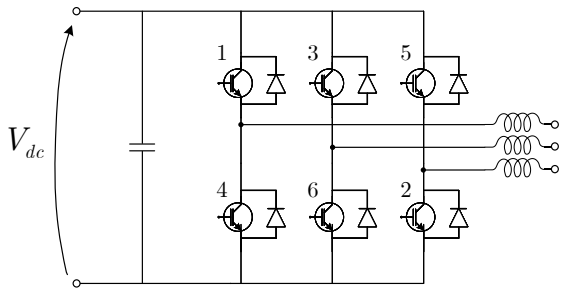

Figure 1.5: Three-phase one-level six-step IGBT inverter simplified scheme.

It should be noted that while VSC are reversible, i.e. active power can flow both from AC site to DC and vice-versa, thyristor-based converters are unidirectional.

Discussing the architectures and control systems of MVDC converters is out of the scope of this work: a vast literature exists on this topic, see e.g. [2]–[4]. In this work, as discussed later in Chapter 2.3, the MVDC interfaces are assumed to be ideal and controlled through DC voltage and reactive power set-points, for which purpose in [5] an adequate control system has been presented.

1.4 MicroGrids

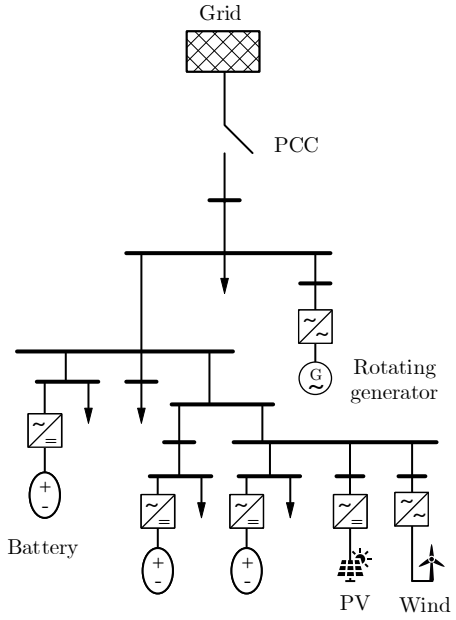

Figure 1.6: Example of an AC MicroGrid topology

In few years, microgrids (MG) have become the main research topic in the field of the Smart Grid. Similarly to any feeder network, a MG is composed by buses connected by links, to which loads, generators and energy storages are connected. Any microgrid, connected to a bus of the feeder by means of the Point of Common Coupling (PCC), may operate in AC or DC. In the first case the PCC may feature an On Load Tap Changer (OLTC) for the slack voltage regulation, while in the second case a DC/AC converter, possibly allowing a reversible power flow, is required.

A microgrid can operate either in *islanded mode*, i.e. detached from the main grid, or in *connected mode*. In the former operating mode the MG control system exploits the generators and energy storages to feed the loads, keeping the voltage (and the frequency, if the MG is AC) within the prescribed limits. In the latter mode, the MG is able to exchange power with the main grid, which imposes its electric frequency thanks to the infinitely larger inertia. Islanded condition is,

of course, the most critical operating mode, due to the diminished inertia of the microgrid. In both operating modes hierarchical control schemes are used to manage the MG, where primary control is usually exerted by simple droop regulators, whereas secondary control can be performed through an MPC architecture, which allows to exploit loads' and non-dispatchable generators' forecasts, see e.g. [6], [7].

As many control schemes already exist and it is not the purpose of this work to go on such a level of detail, microgrids will be considered self-governed entities, equipped with their own control system, providing rewarded ancillary services to the network, namely active and reactive power generation. Each MG is hence supposed to operate in connected mode and to communicate its scheduled - optimal - power profiles, along with the granted margins for the power adjustments. It is worth noticing that, as the grid controller requests an ancillary service to the microgrid, e.g. a variation of active power supplied by its generators, the MG scheduler is supposed to satisfy the request by optimally dispatching its elements. In other words, the microgrid scheduler is considered a low-level controller actuating the references issued by the grid's control system.

1.5 Controllable loads

In the transition towards the Smart Grid, *Demand Side Management* (DMS) activities, i.e. the actions that can be directly or indirectly taken on loads, will play a fundamental role to enhance grid efficiency and reliability, shaving power demand peaks or even actively sustaining the grid. According to [8], depending on how loads are controlled it is possible to distinguish between:

- *Load Management* (LM): the load power absorption profile is directly rescheduled by the tertiary control of the grid, resorting to load interruption or curtailment, provided that the demanded energy is supplied within the declared deadline.
- *Demand Response* (DR): the load is encouraged to reshape its demand patterns either by means of incentives (IBP) or changing electric power price (PBP).

Therefore, virtually all the loads with soft time constraints can be managed with DSM, with advantages for both the consumers and *Distribution Service Operator* (DSO): the former can benefit of lower energy prices, the latter can avoid critical demand peaks, which would require to operate the generators beyond their optimal efficiency point, to oversize the grid devices, and to plan backup generators in order to avoid blackouts.

Although load controllability was initially addressed to industries, nowadays more and more residential loads are being aggregated in *Load Aggregates* (LA), large equivalent controllable loads that can be shifted and re-shaped with the aforementioned advantages.

Even more advanced ancillary services can be provided by the electric vehicles equipped with Vehicle To Grid (V2G) functionality: as EV are static energy storages, while attached they may supply power to the grid during demand peaks, whereas during off-peak periods - when electric power is cheaper - they are fully recharged. Of course this voluntary service is adequately rewarded and the EV must be recharged within a precise deadline.

1.6 Grid control state-of-the-art

The electric power distribution is a service of primary importance, strictly regulated by national and supranational entities to ensure a proper working of the consumer devices, industrial plants, institutional and public services. An adequate resource planning for the successive day and an automatic control structure ensuring requirements' satisfaction is thus necessary.

First, as the day-ahead reliable demand and generation forecasts are available, generally for each node of the grid, a Day-Ahead Market (DAM) takes place with bids. Power dispatches are therefore committed to different generators, depending on energy price.

Still, loads and non-dispatchable generators are not only aleatory and therefore subject to fluctuation, but their forecasts may also be inaccurate. These variations need to be compensated by an automatic control system, in order to meet the aforementioned objectives. Nowadays, a hierarchical control system is implemented to regulate the working point of the grid, possibly minimizing costs and power losses. Each layer constituting the controller operates at different time scales and objectives, and provides for lower-levels supervision.

Primary Control The lower layer of the control system, known as Primary Control, deals with the fastest dynamics and operates with a time scale of few seconds. Due to the fast response required to this layer it must be decentralized, since a centralized control structure would require an excessive amount of time, both for data collection from the entire grid and for computational complexity reasons. The main objective of primary control is frequency regulation: generators are dispatched with power variations to avoid significant deviations of the electric frequency from its nominal value.

Secondary Control The secondary control layer is in charge of restoring the nominal electric frequency and of adequately commissioning the power variations to the different generators according to various criteria. As this layer operates at an higher level than the primary one, the time scale is larger - generally in the order of minutes - and the response is slower, hence the primary control can be considered at steady state. Secondary control can be either centralized or decentralized. The former structure allows an efficient and safe control of the grid, but requires a fixed network topology and all the available measurements from the entire grid,

therefore a robust communication system. Conversely, the latter control architecture is more flexible but leads to a sub-optimal solution, as iterative optimization algorithms are generally characterized by lower convergence rates.

Tertiary Control Power flows are optimized by the tertiary control, the highest control layer which operates in a time-scale ranging from minutes to hours. The main objectives pursued are the generation costs and power losses minimization by means of the generation units coordination. Due to its nature, this control layer generally consists in a static optimization problem, hence it is centralized and usually computationally intensive. This optimization problem, also known as *Optimal Power Flow* (OPF), is based on the power flow equations, which rule the behavior of any electric grid. The interested reader is addressed to [2], Chapters 9.4 and 13.

1.7 Problem summary

The problem addressed in this work is first and foremost the compensation of loads' and RES' uncertainty. This uncertainty is in fact the bottleneck limiting the adoption of RES in the electric grid, as well as the consequent inertia reduction, which entails unacceptable voltage and frequency fluctuations. It should be reminded, however, that in this work the electric frequency is assumed to be imposed by the transmission stage.

Hence, without an adequate control system, the progressive diffusion of RES undermines grid predictability. Depending on actual weather condition, large deviations of the power supplied by generators from their scheduled value might be required, leading to significant costs and power losses increase, as well as complications for power transmission planning.

The challenge is thus to design a control system, possibly decentralized, to exploit the ancillary services offered by local microgrids to mitigate those problems, minimizing the deviations of the power absorbed from transmission stage.

1.8 Proposed solution

In this work, the problem of uncertainty compensation and microgrids' integration is addressed with the introduction of intermediate entities, named *clusters*. Each cluster is defined as a portion of the distribution grid identified on a geographic basis and consists of an aggregate of loads and microgrids. Clusters' rationale is that these entities shall self-compensate exploiting DERs, in such a way that from an external perspective that portion of the grid is behaving as scheduled, contextually limiting the information exchanged with the rest of the grid and the problem's scale by means of local compensation. The clear objective is in fact to keep the active power absorbed from the transmission stage close enough to the day-ahead schedule, hence reducing costs associated to the intra-day energy retrieval from the energy market.

Clusters are characterized by power and energy reserves, achieved through the ancillary services offered by the microgrids therein included. Specifically, power reserves correspond to the margins for variations of the active power requested to microgrids' batteries and generators. Similarly, due to the nature of batteries and - more in general - energy storages, energy reserves are defined as the residual amount of energy which can be stored or supplied. As every microgrid declares its reserves, by means of a proper control architecture it is possible to optimally coordinate microgrids to counteract loads' fluctuations, leading to the minimization of the grid unpredictability.

A MVDC transmission line is also assumed to be introduced into an existing grid in order to reinforce the AC backbone, enabling the transfer of high powers among different clusters of the grid - even clusters of two grids not directly connected -, reducing the transmission lines' saturation and minimizing the power losses, owing to MVDC high efficiency. This solution has been subject to an increasing research interest by the main companies operating in power industry, see [1], [2]. Not only this is fundamental in case of weak AC transmission lines, but it especially allows to transfer power among different nodes (and clusters) of the grid in a controlled fashion, possibly pro-actively balance clusters' reserves to enhance their functionalities. In this way, in fact, load variations can be split among clusters, avoiding the depletion of one's reserves.

For each cluster, a fast *Model Predictive Control* (MPC) algorithm, exploiting loads' and non-dispatchable generators' forecasts, optimally distributes loads deviation among microgrids' generators and storages, requesting power to other clusters via the MVDC line only when is running out of reserves. A supervisor commits the powers flows variations to the AC/DC interfaces of each cluster, amending clusters' power requests and balancing their reserves. Moreover, a slower Optimal Reactive Power Flow (ORPF) periodically adjusts reactive powers and OLTCs' position in such a way to keep voltages, phases and currents within the prescribed limits and to minimize power losses.

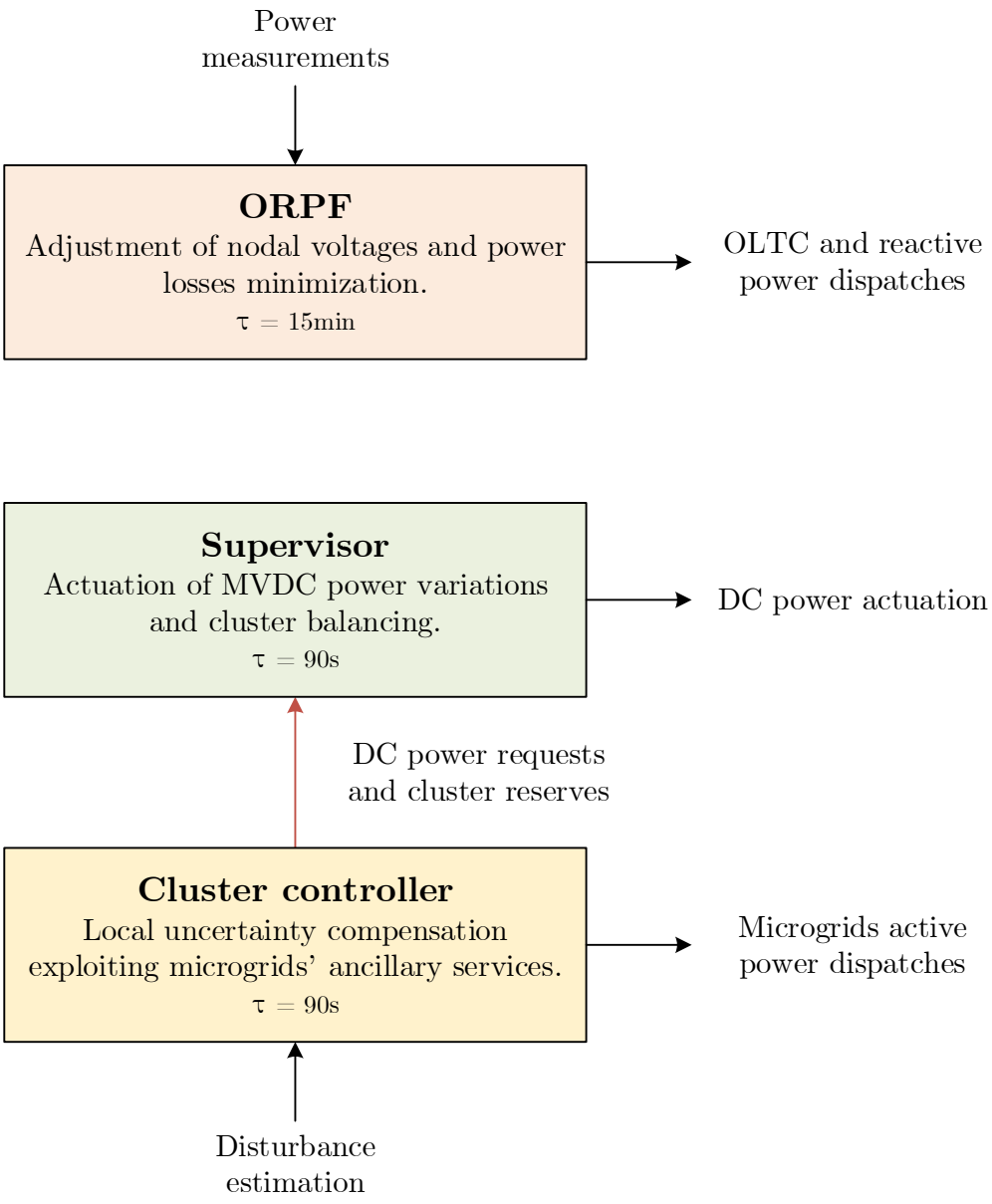

Figure 1.7: Scheme of the implemented control system.

1.9 Literature review

The reference book for the entire work is [2].

In [9] microgrids' motivations and problematics are reviewed, hinting at the main control architectures currently adopted, for both the primary and the secondary control. Politecnico di Milano is really active in the topic of microgrid's control. For example, in [6] a hierarchical control structure is designed to ensure the reliability of an AC microgrid in islanded operating mode, exploiting load and generation forecasts by means of a MPC control strategy. Similarly, in [7] a model for a simple microgrid operating in connected mode is retrieved and two MPC controllers - running at different time scales - are used to minimize the discrepancies between the day-ahead optimization and the actual behavior of the system.

In [10] a novel approach for the day-ahead optimization of multiple microgrids is devised, grouping them in the so-called Aggregator and scheduling the requests of ancillary services by means of a multi-stage distributed algorithm.

As mentioned, MVDC transmission systems are also receiving a lot of interest for both existing grids reinforcement and newly designed distribution systems. In particular, Siemens AG has developed a solution called *MVDC Plus* [1], based on multi-level voltage source converter. In [4], a MVDC grid for a new campus of Aachen University is designed. Specifically, a control system able to regulate the voltages and to manage the power exchanges with the main AC grid is proposed and its dynamic performances, fault rejection capabilities and electromagnetic safety prove to be more than satisfactory.

In this work, the grid model has been retrieved from the *Bus Injection Model*, adapted to consider the MVDC transmission herein implemented. This model is well-explained, along with the fundamentals of centralized Optimal Power Flow, in [11]. Furthermore, it is worth mentioning that as in this work, in [12] an Optimal Reactive Power Flow problem is periodically solved, adjusting DGs' reactive powers to keep nodal voltages' amplitude and angle within regulatory limits.

Model Predictive Control applied to distribution grid has been experiencing an increasing research interest, thanks to its flexibility and to the possibility to exploit forecasts. In the field, a milestone paper is [13], in which a Distributed MPC algorithm is used to control partially overlapping areas equipped with distributed generators and storages. The centralized problem is first defined, then decomposed in multiple sub-problems; distributed solver methods are eventually proposed. Unlike in this work, however, in [13] areas are unbalanced and large deviations from the day-ahead grid schedule are accepted, for the sake of generation cost minimization.

Another meaningful paper featuring MPC is [14], in which two MPC controllers operating at different time scales are used to control nodal voltages, exploiting Distributed Generators ancillary services. A further peculiarity which makes [14] interesting is that the system model has been experimentally identified by means of an impulse response identification procedure.

1.10 Thesis outlook

This thesis is organized as follows.

After this brief introduction, in the following chapter a model for microgrids is first presented. However, since this model is only required for control purposes, it is simplified by aggregating its generators, batteries and loads. Clusters are then introduced explaining their rationale and an energetic model, corresponding to a linear discrete-time system in state-space form, is provided for a generic cluster. Under rather general assumptions, a model of the mixed AC-DC grid based on power flow equations is formalized.

In Chapter 3 the different layers of the control system are presented. First - for each cluster - a Model Predictive Control, based on the new concept of Flexible Receding Horizon principle, is presented, constructing the system's predictive model and formalizing, based on this model, the optimization problem's constraints and cost function. Cluster reserves are moreover introduced to communicate the cluster's residual operative margins to the Supervisor, which is then described in the second part of the chapter. Specifically, after a brief overview of its objectives, a simple non-convex supervisor is presented; a multi-stage supervisor is devised to avoid possible convergence problems, guaranteeing the existence of, at least, a sub-optimal solution to the corresponding optimization problem. The Optimal Reactive Power Flow is eventually formalized.

The results of the defined control systems are illustrated in Chapter 4. In the first part of the chapter, a Benchmark Grid is provided and the retrieval of actual and scheduled power profiles is discussed. The system is then simulated without the control action, hence assessing the violation of regulatory limits and its undesirable behavior. The performances of the controlled systems are eventually discussed, assessing the fitness of the control system by means of some Key Performance Indicators.

In Chapter 5, the possibility to implement a data-driven cluster control strategy is explored. For this purpose, a controller inspired by Scenario-based Model Predictive Control is presented. The scenarios required by this approach are retrieved from historical data, although a scenario-generation technique based on Neural Network is also illustrated. Eventually, the designed control problem is formalized and the resulting performances analyzed.

In the last chapter few final considerations are expressed, providing some hints for possible future research topics.

Chapter 2

System model

2.1 Microgrid model

In Chapter 1.4 a microgrid has been defined as a small-scale grid, connected to the main grid through the Point of Common Coupling, which works as a middle entity between the grid and the distributed energy resources. A microgrid can hence be generally considered an aggregate of dispatchable and non-dispatchable generators, controllable and non-controllable loads and energy storages. A control system is in charge of scheduling dispatchable generators and batteries to sustain internal non-controllable loads, typically based on some economic criterion. Furthermore, it shall execute ancillary services' requests issued by the main grid, thus ensuring their satisfaction.

As mentioned, MG control system is out of the scope of this work: microgrids are indeed considered as entities with power and energy reserves that can be exploited by the cluster control system. From this point of view, as in figure 2.1, MG internal topology can be ignored and an equivalent energetic approximate model can be retrieved, of course under the assumption of grid-connected operating mode.

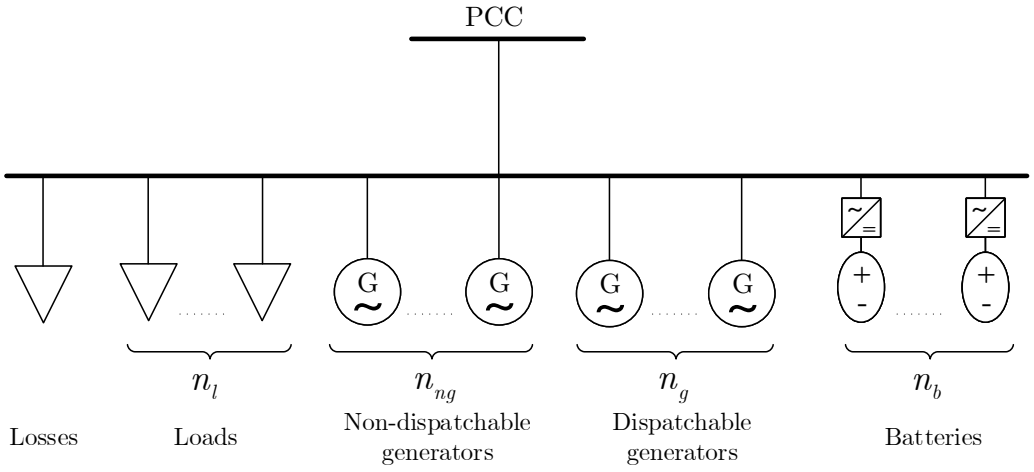

Figure 2.1: Power-based approximate model for a microgrid

Owing to its independence from microgrid's topology, this model entails the following approximations:

- Joule and converters's losses are considered constant.
- Nodal voltages are ignored.

In the following part of the section, models for generators, batteries and loads alone will be first provided; then, an externally-equivalent microgrid's simplified model will be obtained. It should be noted that only active powers are modeled at this stage: although reactive power can also be exchanged, it does not affect the energy stored in the microgrid itself. Hence, reactive power ancillary services are introduced contextually to the simplified model in Chapter 2.1.6.

Notation Each quantity is denoted with a superscript indicating the kind of the element under consideration: G stands for dispatchable generator, NG for non-dispatchable generator, L for load and B for battery. Two subscripts specify respectively the element to which the quantity is referred and the microgrid to which it belongs. Notice that the cluster index is omitted for the sake of simplicity. Indeed, as the model will be exploited by a decentralized cluster controller, only local quantities therein included are accessed. Eventually, the discrete time is denoted by t, and a scheduled quantity, i.e. known from the day-ahead optimization, see e.g. [10], is marked by a super-bar on the variable.

$$P^G_{1,3}(t) \tag{2.1.1a}$$

$$\bar{P}^G_{1,3}(t) \tag{2.1.1b}$$

For example, (2.1.1a) indicates the actual active power of the first generator of the third microgrid belonging to the current cluster, while (2.1.1b) is the scheduled value of the same quantity. In Table 2.1 the notation adopted for the microgrid model has been reported.

Furthermore, it is worth noting that the quantities introduced in the remainder of this work are supposed to be expressed in per units, as customary in the domain of electric power systems. For more details, the interested reader is addressed to Appendix A.

Table 2.1: Microgrid model notation

$\mathcal{G}_{i,j}$, $\mathcal{NG}_{i,j}$, $\mathcal{B}_{i,j}$, $\mathcal{L}_{i,j}$	Abbreviation for the i-th dispatchable generator (non-dispatchable generator, battery, load) of the j-th microgrid
$\bar{P}^G_{i,j}$, $P^G_{i,j}$	Scheduled and actual active power of $\mathcal{G}_{i,j}$
$\Delta P^G_{i,j}$	Dispatched active power variation for $\mathcal{G}_{i,j}$
$P^{G,min}_{i,j}$, $P^{G,max}_{i,j}$	Active powers limits for $\mathcal{G}_{i,j}$
$\bar{R}^{G\uparrow}_{i,j}$, $R^{G\uparrow}_{i,j}$	Scheduled and actual upwards power reserve of $\mathcal{G}_{i,j}$
$\bar{R}^{G\downarrow}_{i,j}$, $R^{G\downarrow}_{i,j}$	Scheduled and actual downwards power reserve of $\mathcal{G}_{i,j}$
$\hat{P}^{NG}_{i,j}$, $P^G_{i,j}$	Forecast and actual power injected by $\mathcal{NG}_{i,j}$
$\Delta P^{NG}_{i,j}$	Forecast error of $\mathcal{NG}_{i,j}$
$\bar{P}^B_{i,j}$, $P^B_{i,j}$	Scheduled and actual active power of $\mathcal{B}_{i,j}$
$\Delta P^B_{i,j}$	Dispatched active power variation for $\mathcal{B}_{i,j}$
$P^{B,min}_{i,j}$, $P^{B,max}_{i,j}$	Active powers limits for $\mathcal{B}_{i,j}$
$\bar{R}^{B,\uparrow}_{i,j}$, $R^{B,\uparrow}_{i,j}$	Scheduled and actual upwards power reserve of $\mathcal{B}_{i,j}$
$\bar{R}^{B,\downarrow}_{i,j}$, $R^{B,\downarrow}_{i,j}$	Scheduled and actual downwards power reserve of $\mathcal{B}_{i,j}$
$C^B_{i,j}$, α_j	Capacity and self discharge rate of $\mathcal{B}_{i,j}$
$\bar{\zeta}_{i,j}$, $\zeta_{i,j}$	Scheduled and actual State Of Charge (SOC) of $\mathcal{B}_{i,j}$
$\zeta^{min}_{i,j}$, $\zeta^{max}_{i,j}$	Minimum and maximum SOC of $\mathcal{B}_{i,j}$
$\Delta E_{i,j}$	Deviation of the energy stored in $\mathcal{B}_{i,j}$ with respect to the scheduled trajectory
$\bar{R}^{E\uparrow}_{i,j}$, $R^{E\uparrow}_{i,j}$	Scheduled and actual upwards energy reserve of $\mathcal{B}_{i,j}$
$\bar{R}^{E\downarrow}_{i,j}$, $R^{E\downarrow}_{i,j}$	Scheduled and actual downwards energy reserve of $\mathcal{B}_{i,j}$
$\hat{P}^L_{i,j}$, $P^L_{i,j}$	Forecast and actual power absorbed by $\mathcal{L}_{i,j}$
$\Delta P^L_{i,j}$	Forecast error of the active power absorbed by $\mathcal{L}_{i,j}$
$\bar{P}^{loss}_j$	Expected power losses inside $\mathcal{M}_j$ in scheduled conditions
$\eta^{NG}_{i,j}$	Efficiency of the power converter of $\mathcal{NG}_{i,j}$
$\eta^B_{i,j}$	Efficiency of $\mathcal{B}_{i,j}$

2.1.1 Dispatchable generators

Dispatchable generators vary the generated power upon controller's request, like fossil-fuel based generators and nuclear, geothermic and hydroelectric power plants. Each generator is constrained to operate within a region of economically sustainable working conditions, which in first approximation can be considered constant. Such generator's capability can be formulated as in (2.1.2).

$$P_{i,j}^{G,min} \leq P_{i,j}^{G}(t) \leq P_{i,j}^{G,max} \quad \forall t \tag{2.1.2}$$

It is supposed that the optimal working point of dispatchable generators is determined by the microgrid scheduler, which schedules the power profiles supplied by generators: $\bar{P}_{i,j}^{G}(t)$ is therefore known and, as mentioned, generally determined by an economic criterion.

In view of (2.1.2), the concept of reserve can be formalized as the available margin for variations of the generated power. In particular, let us define the upwards and downwards scheduled reserves respectively as the available margins for power increase and decrease in scheduled conditions. These reserves can thus be formalized as (2.1.3).

$$\bar{R}_{i,j}^{G\uparrow}(t) = P_{i,j}^{G,max} - \bar{P}_{i,j}^{G}(t) \geq 0 \tag{2.1.3a}$$

$$\bar{R}_{i,j}^{G\downarrow}(t) = P_{i,j}^{G,min} - \bar{P}_{i,j}^{G}(t) \leq 0 \tag{2.1.3b}$$

Therefore, reformulating constraint (2.1.2), if any variation $\Delta P_{i,j}^{G}(t)$ is requested to the generator it shall be compatible with its reserves, as in (2.1.4):

$$\bar{R}_{i,j}^{G\downarrow}(t) \leq \Delta P_{i,j}^{G}(t) \leq \bar{R}_{i,j}^{G\uparrow}(t) \quad \forall t \tag{2.1.4}$$

In figure 2.3 the sign conventions have been represented: a positive $\Delta P_{i,j}^{G}$ corresponds to an increase of the generated power. The actual power is hence determined by the sum of its scheduled value and its variation:

$$P_{i,j}^{G}(t) = \bar{P}_{i,j}^{G}(t) + \Delta P_{i,j}^{G}(t) \tag{2.1.5}$$

For each generator, the power variation $\Delta P_{i,j}^{G}(t)$ is a control variable which must be adequately remunerated; for the sake of simplicity, the extra-generation cost is assumed to be quadratic, as the generator operates away from its optimal working point.

It is worth to note that generators' dynamics can be neglected, as their settling time can be safely limited to few seconds, while the controller which will be designed for the clusters runs with a sampling time of 90 s. An instantaneous relationship between reference and actual power variations is therefore assumed.

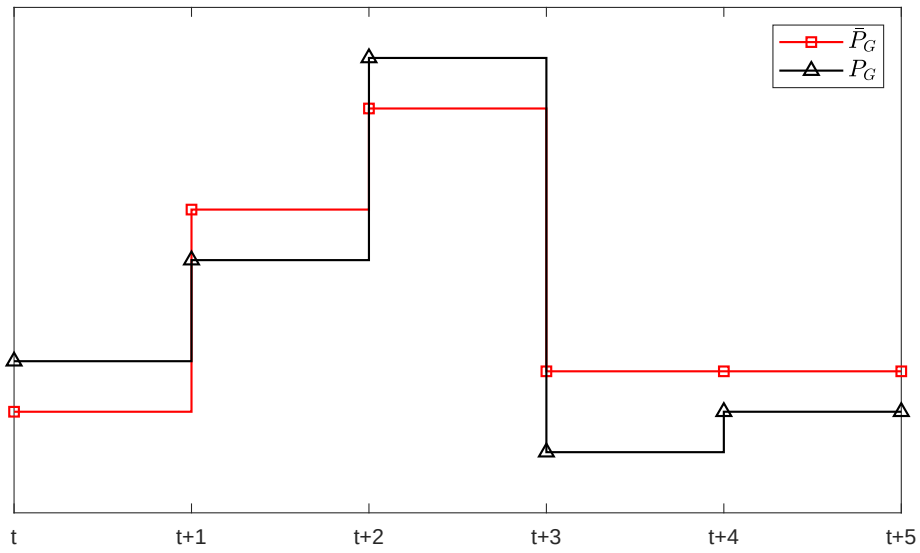

Figure 2.2: Dispatchable generators: example of scheduled power profile versus actual generated power.

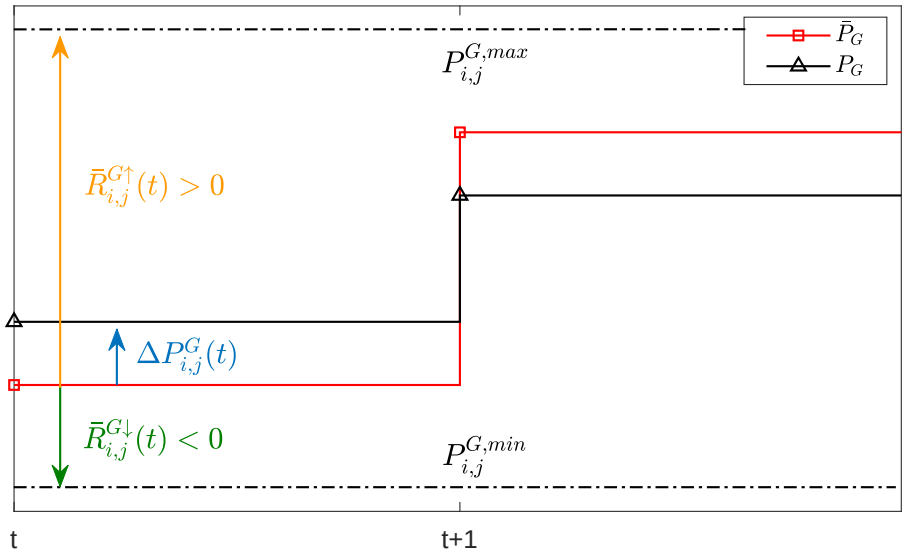

Figure 2.3: Dispatchable generator: graphical interpretation of the power reserves and power variation request.

2.1.2 Non-dispatchable generators

The most common generators based on Renewable Energy Sources, i.e. the PhotoVoltaic (PV) and the Wind Turbine Generators (WTG), are non-dispatchable. This means that the power produced cannot be controlled[2] and is subject to uncertainty, since it strongly depends on the weather. Although forecasts are widely used for the day-ahead optimization, the unpredictability introduced in the grid must be properly accounted and deviations must be compensated.

$$P_{i,j}^{NG}(t) = \hat{P}_{i,j}^{NG}(t) + \Delta P_{i,j}^{NG}(t) \tag{2.1.6}$$

Similarly to dispatchable generators, the actual power produced can be seen as the sum of two components, highlighted in (2.1.6): the former is the forecast power, denoted by $\hat{P}_{i,j}^{NG}(t)$, based on which the day-ahead optimization is performed; the latter, $\Delta P_{i,j}^{NG}(t)$, is the actual (uncontrollable) variation from such forecast, acting as a disturbance associated to weather unpredictability.

Notice that non-controllable generators, in figure 2.1, have been represented as rotating generators. In fact, despite PVs produce DC power, it is implicitly assumed they are connected to the microgrid through ideal power AC/DC converters.

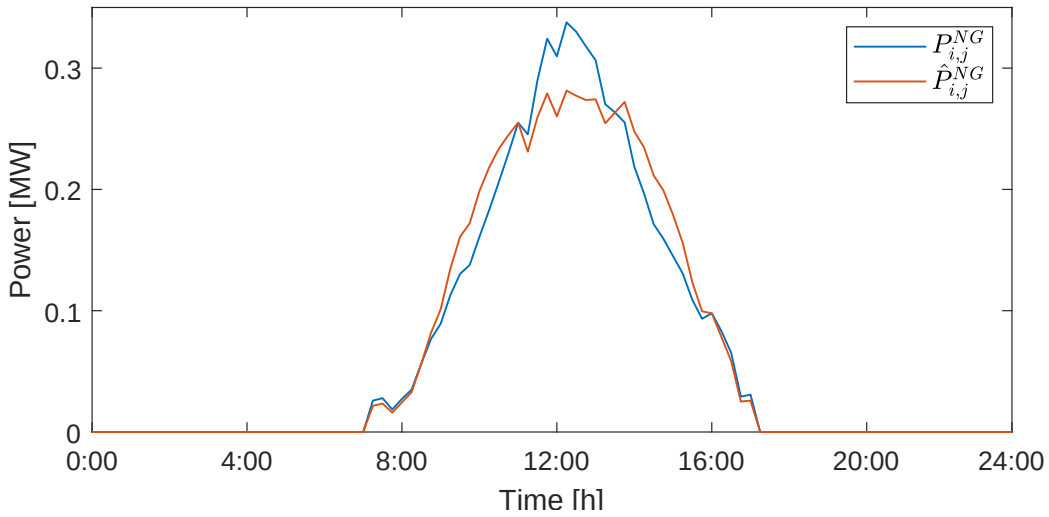

Figure 2.4: Example of non-controllable power generator (PV) forecast versus actual power.

[2]Although it would be actually possible to commit a reduction of the power supplied to the grid (e.g. dissipating the extra power) this additional control variable is not accounted for the sake of simplicity.

2.1.3 Batteries

As mentioned, energy storages are fundamental microgrid components, as they can store energy during low demand periods - when power is cheap - to supply the loads during demand peaks, hence avoiding to operate dispatchable generators in low-efficiency working conditions. In other words, energy storages operate as energy buffers.

Without loss of generality, only batteries are considered in this work, as other energy storages (like supercapacitors) can be analogously modeled. Of course, since batteries produce DC power, a reversible AC/DC converter is required. At the moment, let us consider ideal converters: losses can be adequately accounted later, as explained in Chapter 2.1.5.

Similarly to dispatchable generators, the active power supplied by the battery is scheduled by the microgrid control system, which quantity is denoted by $\bar{P}^B_{i,j}(t)$. Notice that batteries' power is conventionally assumed to be positive when supplied by the battery and negative when the battery is being recharged. Each battery is associated to a control variable, corresponding to variation of the power supplied, namely $\Delta P^B_{i,j}(t)$. The actual outgoing power can hence be defined as in (2.1.7).

$$P^B_{i,j}(t) = \bar{P}^B_{i,j}(t) + \Delta P^B_{i,j}(t) \tag{2.1.7}$$

The exchanged power is bounded by the battery's capability:

$$P^{B,min}_{i,j}(t) \leq P^B_{i,j}(t) \leq P^{B,max}_{i,j}(t) \tag{2.1.8}$$

Once more, the constraint (2.1.8) can be reformulated in terms of power reserves, representing the residual operative margins for power variations.

$$\bar{R}^{B\uparrow}_{i,j}(t) = P^{B,max}_{i,j} - \bar{P}^B_{i,j}(t) \geq 0 \tag{2.1.9a}$$

$$\bar{R}^{B\downarrow}_{i,j}(t) = P^{B,min}_{i,j} - \bar{P}^B_{i,j}(t) \leq 0 \tag{2.1.9b}$$

$$\bar{R}^{B\downarrow}_{i,j}(t) \leq \Delta P^B_{i,j}(t) \leq \bar{R}^{B\uparrow}_{i,j}(t) \tag{2.1.10}$$

Batteries are also characterized by other parameters:

- The nominal energy $C^B_{i,j}$.
- The initial *State Of Charge* (SOC) $\zeta(0) = \bar{\zeta}(0)$.
- The maximum and minimum SOC, respectively denoted by $\zeta^{max}_{i,j}$ and $\zeta^{min}_{i,j}$.
- The self-discharge rate[3] α_j.

The State of Charge represents the residual energy stored in the battery as a percentage of its capacity. It should be noted that, considering the power variation of the battery as a control variable, the SOC is a state of the system.

[3]Required to avoid singularity issues [15], assumed to be equal for each battery of the microgrid

In particular, in (2.1.11) the discrete-time scheduled SOC, i.e. the SOC profile corresponding to the scheduled battery power, is reported, where τ is the sampling time[4].

$$\bar{\zeta}_{i,j}(t+1) = (1-\alpha_j)\ \bar{\zeta}_{i,j}(t) - \frac{\tau}{C^B_{i,j}} \bar{P}^B_{i,j}(t) \tag{2.1.11}$$

The power exchanged by batteries is of course limited by the stored energy, which is in turn is proportional to the SOC. Hence, energy reserves can be formulated as follows.

$$\bar{R}^{E\uparrow}_{i,j}(t) = C^B_{i,j} \cdot (\zeta^{max}_{i,j} - \bar{\zeta}_{i,j}(t)) \tag{2.1.12a}$$

$$\bar{R}^{E\downarrow}_{i,j}(t) = C^B_{i,j} \cdot (\zeta^{min}_{i,j} - \bar{\zeta}_{i,j}(t)) \tag{2.1.12b}$$

In (2.1.12a) the scheduled upwards energy reserve has been defined as the amount of residual energy that can be stored in the battery, whereas in (2.1.12b) the downwards reserve as the amount of residual energy that can be required to the battery.

As soon as the battery is required to supply a power variation $\Delta P^B_{i,j}(t)$, the stored energy deviates from its scheduled trajectory. This deviation is modeled by $\Delta E_{i,j}(t)$, defined in (2.1.13) as the cumulative exceed of stored energy with respect to the scheduled profile. In other words, $\Delta E_{i,j}(t)$ is positive if, at time t, the actual energy is greater than the scheduled one.

$$\Delta E_{i,j}(t+1) = (1-\alpha_j)\ \Delta E_{i,j}(t) - \tau\ \Delta P^B_{i,j}(t) \tag{2.1.13}$$

In figure 2.5 an example is reported, along with a graphic interpretation of power and energy reserves.

The feasibility of a power variation requirement $\Delta P^B_{i,j}(t)$ is not only determined by the fulfillment of power reserves, but also by the compatibility of the corresponding energy deviation with battery's capacity. Specifically, $\Delta P^B_{i,j}(t)$ must be such that the consequent energy deviation $\Delta E_{i,j}$ does not violate the scheduled energy reserves in any future instant up to, at least, the prediction horizon N.

$$\bar{R}^{E\downarrow}_{i,j}(t+k) \leq \Delta E_{i,j}(t+k) \leq \bar{R}^{E\uparrow}_{i,j}(t+k) \qquad \forall k \in [1, N] \tag{2.1.14}$$

As evident from (2.1.10), (2.1.13) and (2.1.14), the advantage of this battery model is that, to correctly operate such component, only few information must be provided to the cluster controller, namely:

- The power reserves, defined in (2.1.9).
- The energy reserves, defined in (2.1.12).
- The self-discharge rate.

Battery characteristics, such as scheduled profiles and capacity, are thus hidden to the cluster controller, which is indeed desirable.

[4]Notice that α_j depends on the choice of τ.

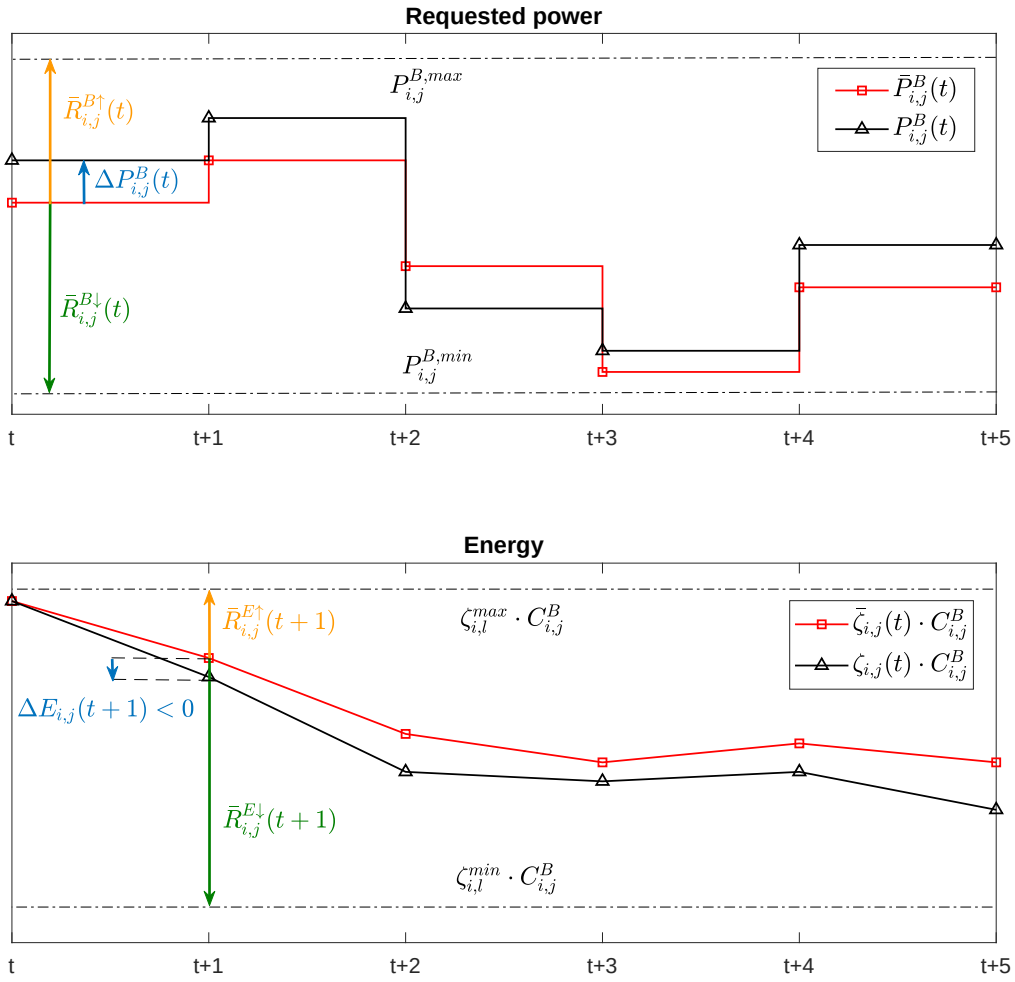

Figure 2.5: Microgrid's batteries: power and energy scheduled profiles, reserves and conventions.

2.1.4 Loads

Loads can either be non-controllable and non-deterministic or controllable and deterministic. The former are - generally - aggregates of smaller loads randomly changing their power profiles, for which forecasts are usually available. The latter are instead characterized by a power profile known to the Grid Operator. Controllable loads offer - as an ancillary service - the possibility to delay or even curtail their power demand, in exchange of a lower energy cost.

In this work only the first group of loads has been considered, although some hints for the modeling of controllable load is later presented.

Non-deterministic loads As mentioned, for each load a forecast denoted by $\hat{P}^L_{i,j}$ is available, generally with a resolution of 15 minutes. These forecasts may be produced with a large variety of techniques, spacing from time-series identification[5], briefly presented in [16], to novel techniques based on Neural Networks, [17]. It is worth noting that not only day-ahead forecasts are available, but they are also updated during the day: these intra-day updates can indeed be exploited by a control system to attain a better power planning. Owing to their reliability and accuracy, forecasts are in fact widely used in both day-ahead optimization procedures and on-line multi-step predictive control systems.

$$P^L_{i,j}(t) = \hat{P}^L_{i,j}(t) + \Delta P^L_{i,j}(t) \tag{2.1.15}$$

In (2.1.15), the actual load power $P^L_{i,j}(t)$ is represented as the sum of its forecast $\hat{P}^L_{i,j}(t)$ and the prediction error $\Delta P^L_{i,j}(t)$, which is a an uncertain variable acting as a disturbance on the system. The control system is hence required to reject it by properly dispatching power variations to microgrid's batteries and generators. Notice, eventually, that loads are generally inductive: they absorb an amount of reactive power, denoted by $Q^L_{i,j}(t)$, which depends on their power factor.

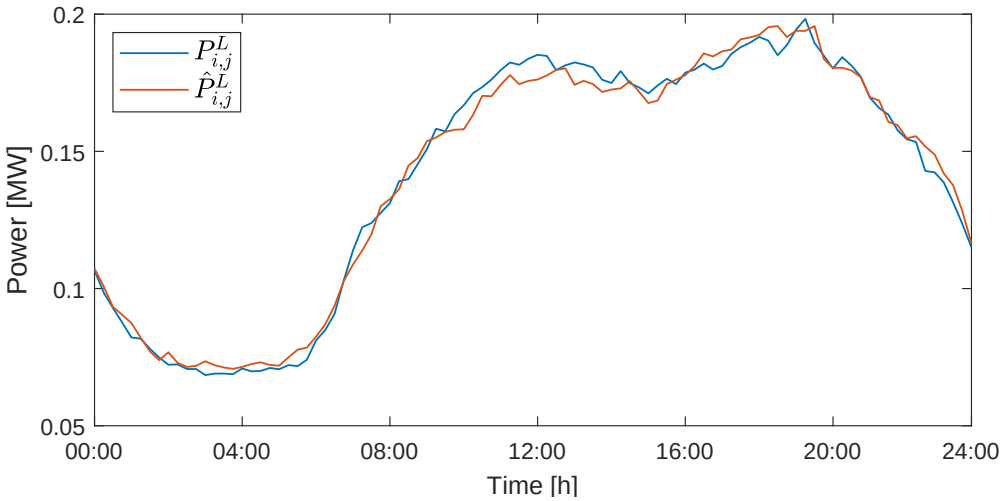

Figure 2.6: Power profile of a load, forecast versus actual value.

[5]Generally, Seasonal ARIMA time-series are adopted for load forecasting.

Controllable loads Controllable loads might be modeled as batteries which can only absorb an amount of power within a discrete set of values, usually 0%, 50% and 100% of the required nominal power. Curtailment is accepted as long as the entire required amount of energy is provided within the prescribed deadline. This condition can be modeled initializing the equivalent battery's SOC to 0 and constraining it to be fully recharged before the deadline. More advanced controllable loads, such as Electric Vehicles, can also supply power to the system during demand peaks.

2.1.5 Losses

In the previous modeling of generators and batteries power losses have been neglected, in particular those related to power converters.

An accurate modeling of the losses is not only out of the scope of this work, but it would involve an unjustified complexity, since converters' efficiencies are non constant quantities. Instead, in equation (2.1.16) an approximate a-posteriori calculation of the power losses is performed: once all generators and batteries are dispatched, joule losses and converter efficiencies are in fact fixed.

$$\bar{P}_j^{loss}(t) \simeq \bar{P}_j^{joule}(t) + \sum_{i=1}^{n_{ng,j}} \left(1 - \eta_{i,j}^{NG}\right) \hat{P}_{i,j}^{NG}(t) + \sum_{i=1}^{n_{b,j}} \left(1 - \tilde{\eta}_{i,j}^{B}(t)\right) \bar{P}_{i,j}^{B}(t) \tag{2.1.16}$$

Of course, batteries' efficiencies depends on the power flow direction:

$$\tilde{\eta}_{i,j}^{B}(t) = \begin{cases} \eta_{i,j}^{B} & \text{if } \bar{P}_{i,j}^{B}(t) > 0 \\ \\ \frac{\eta_{i,j}^{B} - 1}{\eta_{i,j}^{B}} & \text{if } \bar{P}_{i,j}^{B}(t) < 0 \end{cases} \tag{2.1.17}$$

Notice that in this way it is only possible to compute the power losses in scheduled operating conditions, while their variations - associated to loads, generators and batteries power fluctuations - act as disturbances to be automatically compensated by the control system.

Table 2.2: Simplified microgrid model notation

$\mathcal{M}_j$	Abbreviation for the j-th microgrid
$\mathcal{G}_j$, $\mathcal{B}_j$, $\mathcal{L}_j$	Abbreviation for the aggregated generator (or battery or load, respectively) of the j-th microgrid
$n_{g,j}$	Number of dispatchable generators in $\mathcal{M}_j$
$n_{b,j}$	Number of batteries in $\mathcal{M}_j$
$n_{ng,j}$	Number of non-dispatchable generators in $\mathcal{M}_j$
$n_{l,j}$	Number of loads in $\mathcal{M}_j$
$\bar{P}_j^{mg}$	Active scheduled power injected by $\mathcal{M}_j$ into the grid
ΔP_j^G	Dispatched power variation of $\mathcal{G}_j$
$\bar{R}_j^{G\uparrow}$, $R_j^{G\uparrow}$	Scheduled and actual upwards power reserve of $\mathcal{G}_j$
$\bar{R}_j^{G\downarrow}$, $R_j^{G\downarrow}$	Scheduled and actual downwards power reserve of $\mathcal{G}_j$
ΔP_j^B	Dispatched active power variation for $\mathcal{B}_j$
$\bar{R}_j^{B\uparrow}$, $R_j^{B\uparrow}$	Scheduled and actual upwards power reserve of $\mathcal{B}_j$
$\bar{R}_j^{B\downarrow}$, $R_j^{B\downarrow}$	Scheduled and actual downwards power reserve of $\mathcal{B}_j$
C_j^B, α_j	Capacity and self discharge rate of $\mathcal{B}_j$
$\bar{\zeta}_j$, $\zeta_{i,j}$	Scheduled and actual State Of Charge of $\mathcal{B}_j$
ΔE_j	Deviation of the energy stored in the aggregated battery $\mathcal{B}_j$ with respect to the scheduled trajectory
$\bar{R}_j^{E\uparrow}$, $R_j^{E\uparrow}$	Scheduled and actual upwards energy reserve of $\mathcal{B}_j$
$\bar{R}_j^{E\downarrow}$, $R_j^{E\downarrow}$	Scheduled and actual downwards energy reserve of $\mathcal{B}_j$
ΔP_j^L	Aggregate disturbance acting on $\mathcal{M}_j$
Q_j^{mg}	Non-dispatchable aggregated reactive power load of $\mathcal{M}_j$
ΔQ_j^G	Dispatchable aggregated reactive power generated by $\mathcal{M}_j$

2.1.6 Simplified model

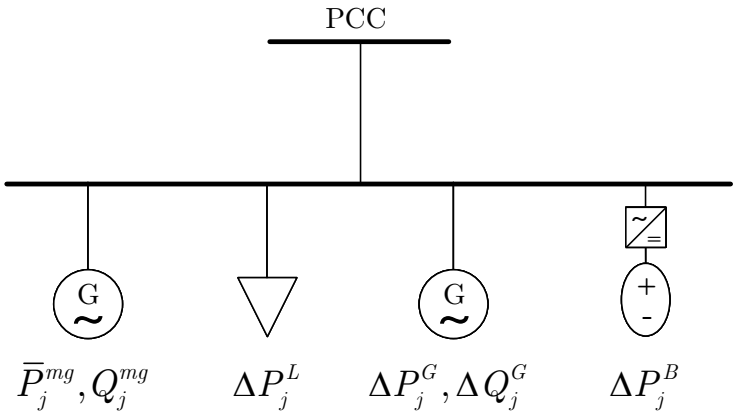

Figure 2.7: Simplified microgrid model.

The formulated microgrid model is fruitlessly detailed and is assuming that individual generators and batteries are directly controlled by the cluster controller. Conversely, the task of such control system is just to split the power demand among microgrids in view of their reserves. The dispatching of the single generators and batteries is then a duty of the microgrid scheduler, according to its own criteria, which are not a matter of concern for the higher-level cluster controller. In other words, we need to develop a simpler model of the microgrid, in which individual elements are aggregated, also reintroducing the demanded and generated reactive powers.

Consider the simplified microgrid model depicted in figure 2.7. It should be noted that it is composed of few different elements:

- A scheduled net active power $\bar{P}_j^{mg}(t)$.
- An actual non-controllable reactive power $Q_j^{mg}(t)$.
- A non-deterministic load absorbing a power $\Delta P_j^L(t)$.
- A dispatchable generator supplying an active power $\Delta P_j^G(t)$ and a reactive power $\Delta Q_j^G(t)$.
- A battery providing a power $\Delta P_j^B(t)$.

The first term corresponds to the scheduled net active power supplied by the microgrid, which is defined in (2.1.18) aggregating the scheduled or expected active powers of each microgrid element.

$$\bar{P}_j^{mg}(t) = \sum_{i=1}^{n_{g,j}} \bar{P}_{i,j}^G(t) + \sum_{i=1}^{n_{ng,j}} \hat{P}_{i,j}^{NG}(t) + \sum_{i=1}^{n_{b,j}} \bar{P}_{i,j}^B(t) - \sum_{i=1}^{n_{l,j}} \hat{P}_{i,j}^L(t) - \bar{P}_j^{loss}(t) \qquad (2.1.18)$$

The second term is, instead, the non-controllable component of the aggregated reactive power. It should be noted that, since the only elements exchanging a non-dispatchable amount of reactive power are the loads, this quantity can be expressed as (2.1.19).

$$Q_j^{mg}(t) = -\sum_{i=1}^{n_{l,j}} Q_{i,j}^L(t) \tag{2.1.19}$$

The third term, defined in (2.1.20), represents instead the aggregated disturbance acting on the microgrid, which is unmeasurable in the time scale of the cluster controller[6].

$$\Delta P_j^L(t) = \sum_{i=1}^{n_{l,j}} \Delta P_{i,j}^L(t) - \sum_{i=1}^{n_{ng,j}} \Delta P_{i,j}^{NG}(t) \tag{2.1.20}$$

The term $\Delta P_j^G(t)$ represents the aggregated variations of active power requested to microgrid's generators, as from (2.1.21). Notice that $\Delta P_j^G(t)$ is limited by the aggregated generators' power reserves, which can be computed according to (2.1.22), resulting in the capability bound (2.1.23).

$$\Delta P_j^G(t) = \sum_{i=1}^{n_{g,j}} \Delta P_{i,j}^G(t) \tag{2.1.21}$$

$$\bar{R}_j^{G\uparrow}(t) = \sum_{i=1}^{n_{g,j}} \bar{R}_{i,j}^{G\uparrow}(t) \qquad \bar{R}_j^{G\downarrow}(t) = \sum_{i=1}^{n_{g,j}} \bar{R}_{i,j}^{G\downarrow}(t) \tag{2.1.22}$$

$$\bar{R}_j^{G\downarrow}(t) \leq \Delta P_j^G(t) \leq \bar{R}_j^{G\uparrow}(t) \tag{2.1.23}$$

The aggregated reactive power requested to microgrid's components, i.e. $\Delta Q_j^G(t)$, is instead bounded by a maximum and minimum, which are supposed to be declared by the microgrid itself[7].

$$Q_j^{G,min} \leq \Delta Q_j^G(t) \leq Q_j^{G,max} \tag{2.1.24}$$

The last term, i.e. $\Delta P_j^B(t)$, corresponds to the aggregated power supplied by microgrid's batteries, see (2.1.25). Batteries are in fact aggregated into an *equivalent battery*, whose capacity and SOC can be computed as in (2.1.26).

$$\Delta P_j^B(t) = \sum_{i=1}^{n_{b,j}} \Delta P_{i,j}^B(t) \tag{2.1.25}$$

$$C_j^B = \sum_{i=1}^{n_{b,j}} C_{i,j}^B \tag{2.1.26a}$$

$$\bar{\zeta}_j(t) = \frac{1}{C_j^B} \sum_{i=1}^{n_{b,j}} C_{i,j}^B \bar{\zeta}_{i,j}(t) \tag{2.1.26b}$$

[6]Aggregate loads measurements are generally hourly updated

[7]Constant bounds are in fact assumed. This implies to constraint generators' and converters' active and reactive powers within a constant rectangular P-Q region, in such a way that reactive power capability is independent from the supplied active power and vice-versa, see [6].

The associated power and energy reserves can be accordingly computed as the sums of the respective reserves of all microgrid's batteries.

$$\bar{R}_j^{B\uparrow}(t) = \sum_{i=1}^{n_{b,j}} \bar{R}_{i,j}^{B\uparrow}(t) \qquad \bar{R}_j^{B\downarrow}(t) = \sum_{i=1}^{n_{b,j}} \bar{R}_{i,j}^{B\downarrow}(t) \tag{2.1.27a}$$

$$\bar{R}_j^{E\uparrow}(t) = \sum_{i=1}^{n_{b,j}} \bar{R}_{i,j}^{E\uparrow}(t) \qquad \bar{R}_j^{E\downarrow}(t) = \sum_{i=1}^{n_{b,j}} \bar{R}_{i,j}^{E\downarrow}(t) \tag{2.1.27b}$$

The deviation of the stored energy in the equivalent battery can be then expressed as in (2.1.28). Denoting by N the control horizon, as for individual batteries, a power variation request $\Delta P_j^B(t)$ is feasible if it compatible with the aggregated power reserves and if the corresponding state deviation $\Delta E_j(t)$ lies within the aggregated energy reserves, at least up the end-of-horizon $t + N$.

$$\Delta E_j(t+1) = \sum_{i=1}^{n_{b,j}} \Delta E_{i,j}(t+1) = (1-\alpha_j)\ \Delta E_j(t) - \tau \Delta P_j^B(t) \tag{2.1.28}$$

$$\bar{R}_j^{B\downarrow}(t) \leq \Delta P_j^B(t) \leq \bar{R}_j^{B\uparrow}(t) \tag{2.1.29}$$

$$\bar{R}_j^{E\downarrow}(t+k) \leq \Delta E_j(t+k) \leq \bar{R}_j^{E\uparrow}(t+k) \qquad \forall k \in [1, N] \tag{2.1.30}$$

Eventually, the *actual reserves* are defined as the residual reserves available after commitment of the requested power variations.

$$R_j^{G\uparrow}(t) = \bar{R}_j^{G\uparrow}(t) - \Delta P_j^G(t) \qquad R_j^{G\downarrow}(t) = \bar{R}_j^{G\downarrow}(t) - \Delta P_j^G(t) \tag{2.1.31a}$$

$$R_j^{B\uparrow}(t) = \bar{R}_j^{B\uparrow}(t) - \Delta P_j^B(t) \qquad R_j^{B\downarrow}(t) = \bar{R}_j^{B\downarrow}(t) - \Delta P_j^B(t) \tag{2.1.31b}$$

$$R_j^{E\uparrow}(t) = \bar{R}_j^{E\uparrow}(t) - \Delta E_j(t) \qquad R_j^{E\downarrow}(t) = \bar{R}_j^{E\downarrow}(t) - \Delta E_j(t) \tag{2.1.31c}$$

As a simplified microgrid model has been retrieved, it is now possible to define an energetic model for the cluster, which will later be adopted for control purposes.

Table 2.3: Cluster model notation

n_P	Number of AC ports of the cluster
n_M	Number of microgrids
n_L	Number of loads directly attached to the grid
$\bar{P}_j^{ac}$, P_j^{ac}	Scheduled and actual power flowing out of the cluster through the j-th AC port
$\bar{P}^{net}$, P^{net}	Scheduled and actual net active power of the cluster
ΔP^{net}	Cluster net active power mismatch with respect to the day-ahead scheduling
$\bar{P}_k^{dc}$	Day-ahead scheduled value of the power injected into the cluster through the DC port
ΔP_k^{dc}	DC power variation requested to the cluster supervisor
$\hat{\tilde{P}}_i^L$	Forecast power demand for the i-th load directly connected to the cluster portion of grid
$\Delta\tilde{P}_i^L$	Forecast error of the i-th cluster load
$\bar{P}^{loss}$	Scheduled cluster power losses
ΔP^{loss}	Power losses mismatch with respect to the scheduled value
$R^{G\uparrow}$, $R^{G\downarrow}$	Aggregated generators reserves
$R^{B\uparrow}$, $R^{B\downarrow}$	Aggregated batteries power reserves
$R^{E\uparrow}$, $R^{E\downarrow}$	Aggregated energy reserves
$P_k^{dc,min}$, $P_k^{dc,min}$	MVDC power converter's capability bound
$\mathcal{X}(t), \mathcal{U}(t)$	Space of admissible states and inputs trajectories at time t
$1_{n,m}$	n-by-m matrix of ones
$\emptyset_{n,m}$	n-by-m matrix of zeros
$I_{n,m}$	n-by-m identity matrix

2.2 Energetic cluster model

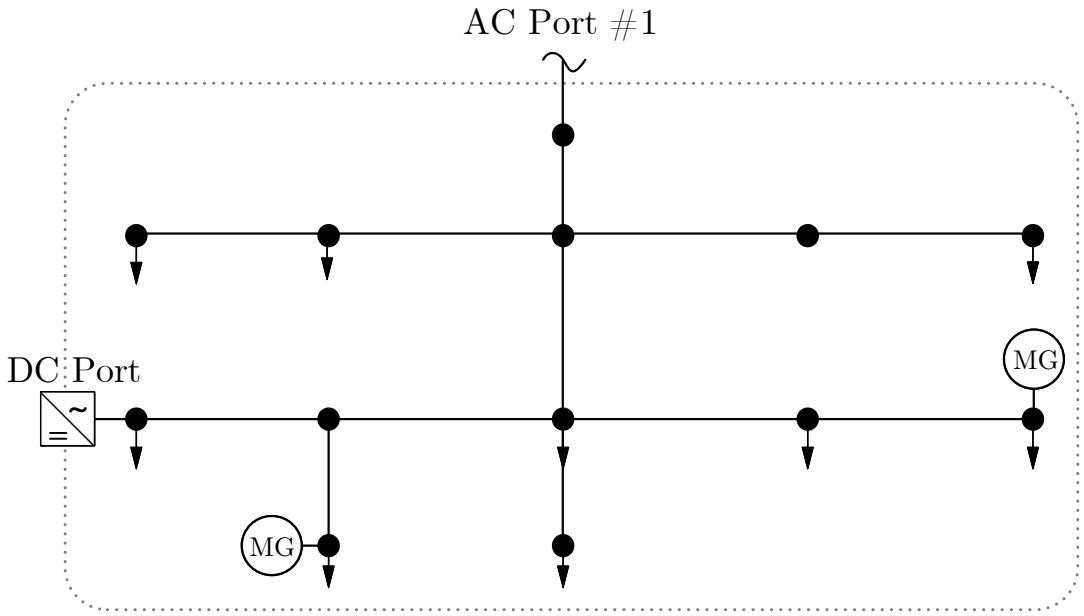

Figure 2.8: Example of a cluster with two microgrids, nine loads and one AC port.

Previously, clusters have been defined as portions of the grid aggregating loads and microgrids, which are attached to buses, interconnected by links. Each cluster is characterized by aggregated power and energy reserves that represent its operative margins. As an energetic model of the cluster is developed, its topology - which defines the internal power flows and determines the nodal voltages - is not herein modeled.

Clusters' rationale is their ability to internally compensate local loads' fluctuations, in such a way that they externally behave as scheduled. If the reserves of a cluster run out, an additional[8] (controlled) amount of power can be transferred from other clusters to the hindered one exploiting the MVDC transmission, which allows to exchange controlled amounts of power at high efficiencies. Moreover, each cluster is connected with one or more other clusters by AC ports, through which an uncontrolled amount of active and reactive power flows. Ports of different clusters are indeed connected by transmission lines, modeled as impedances[9]: the power flows through the AC connections only depend on the voltage phase and amplitude of the clusters' AC ports, as they determine the voltage drops across the lines.

It should be noted that, although the partitioning of the grid in clusters is arbitrary, each of them should have at least one microgrid and exactly one MVDC interface.

[8]The day ahead optimization already scheduled power flows through each DC interface, $\bar{P}_k^{dc}(t)$
[9]See chapter 2.3

It is assumed that the outgoing power flow through each AC port of the cluster, namely $P_j^{ac}(t)$, is measured. It is worth reminding the reader that, for the sake of compactness, the index associated to the cluster number is omitted, as each cluster operates independently from the others and there is no direct exchange of information among them. From Table 2.3, which reports the notation adopted for this model, we stress that the quantities referred to the loads directly connected to the grid are denoted by a tilde, to distinguish them from the microgrids' internal loads.

Let P^{net} be the *cluster's net power*, i.e. the total power outgoing from the cluster, which can be computed as in (2.2.1). Notice that, being the sum of measurable quantities, $P^{net}(t)$ is measurable as well.

$$P^{net}(t) = \sum_{j=1}^{n_P} P_j^{ac}(t) \tag{2.2.1}$$

According to the usual notation, $\bar{P}^{net}(t)$ is the scheduled cluster net power, whereas $\Delta P^{net}(t)$ is the mismatch of actual net power from the schedule.

Since the goal is to provide a control-oriented energetic model of the cluster, in the form of (2.2.2), reactive powers are not considered in this model. In fact, neither they are controlled by cluster controller, nor they affect the stored energy.

$$\begin{cases} x(t+1) = A \cdot x(t) + B \cdot u(t) \\ y(t) = C \cdot x(t) + D \cdot u(t) + M \cdot h(t) + H \cdot d(t) \end{cases} \tag{2.2.2}$$

The states are the energy deviations of the microgrids' batteries from their scheduled trajectories, while the control variables are of course the power variations dispatched to batteries and generators, as well as the variation of the power flowing through the DC port of the cluster.

$$x(t) = \begin{bmatrix} \Delta E_1(t) \\ \Delta E_2(t) \\ \vdots \\ \Delta E_{n_M}(t) \end{bmatrix} \in \mathbb{R}^{n_M} \tag{2.2.3}$$

$$u(t) = \left[\begin{array}{c} \Delta P_1^B(t) \\ \Delta P_2^B(t) \\ \vdots \\ \Delta P_{n_M}^B(t) \\ \hline \Delta P_1^G(t) \\ \Delta P_2^G(t) \\ \vdots \\ \Delta P_{n_M}^G(t) \\ \hline \Delta P_k^{dc}(t) \end{array}\right] \in \mathbb{R}^{2 \cdot n_M + 1} \tag{2.2.4}$$

Notice that $\Delta P_k^{dc}(t)$ is not directly manipulated by cluster controller, but rather a request is issued to the so-called Clusters Supervisor, which is in charge of conciliating and actuating the DC power requests, see Chapter 3.3.

From (2.1.21), (2.1.25) and (2.1.28) the A and B matrices can be straightforwardly computed as follows.

$$A = \begin{bmatrix} 1-\alpha_1 & & \\ & \ddots & \\ & & 1-\alpha_{n_M} \end{bmatrix} \tag{2.2.5}$$

$$B = \begin{bmatrix} -\tau \cdot I_{n_M,n_M} \mid \emptyset_{n_M,n_M} \mid \emptyset_{n_M,1} \end{bmatrix} \tag{2.2.6}$$

The outputs of the model are the actual cluster net power $P^{net}(t)$ - which is, as mentioned, trivially measurable - and the residual aggregated power and energy reserves, which are communicated to the supervisor for monitoring purposes.

$$y(t) = \begin{bmatrix} P^{net}(t) \\ R^{G\uparrow}(t) \\ R^{G\downarrow}(t) \\ R^{B\uparrow}(t) \\ R^{B\downarrow}(t) \\ R^{E\uparrow}(t) \\ R^{E\downarrow}(t) \end{bmatrix} \in \mathbb{R}^7 \tag{2.2.7}$$

The former, by definition, can be expressed as a function of control variables, disturbances and exogenous known quantities according to (2.2.8).

$$\begin{aligned} P^{net}(t) = \sum_{j=1}^{n_M} \bar{P}_j^{mg}(t) - \sum_{i=1}^{n_L} \hat{\tilde{P}}_i^L(t) + \sum_{j=1}^{n_M} \left(\Delta P_j^G(t) + \Delta P_j^B(t) - \Delta P_j^L(t)\right) - \sum_{i=1}^{n_L} \Delta \tilde{P}_i^L(t) \\ + \bar{P}_k^{dc}(t) + \Delta P_k^{dc}(t) - \bar{P}^{loss}(t) - \Delta P^{loss}(t) \end{aligned} \tag{2.2.8}$$

The vectors $d(t)$ and $h(t)$ appearing in (2.2.2) are respectively the vector of unmeasurable disturbances acting on the system and the vector of known quantities, i.e. scheduled powers and forecasts.

$$d(t) = \begin{bmatrix} \Delta P_j^L(t) \\ \vdots \\ \Delta P_{n_L}^L(t) \\ \Delta \tilde{P}_1^L(t) \\ \vdots \\ \Delta \tilde{P}_{n_M}^L(t) \\ \Delta P^{loss}(t) \end{bmatrix} \in \mathbb{R}^{n_L+n_M+1} \tag{2.2.9}$$

$$h(t) = \begin{bmatrix} \bar{P}^{mg}_{1..n_M}(t) \\ \hat{\bar{P}}^{L}_{1..n_L}(t) \\ \bar{P}^{dc}_{k}(t) \\ \bar{P}^{loss}(t) \\ \bar{R}^{G\uparrow}_{1..n_M}(t) \\ \bar{R}^{G\downarrow}_{1..n_M}(t) \\ \bar{R}^{B\uparrow}_{1..n_M}(t) \\ \bar{R}^{B\downarrow}_{1..n_M}(t) \\ \bar{R}^{E\uparrow}_{1..n_M}(t) \\ \bar{R}^{E\downarrow}_{1..n_M}(t) \end{bmatrix} \in \mathbb{R}^{7\cdot n_M + n_L + 2} \tag{2.2.10}$$

The output transformation is therefore described by the matrices (2.2.11), (2.2.12), (2.2.13) and (2.2.14).

$$C = \begin{bmatrix} \emptyset_{5,n_M} \\ -1_{2,n_M} \end{bmatrix} \tag{2.2.11}$$

$$D = \left[\begin{array}{c|c|c} 1_{1,n_M} & 1_{1,n_M} & 1 \\ \emptyset_{2,n_M} & -1_{2,n_M} & \emptyset_{2,1} \\ -1_{2,n_M} & \emptyset_{2,n_M} & \emptyset_{2,1} \\ \emptyset_{2,n_M} & \emptyset_{2,n_M} & \emptyset_{2,1} \end{array}\right] \tag{2.2.12}$$

$$M = \left[\begin{array}{cccc|c} 1_{1,n_M} & -1_{1,n_L} & 1 & -1 & \emptyset_{1,6n_M} \\ \hline & & & & 1_{1,n_M} \\ & \emptyset_{6,n_M+n_L+2} & & & \ddots \\ & & & & 1_{1,n_M} \end{array}\right] \tag{2.2.13}$$

$$H = \begin{bmatrix} -1_{1,n_M+n_L+1} \\ \emptyset_{6,n_M+n_L+1} \end{bmatrix} \tag{2.2.14}$$

It should be noted that the aforementioned DC power variation request, namely $\Delta P^{dc}_k(t)$, is bounded by the power converter capability.

$$P^{dc,min}_k - \bar{P}^{dc}_k(t) \leq \Delta P^{dc}_k \leq P^{dc,max}_k - \bar{P}^{dc}_k(t) \tag{2.2.15}$$

For the sake of simplicity, $P^{dc,min}_k$ and $P^{dc,max}_k$ are supposed to be constant and independent from the reactive power supplied by the converter itself.

Notice that the state and control variable constraints formalized in (2.1.23), (2.1.29), (2.1.30) and (2.2.15) can be generically reformulated as (2.2.16).

$$\begin{aligned} x(t) &\in \mathcal{X}(t) \\ u(t) &\in \mathcal{U}(t) \end{aligned} \tag{2.2.16}$$

2.3 Grid model

Albeit in Chapter 2.2 a control-oriented energetic model of clusters has been retrieved, an electrical model of the grid is required for both simulation and OPF problem formulation. The grid model shall establish a relationship between the input quantities, corresponding to:

- the active power supplied by each microgrid, given by the sum of the scheduled net power $\bar{P}_j^{mg}(t)$ and the power variation dispatches $\Delta P_j^G(t)$ and $\Delta P_j^B(t)$.
- the loads' forecasts $\hat{P}_j^L(t)$ and $\hat{\tilde{P}}_j^L(t)$ and their mismatch $\Delta P_j^L(t)$ and $\Delta \tilde{P}_j^L(t)$.
- the microgrid scheduled reactive power $\bar{Q}_j^{mg}(t)$ and dispatched reactive power variation $\Delta Q_j^G(t)$, as well as the reactive power absorbed by the grid loads $\tilde{Q}_j^L(t)$.
- the power flow through the MVDC interfaces.
- the On-Load Tap Changers (OLTCs) position.

and the dependent electric quantities of interest:

- the voltage amplitude and phase at each bus of the grid.
- the current and power flows through each transmission line.
- the power losses.
- the power imported from the the transmission stage through the primary substation, i.e. from the grid slack bus.

In this work, the well known Bus Injection model[10], extended to included the MVDC transmission, has been used to model the grid.

Notation In order to ensure a compact and easily readable model, a change of notation is required. As a matter of fact, clusters are not considered in this model, since they are fictitious entities introduced just for control purposes. Since the quantities adopted in previous models have been indexed on a cluster basis, indexing needs indeed to be re-defined. Hence, in order to avoid any ambiguity, lowercase letters are used in this model, as reported in Table 2.4.

Simplifying assumptions The electric grid to model is supposed to be composed by two or more radial AC feeder[11], corresponding to isolated areas not directly connected by AC transmission lines. Different nodes of the grids are connected by a DC transmission grid, through which the power flows are controlled by AC/DC power converters.

For the sake of simplicity it is assumed that these MVDC converters are ideal, i.e. that they convert an active AC power into the exact same amount of DC

[10] For more details see [2]

[11] Acyclicity is a legit assumption for feeders, possible transmission loops are activated only in case of faults

power and vice versa. As in [6], these converters are supposed to be characterized by rectangular P-Q regions [6], which means that - regardless the active power exchanged - the interface can absorb or generate an arbitrary amount of reactive power within the minimum and maximum bound. Furthermore, the MVDC converters are supposed to be controlled providing reactive power and DC voltage set-points, see [5].

A grid area is modeled as an acyclic tree, whose nodes are the grid buses (unequivocally identified by an ID), connected by oriented tree links, corresponding to the transmission lines. Each area has exactly one slack bus, representing the primary substation through which power is exchanged with the transmission stage of the power grid. Although voltage amplitude and phase of this bus are imposed by the transmission stage itself, the former is supposed to be slightly controllable through a dispatchable On-Load Tap Changer. For the sake of simplicity, the OLTC turns ratio is assumed to be a continuous control variable, hence relieving the computational complexity involved by the *Binary Mixed Integer* (BMI) problem which would arise if a discrete set of possible turns ratios were adopted. It is worth noting that this assumption marginally affects the accuracy of the solution and only requires - when the turns ratio is dispatched to the OLTC - an approximation to the closest discrete tap ratio.

A fundamental assumption is that the electric frequency is imposed by the transmission stage, therefore frequency is supposed to be constantly equal to its nominal value and hence is not modeled. Furthermore, no FACT device other than the slack OLTCs is considered.

The distribution grid is supposed to be three-phase and balanced, so that choosing a coherent set of base quantities (see Appendix A) it is possible to model the feeder through its single-phase equations, [2].

Without loss of generality the microgrids' loads fluctuations are aggregated to the loads directly connected to the grid, namely $\Delta\tilde{p}_j^L$.

$$\Delta p_h^L = 0 \quad \forall h \tag{2.3.1}$$

2.3.1 Admittance matrix construction

As in this work the Bus Injection model is adopted, it is necessary to construct the so called *Admittance Matrix*, which is the matrix $\mathbf{Y}$ such that (2.3.2) holds, where $\mathbf{V} = [\tilde{v}_1 \dots \tilde{v}_{N_m}]^T$ is the vector of complex nodal voltages and $\mathbf{I} = [\,\tilde{c}_1 \dots \tilde{c}_{N_m}\,]^T$ is the vector of complex net currents injected at each node of the grid.

$$\mathbf{I} = \mathbf{Y}\ \mathbf{V} \tag{2.3.2}$$

In order to determine the elements Y_{jk} of the admittance matrix, a model for transmission lines is first required.

[12] Grouped with $\Delta\tilde{p}_j^L$, see the assumptions paragraph in Chapter 2.3

[13] Links are considered unidirectional, quantities are positive when flowing in the link direction

Table 2.4: Grid model notation

v_j	Voltage amplitude of the j-th bus
δ_j	Voltage phase of the j-th bus
$\tilde{v}_j$	Complex voltage of the j-th bus, defined as $\tilde{v}_j = v_j\ e^{i\delta_j}$
p_j, q_j	Net active and reactive power of the j-th bus
$\bar{p}_h^{mg}$	Scheduled net active of the h-th MG
q_h^{mg}	Aggregated non-controllable reactive power of the h-th MG
Δp_h^G, Δp_h^B	Active power variation requested respectively to the aggregated generator and battery of the h-th microgrid
Δq_h^G	Reactive power variation committed to the h-th microgrid
Δp_h^L	Aggregated forecast error of the h-th microgrid[12]
$\hat{\tilde{p}}_j^L$	Forecast of the aggregated active power absorbed by the grid load connected to the j-th bus
$\Delta\tilde{p}_j^L$	Forecast error for the grid load connected to the j-th bus
$\tilde{q}_j^L$	Aggregated reactive power absorbed by the grid load connected to the j-th bus
p_{jk}, q_{jk}	Active and reactive power flowing through the branch connecting bus j to bus k
p_j^{grid}, q_j^{grid}	Active and reactive power imported from transmission grid, defined only for slack buses
y_{jk}	Admittance of the j-to-k branch
v_j^{nom}	Nominal voltage of the slack bus j
τ_j	OLTC tap ratio of slack bus j
p_i^{dc}, q_i^{dc}	Active and reactive power injected by the i-th AC/DC interface into the corresponding AC node
$p^{dc,loss}$	Power losses along DC transmission
v_j^{dc}	Voltage of the j-th DC transmission line
r_{jk}^{dc}	Resistance of the j-to-k DC line
$S_m(j)$	Set of microgrids connected to the j-th node
S_s	Set of slack nodes
$S_{ac}(j)$, $S_{dc}(j)$	Set of AC/DC interfaces connected respectively to the j-th AC bus and to the j-th DC node
$S_i(j)$, $S_o(j)$	Set of AC nodes connected to the j-th node respectively by ingoing and outgoing links[13]
$S_i^{dc}(j)$, $S_o^{dc}(j)$	Set of DC nodes connected to the j-th node by ingoing and outgoing links
$S_{io}(j)$	Set of AC nodes connected to the j-th, $S_{io}(j) = S_i(j) \cup S_o(j)$
$S_{io}^{dc}(j)$	Set of DC nodes connected to the j-th, $S_{io}^{dc}(j) = S_i^{dc}(j) \cup S_o^{dc}(j)$
S_b	Set of AC branches, identified by a tuple (i, j) corresponding to the connected buses
$S_a(i)$	Set of AC buses in the i-th grid area
N_n, N_i, N_d, N_m, N_s	Number of AC nodes, AC/DC interfaces, DC nodes, microgrids and slack nodes (areas), respectively

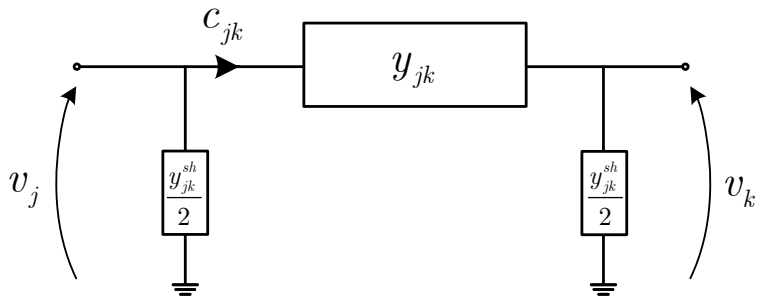

Figure 2.9: π branch model for a transmission line.

Each transmission line, generically connecting bus j to bus k, is characterized by different parameters:

- Cable length, l_{jk}.
- Cable resistance and reactance per unit of length, respectively $r_{jk,n}$ and $x_{jk,n}$.
- A capacitive shunt susceptance per unit of length, associated to parassitic phenomena $b_{jk,n}$.
- A rated current c_{jk}^{max}.

Since the goal is to determine the admittance matrix elements from lines parameters, the so-called π branch model is adopted, in which each transmission line is composed by a line admittance y_{jk} and two lumped shunt admittances $\frac{y_{jk}^{sh}}{2}$ directly connected to two buses, namely j and k, as shown in figure 2.9. The line and shunt admittances can be computed as in (2.3.3), where of course $y_{jk} = y_{kj}$.

$$y_{jk} = \frac{Z_{base}}{l_{jk}\left(r_{jk,n} + i x_{jk,n}\right)} \tag{2.3.3a}$$

$$y_{jk}^{sh} = -i\ l_{jk}\ b_{jk,n}\ Z_{base} \tag{2.3.3b}$$

As shown in [11], the admittance matrix can hence be constructed applying the equations reported in (2.3.4).

$$Y_{jk} = -y_{jk} \tag{2.3.4a}$$

$$Y_{jj} = \sum_{k \in S_o(j)} \frac{y_{jk}^{sh}}{2} + \sum_{k \in S_i(j)} \frac{y_{kj}^{sh}}{2} \tag{2.3.4b}$$

Analogously, MVDC transmission lines are characterized by the following parameters:

- Line length, l_{jk}^{dc}.
- Cable resistance per unit of length $r_{jk,n}^{dc}$.
- A rated current $c_{jk}^{dc,max}$ and nominal voltage $\bar{v}^d c_j$.

It should be noted that not only the transmission dynamics are surely negligible, but the system is also operated at constant voltages, therefore links' reactance and susceptance can be neglected, while lines' resistance can be computed as in (2.3.5).

$$r_{jk}^{dc} = l_{jk}^{dc}\, r_{jk,n}^{dc} \tag{2.3.5}$$

2.3.2 Power flow equations

The bus injection is the most intuitive model of the grid, as it simply consists in a balance of powers at each bus: specifically, the net active power of any node of the grid must be equal to the sum of active powers flowing through the branches connected to that node. The very same holds, of course, for reactive powers.

Hence, adopting the notation reported in Table 2.4, the net active power injected in the j-th bus can be computed as in (2.3.6a). It should be noted that for slack buses, since there is no microgrid, load or DC interface connected, the net power injected equals the total power absorbed from the transmission stage by the corresponding grid area.

$$p_j = \sum_{h \in S_m(j)} \left(\bar{p}_h^{mg} + \Delta p_h^G + \Delta p_h^B\right) - \left(\hat{\tilde{p}}_j^L + \Delta \tilde{p}_j^L\right) + \sum_{h \in S_{ac}(j)} p_h^{dc} \tag{2.3.6a}$$

$$p_j = p_j^{grid} \tag{2.3.6b}$$

Analogously, the net reactive power injected into the buses is determined by equations (2.3.7).

$$q_j = \sum_{h \in S_m(j)} \left(\bar{q}_h^{mg} + \Delta q_h^G\right) - \tilde{q}_j^L + \sum_{h \in S_{ac}(j)} q_h^{dc} \tag{2.3.7a}$$

$$q_j = q_j^{grid} \tag{2.3.7b}$$

As mentioned, the net power injected in any node must be equal to the total power outgoing through the connected links, which is solely determined by nodal voltages and branches' admittances. In view of Kirchhoff's Laws[14], equations (2.3.8) indeed hold for all the nodes of the grid.

$$p_j = v_j \sum_{k \in S_{io}(j)} v_k \left(G_{jk} \cos\left(\delta_j - \delta_k\right) + B_{jk} \sin\left(\delta_j - \delta_k\right)\right) + G_{jj} v_j^2 \tag{2.3.8a}$$

$$q_j = v_j \sum_{k \in S_{io}(j)} v_k \left(G_{jk} \sin\left(\delta_j - \delta_k\right) - B_{jk} \cos\left(\delta_j - \delta_k\right)\right) - B_{jj} v_j^2 \tag{2.3.8b}$$

The conductance G_{jk} and susceptance B_jk are directly computed respectively as the real and imaginary part of the admittance matrix elements.

$$G_{jk} = \Re(Y_{jk}) \tag{2.3.9a}$$

$$B_{jk} = -\Im(Y_{jk}) \tag{2.3.9b}$$

[14] See [2] and [11] for more details.

Moreover, as mentioned above, the voltage amplitude of the slack nodes can be controlled dispatching the OLTCs, while their voltage phase is customarily set to 0.

$$\delta_j = 0 \qquad \forall j \in S_s \tag{2.3.10a}$$

$$v_j = \tau_j \, v_j^{nom} \qquad \forall j \in S_s \tag{2.3.10b}$$

An adequate model of the MVDC transmission grid is also required, as the active powers injected in the connected AC buses, namely p_h^{dc}, are not completely-free variables, but they are constrained by DC power flow equations. The assumption of ideal AC/DC converters, dictated by simplicity purposes[15], implies that the DC power absorbed (resp. emitted) by the converter equals[16] the active AC power emitted (resp. absorbed), which are - in fact - both denoted by the variable p_h^{dc}.

Similarly to the AC case, DC power flow equations, reported in (2.3.11), can be easily retrieved combining power balances to Kirchhoff's and Ohm's laws.

$$-\sum_{h \in S_{dc}(j)} p_h^{dc} = v_j^{dc} \sum_{k \in S_{io}^{dc}(j)} \frac{v_j^{dc} - v_k^{dc}}{r_{jk}^{dc}} \tag{2.3.11}$$

It is worth to stress that the aforementioned constraint on the set of p_h^{dc} variables is implied by the power flow equations themselves. In fact, summing (2.3.11) over the DC nodes, the set of power flow equations can be re-written as (2.3.12), in which it is evident that at most $N_i - 1$ out of all the p_h^{dc} variables can be controlled, while the remaining one shall be such that (2.3.12) is feasible.

$$\sum_{h=1}^{N_i} p_h^{dc} + p^{dc,loss} = 0 \tag{2.3.12a}$$

$$p^{dc,loss} = \sum_{j=1}^{N_d} \sum_{k \in S_o^{dc}(j)} \frac{(v_j^{dc} - v_k^{dc})^2}{r_{jk}^{dc}} \tag{2.3.12b}$$

Eventually, exactly one MVDC converter shall be selected as DC slack node. The voltage of this node, namely j^*, is hence fixed to the nominal voltage, corresponding to 1 *p.u.*. This constraint is required to ensure the problem feasibility: without a fixed voltage, in fact, it would admit infinite combinations of nodal DC voltages realizing the same power flows through the transmission lines.

$$v_{j^*}^{dc} = 1 \tag{2.3.13}$$

[15] To include converters efficiency, power flow direction should have been accounted by means of Boolean variables, leading to a notation over-complication and to a computationally tougher problem.

[16] This holds only if the DC base power has been coherently selected, see Appendix A.

2.3.3 Operating constraints

Albeit in the previous section power flow equations for a multi-area mixed AC-DC have been formalized, the power flow problem formulation is still incomplete, as it is missing the restrictions associated to electric regulations and to devices' capabilities.

In particular, the voltage amplitude and phase must lay within a narrow band centered around their nominal values.

$$v_j^{min} \leq v_j \leq v_j^{max} \tag{2.3.14a}$$

$$-\delta_j^{max} \leq \delta_j \leq \delta_j^{max} \tag{2.3.14b}$$

Where the voltage amplitude limits are usually $\pm 10\%$ the nominal voltage of the corresponding slack node k, while the voltage phase deviation is bounded to a fraction of π.

$$v_j^{min} = 0.9\ v_k^{slack} \tag{2.3.15a}$$

$$v_j^{max} = 1.1\ v_k^{slack} \tag{2.3.15b}$$

$$\delta_j^{max} = \frac{\pi}{20} \tag{2.3.15c}$$

As far as the OLTC is concerned, the tap ratio is limited within a narrow window centered in 1, e.g. 1 ± 0.075.

$$\tau^{min} \leq \tau_j \leq \tau^{max} \qquad \forall j \in S_s \tag{2.3.16}$$

Furthermore, owing to transmission lines capabilities, a limit must be prescribed to the current flowing through grid branches. The formulation of this constraint, which isn't straightforward because currents do not appear explicitly in the Bus Injection model, as shown in [11], leads to the non-linear non-convex expression reported in equation (2.3.17).

$$\left(v_j \cos\delta_j - v_k \cos\delta_k\right)^2 y_{jk}^2 + \left(v_j \sin\delta_j - v_k \sin\delta_k\right)^2 y_{jk}^2 \leq \left(c_{jk}^{max}\right)^2 \qquad \forall (j,k) \in S_b \tag{2.3.17}$$

2.3.4 Problem formulation

The grid model can hence be formalized exploiting the equations described in 2.3.2 and 2.3.3, so that it can be implemented in either a Power Flow or an Optimal Power Flow problem.

Let us denote by h the vector of exogenous inputs, by u the independent decision variables and by x the so-called state variables, i.e. the problem's quantities depending on the previous two sets.

$$h = \left(\Delta\tilde{p}_{1\ldots N_n}^{L}, \tilde{q}_{1\ldots N_n}^{L}\right) \tag{2.3.18a}$$

$$u = \left(\Delta p_{1\ldots N_m}^{G}, \Delta p_{1\ldots N_m}^{B}, v_{1\ldots N_d}^{dc}, \Delta q_{1\ldots N_m}^{G}, q_{1\ldots N_i}^{dc}, \tau_{j\in S_s}\right) \tag{2.3.18b}$$

$$x = \left(v_{1\ldots N_n}, \delta_{1\ldots N_n}, p_{1\ldots N_i}^{dc}\right) \tag{2.3.18c}$$

As an example, this model could be utilized to formulate an OPF, i.e. an optimization problem in which - given a realization of h - the vector of control variables u minimizing a given cost function is sought. In such a problem, the power flow equations introduced in (2.3.6)-(2.3.13) and (2.3.10) can be reformulated as a set of equality constraints tying all the electric quantities in u and x.

$$f(x, u) = 0 \tag{2.3.19}$$

Similarly, the operative and regulatory limitations expressed in (2.3.14), (2.3.16) and (2.3.17) correspond to a set of inequality constraints:

$$g(x, u) \leq 0 \tag{2.3.20}$$

2.4 Brief summary

In this Chapter, a simplified microgrid model characterized by an equivalent generator, battery and load has been first provided. Each microgrid has been also associated to time-varying power and energy reserves, which are exploited to declare their operative margins to the cluster controller.

The concept of cluster has been introduced, along with motivations of its necessity for the achievement of the main goal of this work, i.e. compensating the effects of loads' fluctuations on the transmission stage. A control-oriented cluster energetic model has been provided.

Eventually, under rather general assumptions a model for a multi-area mixed AC/DC electric grid has been provided for both simulation and optimization purposes.

Chapter 3

Control strategy

3.1 Introduction

As mentioned in Chapter 1, one of the main problems preventing a wider RES integration is the intrinsic uncertainty they introduce in the electric grid. Indeed, the traditional control structure presented in Chapter 1.6 is based on an dated model of the grid, in which power flows are unidirectional - from distribution stage to the consumers - and the only non-deterministic components are the loads. This concept has been progressively overtaken by the diffusion of RES-based DERs, which entails the necessity of a control system for an adequate coordination of available resources.

In this work, the primary goal of the control system is indeed exploiting microgrids' ancillary services to locally compensate the uncertainty introduced by non-dispatchable generators and non-deterministic loads, limiting its propagation to transmission stage and allowing a more accurate day-ahead generation planning. Moreover, it is worth noticing that local compensation is fundamental also to avoid significant voltage drops across the feeder and to enhance the grid reliability itself.

Secondary goals consist in balancing clusters' power reserves, thus preventing an overloaded cluster from running out of power, and maintaining the nodal voltages within the prescribed limits.

More specifically, the multi-layer control system herein implemented is articulated in three layers:

- A *Cluster Model Predictive Control* (C-MPC)
- A *Clusters Supervisor* (CS)
- A periodic *Optimal Reactive Power Flow* (ORPF)

In order to provide the reader with a better overview of the control system, the purpose of each layer and their mutual interaction will be briefly anticipated in the following paragraphs. Each of them is then extensively explained in the remaining part of the chapter.

C-MPC For each cluster, a fast MPC-based decentralized controller optimally exploiting microgrids' ancillary services to compensate the inherent grid uncertainty. Due to the restrained time-step, this layer has been designed to work with few measurements only, i.e. the active power flowing through the AC ports of the cluster[17], by means of which it is possible to estimate the disturbance acting on the cluster itself. Based on such disturbance estimation, active power variations are dispatched to microgrids' batteries and generators. Furthermore, owing to the predictive capabilities of the C-MPC, updated forecasts are exploited for a better usage of the resources. If the disturbance is so large that it can not be locally compensated, to preserve the control problem feasibility a power variation can be requested to the MVDC interface. As already mentioned, the cluster controller does not directly command the interface, which would require a consensus among all clusters, but rather it communicates its request to the cluster supervisor.

CS A centralized control layer, called Clusters Supervisor, receives from the cluster controllers their DC power request, as well as the so-called cluster reserves, which will be later introduced. Based on this knowledge of the complete system, it conciliates the active power variations committed to the MVDC interfaces, fulfilling as much as possible the requests and maintaining the reserves well balanced.

ORPF With a much larger time frame, a periodic centralized Optimal Reactive Power Flow commits reactive power variations to microgrids and AC/DC interfaces and controls the OLTCs, in such a way to minimize power losses and to limit nodal voltage deviations, so as to respect regulations. Owing to the larger time-step, it is assumed that measurements of each load are available. It should be noted that this layer is completely independent from the others, as it only acts on reactive powers and on the OLTC, while the previous layers control active powers only.

In figure 3.1 the scheme of the control system is reported.

3.2 Cluster Model Predictive Control

When in Chapter 2.2 we introduced the concept of cluster, we mentioned that its rationale is to define a region of the grid which should internally balance loads' and DERs' fluctuations, avoiding their propagation to the transmission grid, thus mitigating the overall uncertainty of the power system. To attain these goals, of course, an adequate cluster control system is required.

In particular, such controller should be decentralized, i.e. each cluster controller shall be independent from the others and it shall also work with few output measurements only, such as the power flows measured through the AC ports of the cluster, which are easily measurable by the DSO. Moreover, intra-day forecast updates should be exploited for a better power planning.

For this purpose, a Model Predictive Control (MPC) architecture has been adopted, which is indeed well suited to the given control specifications.

[17] See the energetic cluster model in Chapter 2.2.

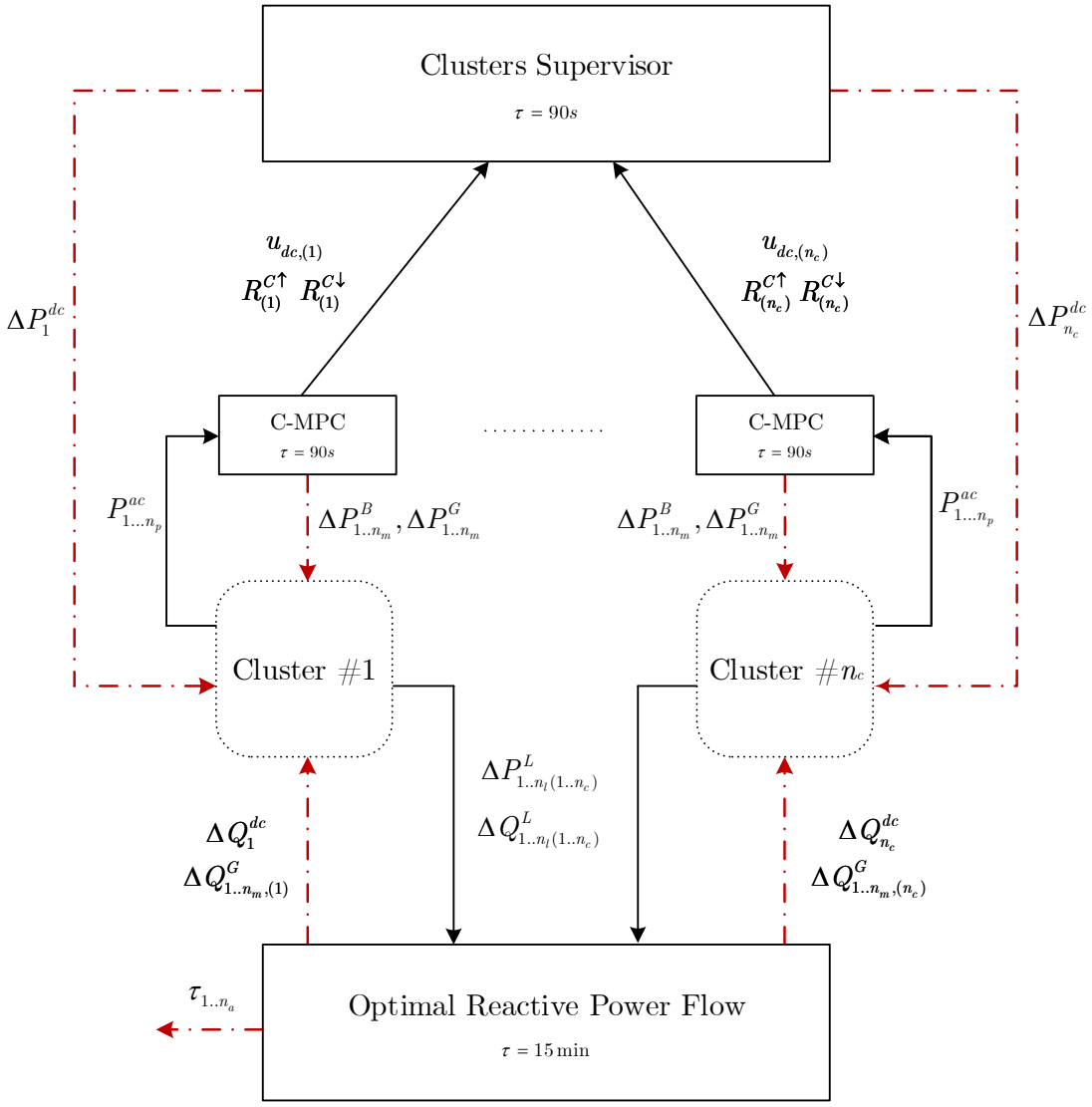

Figure 3.1: Multi-layer control scheme, where subscript (k) indicates a signal exchanged with the k-th cluster and red dash-dotted arrows correspond to control variables.

3.2.1 Introduction to MPC

Model Predictive Control is an advanced control technique remarkably different from traditional linear controllers, such as LQ or PID. It was originally introduced in the 1980s mainly for the chemical industry, where, thanks to the slowness of the processes to be controlled, an on-line optimization algorithm could be solved at each time step despite the limited computational power available at that time. The progressive increase of computational power, combined with the MPC extreme flexibility, encouraged a wide application to faster and faster processes and drove a deep research interest on this technique. A milestone reference for Model Predictive Control is surely [18], in which not only strong theoretical foundations are posed, but the further development of Robust MPC and Stochastic MPC is also devised, which are nowadays the most powerful control strategies for uncertain systems [19], [20]. Moreover, the main reference adopted in this work for the MPC problem definition and implementation is [21].

The name *Model Predictive Control* hints to the fact that this control strategy is grounded on the model-based prediction of future states and outputs trajectories as functions of the control variables and known (or measurable) quantities. In particular, these trajectories are predicted within a finite prediction horizon N, which must be large enough to capture all system's dynamics. For linear systems with linear constraints, a constrained *Quadratic Programming* (QP) problem[21] is hence solved to find the optimal control sequence $u(t), ..., u(t_N - 1)$, i.e. the control sequence minimizing a defined quadratic cost function J while - of course - respecting the prescribed constraints on the trajectories.

In accordance with the *Receding Horizon* principle only the first control action $u(t)$ is applied, before shifting the prediction horizon of one time step and recursively applying the same procedure.

Considering the aforementioned class of systems and a quadratic cost function J, the main peculiarities of Model Predictive Control, which entailed such an innovation with respect to traditional linear control strategies and heavily contributed to its popularity, have been reported below:

- **Optimality**: As MPC consists in a QP optimization problem, its control action is guaranteed to be optimal with respect to the expressed cost function, provided - of course - that the system model is exact. Furthermore, as J is a free design choice, differently from LQ control in which the cost function have a predefined structure, multiple objectives can be pursued.
- **Explicit constraints**: Differently from any other controller, MPC allows the formulation of explicit constraints on optimization variables, making it well suited in contexts where the fulfillment of hard constraints is particularly crucial. Unnecessarily conservative solutions can hence be avoided. It should be noted that this feature is particularly useful in our problem, since it allows to consider not only the physical limits of the cluster elements, but also to enforce a prescribed system behavior.

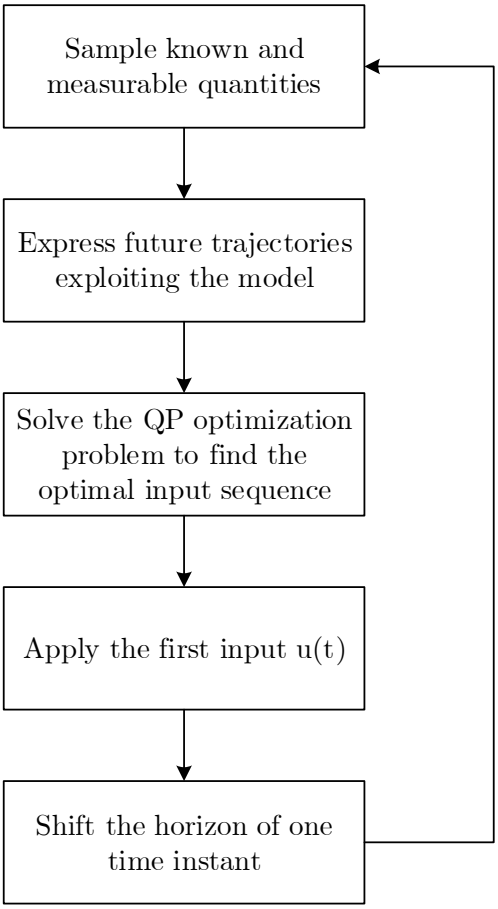

Figure 3.2: Scheme of the main steps performed at each MPC time step.

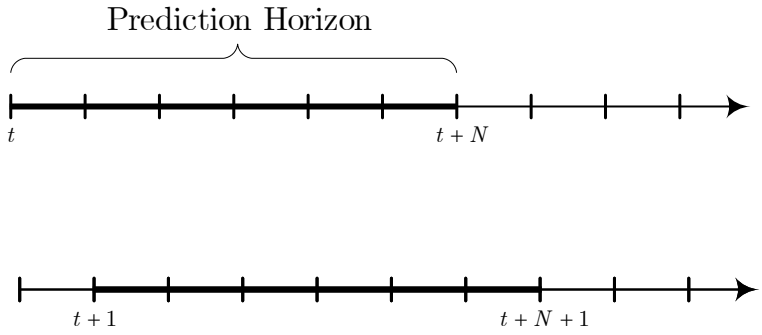

Figure 3.3: Receding Horizon principle: once that the optimal control variable's trajectory is computed for the interval $[t, t_N]$, only the first control action $u(t)$ is applied and the prediction horizon is shifted of one time step.

- **Predictive approach**: As mentioned, MPC exploits the system model to predict the states' and outputs' trajectories throughout the prediction horizon, determining the control variable sequence which minimizes the cost function J while fulfilling the given constraints. Since the optimization procedure also considers future time instants, potential forecasts of the involved exogenous quantities can be used to improve the quality of the solution. This is indeed of paramount importance in the domain of power systems, as updated intra-day forecasts can be exploited to attain lower generation costs and stationary power dispatches.
- **Robustness to faults**: For a safety-critical and highly regulated environment such as the electric grid, strong fault-rejection capabilities are a fundamental property for the control system. Thanks to the flexibility of its formulation, MPC is recognized as one of the most fault-tolerant control strategies, since in case of fault only the formulation of few additional constraints is required, see e.g. [22].
- **System model identification**: If a model of the system is not available, simple identification procedures based on impulse response can be periodically performed by the MPC algorithm, as in [14].

These features make MPC one of the most promising control strategies, as it can combine an optimal usage of energy storages, uncertainty compensation, forecasts employment and the fulfillment of operative constraints.

Before proceeding with the problem formalization, however, the choice of the time-step needs to be briefly discussed, as it significantly affects MPC's stabilizing properties and performances. The general rule is to take the time-step larger the settling time of the neglected dynamics, but small enough to guarantee the desired responsiveness to disturbances. Moreover, the time-step must be larger than the computational time required for the optimization problem resolution. The model presented in Chapter 2.2 neglects two dynamics of the system:

- Electric dynamics associated to transmission lines' inductance, which, being in the order of few milliseconds, can be safely ignored.
- The dynamics of microgrids' generators, since they usually fulfill the power dispatches with a first order fashion, with a settling time ranging from few second to some tens.

Another factor driving the time step choice is the resolution of loads' and DERs' forecasts, which inthis work is assumed to be 15 minutes[18]: in each of these time windows, there must be a fixed integer number of MPC steps.

In accordance with the aforementioned criteria, the chosen MPC time step is 90 seconds, which is enough to guarantee the settling of neglected dynamics, the convergence of the optimization problem solution, and a quick disturbance compensation.

[18]Usual values of forecasts resolutions are 15 and 30 minutes.

3.2.2 Flexible Receding Horizon

Although the traditional Receding Horizon implementation of MPC has proven to guarantee the system stability if the prediction horizon is sufficiently large[18], [21], a slight modification of this principle is required to cope with some peculiarity of the actual control problem.

First and foremost, at the end of the day the SOCs of microgrids' batteries must coincide to their scheduled values. In fact, since microgrids' schedulers have to execute the day-ahead optimal power planning, an initial SOC for the batteries needs to be assumed. The most straightforward choice is indeed to adopt as initial SOCs the scheduled values at the end of the previous day. Reminding that the states of cluster's model are the batteries' energy deviations, this behavior can be enforced constraining the final states to be null.

Another peculiarity concerns the updated forecasts availability. Let us suppose that intra-day forecasts are only known for the successive three quarters of hour, in addition - of course - to the current one. In view of this, if the traditional receding horizon technique were applied, for some of the prediction horizon's terminal time instants the updated forecast would not be available. As an example, consider a prediction horizon of one hour. At instant 01:00:00 updated forecasts are known up to 02:00:00, therefore a 40-steps[19] prediction horizon could be applied. Conversely, at instant 01:24:00 only forecasts up to 02:15:00 are assumed to be available, corresponding to 34 time-steps. Hence, in the latter case, a fixed 40-steps prediction horizon could not be applied, due to the lack of forecasts in the final time interval 02:15:00-02:24:00.

It should be noted that there are several possible workarounds to overcome this problem:

- The prediction horizon could be shrunk to 45 minutes, i.e. 30 steps, so that the Receding Horizon principle could be safely applied. A shorter horizon implies however a worse usage of energy storages and an under-usage of available intra-day forecasts.
- Day-ahead forecasts could be used in place of the missing intra-day ones. Since renewable energy sources are extremely weather-dependent, however, day-ahead projections could be significantly wrong, thus leading to a degradation of the control system performances.

The proposed solution, named *Flexible Receding Horizon* (FRH), as shown in figure 3.4 consists in adopting a time-varying prediction horizon - intuitively corresponding to the whole timespan for which the intra-day forecasts are available - determined by the following mathematical formulation.

Let us denote by t discrete-time index, where $t = 0+mM_d$ corresponds to 00:00 and $t = (m+1)M_d$ to 24:00 of day m, being $M_d = 960$ the number of time-steps per day.

[19] Recall that, since one MPC time step is 90 seconds, in each quarter of hour there are exactly 10 steps

Let the parameters M_p and M_s be respectively the maximum number of periods, i.e. quarter of hours, in the prediction horizon and the amount of time-steps in a single periods. In light of our previous considerations, $M_p = 4$ and $M_s = 10$. Hence, denoting by $N(t)$ the time-varying length of the prediction horizon and by $t_N(t)$ the corresponding final instant, it holds that:

$$t_N(t) = min\left(\left(\left\lfloor \frac{t}{M_s} \right\rfloor + M_p\right) M_s, \left(\left\lfloor \frac{t}{M_d} \right\rfloor + 1\right) M_d\right) \tag{3.2.1a}$$

$$N(t) = t_N(t) - t \tag{3.2.1b}$$

Where $\lfloor \cdot \rfloor$ and $\lceil \cdot \rceil$ correspond respectively to the floor and ceiling operators.

As depicted in figure 3.5 , the law introduced in (3.2.1) corresponds to an horizon ranging from 31 to 40, except in the last hour of the day when - owing to the min operator - it becomes a pure *shrinking horizon*, see figure 3.6. It is worth noting that this shrinking horizon behavior is adopted to enforce the fulfillment of the zero end-states constraint, i.e. batteries' SOCs restoration. As a matter of fact, during the last hour of the day the deadline of this constraint is kept fixed at 24:00. Therefore - as the end of the day approaches - the SOC restoration becomes more and more compelling, until at 23:58:30 the deadline of this constraint is at the next time-step and hence it must be necessarily fulfilled.

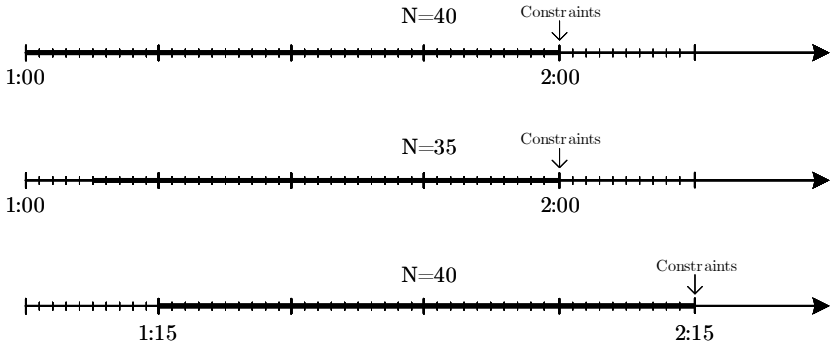

Figure 3.4: Working principle of the Flexible Receding Horizon. The prediction horizon is highlighted in strong black, while the final constraints are represented by an downward arrow.

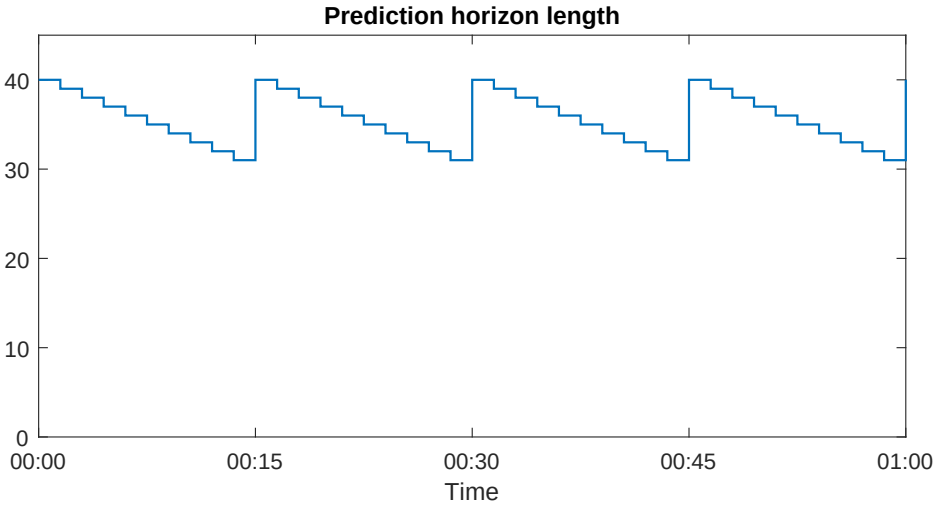

Figure 3.5: Throughout each quarter of hour the end of the prediction horizon is kept fixed. At the end of the quarter the horizon is shifted by other 15 minutes.

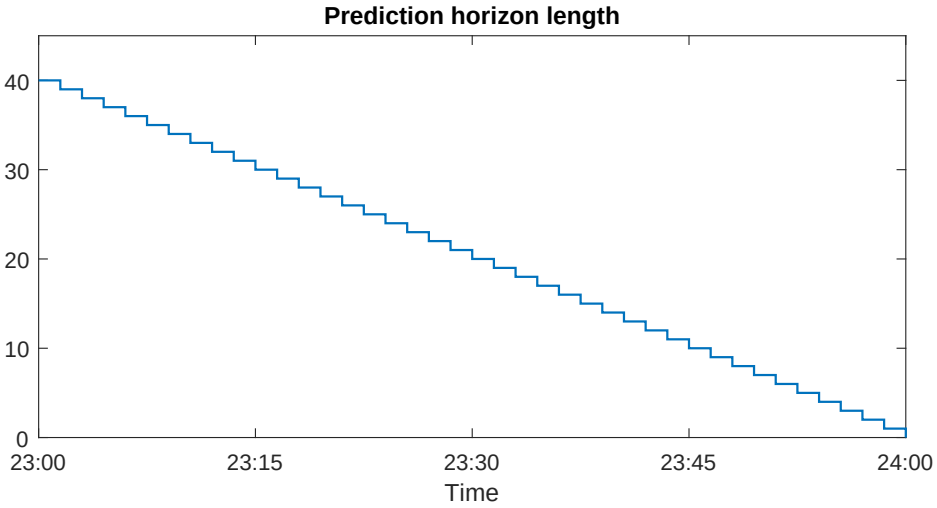

Figure 3.6: During the last hour of the day the prediction horizon progressively shrink and the zero end-state constraint approaches.

3.2.3 Predictive model

In order to formalize the MPC problem, the energetic cluster model needs to be reformulated in the so-called prediction form, which relates the future states and outputs trajectories to the current states and future inputs. As MPC is a model-based control strategy, the construction of the predictive model is fundamental and is therefore discussed in detail.

In Chapter 2.2 the control-oriented cluster model has been provided in its generic state space representation, see equation (2.2.2). Although it would be possible to adopt this model to formulate the control problem, it is convenient to partition the system according to the following criteria:

- The three types of control variables, i.e. generators, batteries and DC power request, should be separated, for a more compact formulation of the constraints later in this chapter.
- The only output which affects the optimal control sequence, i.e. the cluster net power, should be isolated from the outputs which are information merely issued to the supervisor, i.e. the cluster reserves.

Recalling that, since there is no exchange of information among the decentralized C-MPCs, the index of the cluster to which the model is related has been dropped, the aforementioned partitioning criteria correspond to (3.2.2).

$$u(t) = \begin{bmatrix} \Delta P_1^B(t) \\ \vdots \\ \Delta P_{n_M}^B(t) \\ \hline \Delta P_1^G(t) \\ \vdots \\ \Delta P_{n_M}^G(t) \\ \hline \Delta P_k^{dc}(t) \end{bmatrix} \begin{matrix} \Big\} \\ \\ \Big\} \\ \\ \Big\} \end{matrix} \begin{matrix} u_b(t) \\ \\ u_g(t) \\ \\ u_{dc}(t) \end{matrix} \qquad y(t) = \begin{bmatrix} P^{net}(t) \\ \hline R^{G\uparrow}(t) \\ R^{G\downarrow}(t) \\ R^{B\uparrow}(t) \\ R^{B\downarrow}(t) \\ R^{E\uparrow}(t) \\ R^{E\downarrow}(t) \end{bmatrix} \begin{matrix} \Big\} \\ \\ \Big\} \end{matrix} \begin{matrix} y_1(t) \\ \\ y_2(t) \end{matrix} \tag{3.2.2}$$

By partitioning the system matrices in accordance with the dimensions of the partitioned inputs and outputs, one can easily re-write the system in state-space form as (3.2.3).

$$\begin{cases} x(t+1) = A \cdot x(t) + B \cdot u(t) \\ y_1(t) = D_1 \cdot u(t) + M_1 \cdot h(t) + H_1 \cdot d(t) \\ y_2(t) = C_2 \cdot x(t) + D_2 \cdot u(t) + M_2 \cdot h(t) \end{cases} \tag{3.2.3}$$

Notice that, owing to the system sparsity, the output transformations are slightly simplified. Indeed, cluster net power does not depend on the states, while the cluster reserves do not directly depend on the disturbances. For the sake of completeness, the partitioned system matrices are reported below, where the $x(t)$, $d(t)$ and $h(t)$ vectors are those defined in (2.2.3), (2.2.9), (2.2.10) respectively. It is assumed that the vector $h(t)$ contains the most up-to-date intra-day forecasts[20].

[20]These up-to-date forecasts are guaranteed to be available owing to the adequate choice of the prediction horizon, see Chapter 3.2.2.

$$A = \begin{bmatrix} 1-\alpha_1 & & \\ & \ddots & \\ & & 1-\alpha_{n_M} \end{bmatrix} \tag{3.2.4a}$$

$$B = \begin{bmatrix} -\tau \cdot I_{n_M,n_M} & \emptyset_{n_M,n_M} & \emptyset_{n_M,1} \end{bmatrix} \tag{3.2.4b}$$

$$C_2 = \begin{bmatrix} \emptyset_{4,n_M} \\ -1_{2,n_M} \end{bmatrix} \tag{3.2.4c}$$

$$D_1 = 1_{1,2\cdot n_M+1} \tag{3.2.4d}$$

$$D_2 = \begin{bmatrix} \emptyset_{2,n_M} & -1_{2,n_M} & \emptyset_{2,1} \\ -1_{2,n_M} & \emptyset_{2,n_M} & \emptyset_{2,1} \\ \emptyset_{2,n_M} & \emptyset_{2,n_M} & \emptyset_{2,1} \end{bmatrix} \tag{3.2.4e}$$

$$M_1 = \begin{bmatrix} 1_{1,n_M} & -1_{1,n_L} & 1 & -1 & \emptyset_{1,6n_M} \end{bmatrix} \tag{3.2.4f}$$

$$M_2 = \left[\begin{array}{c|ccc} \emptyset_{6,n_M+n_L+2} & 1_{1,n_M} & & \\ & & \ddots & \\ & & & 1_{1,n_M} \end{array}\right] \tag{3.2.4g}$$

$$H_1 = -1_{1,n_M+n_L+1} \tag{3.2.4h}$$

Moreover, it is convenient to group the microgrids' reserves into vectors.

$$\bar{r}_g^{\uparrow}(t) = \begin{bmatrix} \bar{R}_1^{G\uparrow}(t) \\ \bar{R}_2^{G\uparrow}(t) \\ \vdots \\ \bar{R}_{n_M}^{G\uparrow}(t) \end{bmatrix} \qquad \bar{r}_b^{\uparrow}(t) = \begin{bmatrix} \bar{R}_1^{B\uparrow}(t) \\ \bar{R}_2^{B\uparrow}(t) \\ \vdots \\ \bar{R}_{n_M}^{B\uparrow}(t) \end{bmatrix} \qquad \bar{r}_e^{\uparrow}(t) = \begin{bmatrix} \bar{R}_1^{E\uparrow}(t) \\ \bar{R}_2^{E\uparrow}(t) \\ \vdots \\ \bar{R}_{n_M}^{E\uparrow}(t) \end{bmatrix}$$

$$\bar{r}_g^{\downarrow}(t) = \begin{bmatrix} \bar{R}_1^{G\downarrow}(t) \\ \bar{R}_2^{G\downarrow}(t) \\ \vdots \\ \bar{R}_{n_M}^{G\downarrow}(t) \end{bmatrix} \qquad \bar{r}_b^{\downarrow}(t) = \begin{bmatrix} \bar{R}_1^{B\downarrow}(t) \\ \bar{R}_2^{B\downarrow}(t) \\ \vdots \\ \bar{R}_{n_M}^{B\downarrow}(t) \end{bmatrix} \qquad \bar{r}_e^{\downarrow}(t) = \begin{bmatrix} \bar{R}_1^{E\downarrow}(t) \\ \bar{R}_2^{E\downarrow}(t) \\ \vdots \\ \bar{R}_{n_M}^{E\downarrow}(t) \end{bmatrix}$$

As previously mentioned, the predictive model describes the evolution of states and outputs trajectories as a function of the current states (which are supposed to be known), the control sequence and the future exogenous quantities.

Let $x(t+i)$ (where $i \in \mathbb{N} \setminus 0$) be a compact notation for $x(t+i|t)$, i.e. the states' prediction for the step $t+i$ made at time t. The states trajectories can be computed by recursively applying the system difference equation:

$$\begin{aligned} &x(t+1) = A\ x(t) + B\ u(t) \\ &x(t+2) = A\ x(t+1) + B\ u(t+1) = A^2\ x(t) + A\ B\ u(t) + B\ u(t) \\ &\quad\vdots \end{aligned} \tag{3.2.5}$$

Generically, in view of Lagrange equation for discrete-time systems, the states trajectories are described by:

$$x(t+i) = A^i\ x(t) + \sum_{k=0}^{i-1} A^{i-k-1}\ B\ u(t+k) \tag{3.2.6}$$

The outputs' predicted trajectories can then be calculated replacing the states trajectories and the input sequence in the output transformation.

$$\begin{aligned} y_1(t+i) &= D_1\ u(t+i) + M_1 h(t+i) + H_1\ d(t+i) \\ y_2(t+i) &= C_2\ x(t+i) + D_2\ u(t+i) + M_2\ h(t+i) \end{aligned} \tag{3.2.7}$$

The predictive model can be conveniently formulated in a set of compact matrix equations. To do so, as shown in [21], the predicted trajectories for the entire horizon shall first be grouped in vectors. Notice that, owing to the FRH principle presented in Chapter 3.2.2, at time t the prediction horizon is $[t, t_N(t)]$, where $t_N(t)$ is the end-of-horizon introduced in (3.2.1) and $N(t)$ the corresponding length. It should also be highlighted that, for the sake of compactness, the explicit dependency of t_N and N from t is dropped.

$$\underline{x}(t) = \begin{bmatrix} x(t+1) \\ x(t+2) \\ \vdots \\ x(t_N) \end{bmatrix} \qquad \underline{y}_1(t) = \begin{bmatrix} y_1(t) \\ y_1(t+1) \\ \vdots \\ y_1(t_N-1) \end{bmatrix} \qquad \underline{y}_2(t) = \begin{bmatrix} y_2(t) \\ y_2(t+1) \\ \vdots \\ y_2(t_N-1) \end{bmatrix}$$

$$\underline{u}(t) = \begin{bmatrix} u(t) \\ u(t+1) \\ \vdots \\ u(t_N-1) \end{bmatrix} \qquad \underline{h}(t) = \begin{bmatrix} h(t) \\ h(t+1) \\ \vdots \\ h(t_N-1) \end{bmatrix} \qquad \underline{d}(t) = \begin{bmatrix} d(t) \\ d(t+1) \\ \vdots \\ d(t_N-1) \end{bmatrix}$$

In (3.2.8) the predictive model structure has thus been reported.

$$\begin{cases} \underline{x}(t) = A_c \cdot x(t) + B_c \cdot \underline{u}(t) \\ \underline{y}_1(t) = D_{c1} \cdot \underline{u}(t) + M_{c1} \cdot \underline{h}(t) + H_{c1} \cdot \underline{d}(t) \\ \underline{y}_2(t) = C_{c2} \cdot \underline{x}(t) + D_{c2} \cdot \underline{u}(t) + M_{c2} \cdot \underline{h}(t) \end{cases} \tag{3.2.8}$$

Let $\otimes$ be the Kronecker matrix product; in view of (3.2.6) and (3.2.7) the system matrices can be constructed as follows, where it is reminded that $I_{N,N}$ is the N-by-N identity matrix.

$$A_c = \begin{bmatrix} A \\ A^2 \\ \vdots \\ A^{N-1} \end{bmatrix} \qquad B_c = \begin{bmatrix} B & & & \\ BA & B & & \\ \vdots & & \ddots & \\ BA^{N-1} & \dots & BA & B \end{bmatrix}$$

$$D_{c1} = I_{N,N} \otimes D_1 \qquad M_{c1} = I_{N,N} \otimes M_1 \qquad H_{c1} = I_{N,N} \otimes H_1$$

$$C_{c2} = I_{N,N} \otimes C_2 \qquad D_{c2} = I_{N,N} \otimes D_2 \qquad M_{c2} = I_{N,N} \otimes M_2$$

3.2.4 Disturbance estimation

Unfortunately, the model presented in (3.2.8) shows a dependency of the output trajectory $\underline{y}_1(t)$ on the future values of the disturbance, collected in $\underline{d}(t)$. In order to use such model for control purposes, the unknown future disturbance must be replaced by some reasonable estimation.

First and foremost, notice that in (3.2.3) the term $H_1 d(t)$ is a scalar, since H_1 is a $1 \times (n_L + n_M + 1)$ matrix and $d(t)$ is a column vector with $n_L + n_M + 1$ elements. Therefore, let us introduce the scalar quantity $\tilde{d}(t)$ corresponding to that product.

$$\tilde{d}(t) = H_1 \cdot d(t) = -\sum_{i=1}^{n_L} \Delta \tilde{P}_i^L(t) - \sum_{j=1}^{n_M} \Delta P_j^L(t) - \Delta P^{loss} \tag{3.2.9}$$

Consequently, the product $H_{c1}\ \underline{d}(t)$ appearing in the predictive model can be replaced by the vector $\underline{\tilde{d}}(t)$ defined below.

$$\underline{\tilde{d}}(t) = H_{c1}\ \underline{d}(t) = \begin{bmatrix} \tilde{d}(t) \\ \vdots \\ \tilde{d}(t_N - 1) \end{bmatrix} \tag{3.2.10}$$

Albeit this expression is more compact, the vector $\underline{\tilde{d}}(t)$ still depends on future unknown quantities. The great advantage, however, is that $\tilde{d}(t)$ can be estimated from measurements as described below.

Let us denote by t^- a (continuous) time instant immediately preceding the time step t. $P^{net}(t^-)$, for example, denotes the cluster net power measured immediately before the time instant t. It should be reminded that the cluster net power is computed by summing the measured power outgoing through the cluster AC ports as shown in (2.2.1), while it can also be expressed as a function of cluster powers, as in (2.2.8). Furthermore, the scheduled cluster net power can be straightforwardly computed setting all the variations appearing in (2.2.8) to zero.

$$\bar{P}^{net}(t) = \sum_{j=1}^{n_M} \bar{P}_j^{mg}(t) - \sum_{i=1}^{n_M} \hat{\bar{P}}_i^L(t) + \bar{P}_k^{dc}(t) - \bar{P}^{loss}(t) \tag{3.2.11}$$

Remarking that the control variables, at the end of the previous time step, can be safely considered at steady state, it holds that:

$$\begin{aligned}\Delta P_j^G(t^-) &= \Delta P_j^G(t-1)\\ \Delta P_j^B(t^-) &= \Delta P_j^B(t-1)\\ \Delta P_k^{dc}(t^-) &= \Delta P_k^{dc}(t-1)\end{aligned}$$

Exploiting (3.2.11) equation (2.2.8) can be thus re-written as (3.2.12).

$$\begin{aligned}P^{net}(t^-) = \bar{P}^{net}(t-1) + \sum_{j=1}^{n_M}(\Delta P_j^G(t-1) + \Delta P_j^B(t-1)) + \Delta P_k^{dc}(t-1) + \\ \underbrace{-\sum_{j=1}^{n_M}\Delta P_j^L(t^-) - \sum_{i=1}^{n_L}\Delta \tilde{P}_j^L(t^-) - \Delta P^{loss}(t^-)}_{\tilde{d}(t^-)}\end{aligned} \tag{3.2.12}$$

The disturbance acting at the current time instant can thus be estimated by isolating $\tilde{d}(t^-)$:

$$\tilde{d}(t) \approx \tilde{d}(t^-) = P^{net}(t^-) - \bar{P}^{net}(t-1) - \sum_{j=1}^{n_M}(\Delta P_j^G(t-1) + \Delta P_j^B(t-1)) - \Delta P_k^{dc}(t-1) \tag{3.2.13}$$

To estimate the future values of the disturbance, it is customary to assume $\tilde{d}(t) = \tilde{d}(t+1) = ... = \tilde{d}(t_N - 1)$, i.e. a constant disturbance, see [21].

$$\underline{\tilde{d}}(t) = 1_{N(t),1}\ \tilde{d}(t) \tag{3.2.14}$$

At the successive time instant the whole procedure is repeated, and a new value for the constant disturbance is estimated from measurements. The final predictive model is reported below.

$$\begin{cases}\underline{x}(t) = A_c \cdot x(t) + B_c \cdot \underline{u}(t)\\ \underline{y}_1(t) = D_{c1} \cdot \underline{u}(t) + M_{c1} \cdot \underline{h}(t) + \underline{\tilde{d}}(t)\\ \underline{y}_2(t) = C_{c2} \cdot \underline{x}(t) + D_{c2} \cdot \underline{u}(t) + M_{c2} \cdot \underline{h}(t)\end{cases} \tag{3.2.15}$$

3.2.5 Problem formalization

Given the predictive model of the system expressed in (3.2.15), the optimization problem will now be formalized. As any optimization problem, it consists of minimizing a *cost function* J subject to some sets of constraints, usually represented by $\mathcal{X}$, $\mathcal{U}$ and $\mathcal{Y}$, corresponding respectively to the sets of admissible states, inputs and outputs trajectories.

An adequate design of both these component is necessary to attain the desired performances of the MPC. Indeed, the cost function defines the objectives pursued by the control system, while the constraints ensure that the variables' physical limits and desired bounds are not violated by the control sequence.

Constraints

Since MPC is based on an on-line optimization procedure, it is crucial that the problem feasibility is guaranteed. Indeed, if there does not exist any feasible control sequence, i.e. a control sequence for which all constraints are respected, there is no way to determine which control action $u(t)$ should be applied at the current time step. In order to prevent possible unfeasibilities, typically associated to an excessive constraints' tightness, *slack variables* can be introduced to perform a *constraints relaxation*. Slack variables are levers exploited by the solver to widen the constraints which are determining the problem unfeasibility, turning *hard constraints*, i.e. constraints which must be fulfilled in any instant, into *soft constraints*, whose violation is possible yet strongly penalized by the cost function.

$$x^{min} \leq x \leq x^{max} \tag{3.2.16}$$

$$\begin{gathered} x^{min} - \epsilon \leq x \leq x^{max} + \epsilon \\ \epsilon \geq 0 \end{gathered} \tag{3.2.17}$$

As an example, in (3.2.16) an hard inequality constraint is presented, which therefore needs to be satisfied, by any solution of the optimization problem. While the decision variables can always be hard-constrained, for dependent variables it might be the case that an exceptional violation of this restriction could be accepted for the sake of problem feasibility. This is particularly true when the constraint does not represent a physical limit but just some desired behavior in normal operating conditions: in (3.2.17) a slack variable ϵ is hence introduced to relax the constraint. Of course ϵ must be adequately weighted in the cost function to ensure that soft constraints are violated only when strictly necessary to restore the problem feasibility.

In the following part of the chapter, the implemented constraints are presented.

Generators limits As mentioned in Chapter 2.1, the active power capabilities of the microgrids' aggregated generators can be reformulated as hard constraints on the power variations' dispatches. Being these bounds associated to physical limits, no relaxation is possible, since a generator cannot be operated beyond its declared capabilities.

$$\bar{r}_g^{\downarrow}(\tau) \leq u_g(\tau) \leq \bar{r}_g^{\uparrow}(\tau) \qquad \forall \tau \in [t, t_N - 1] \tag{3.2.18}$$

Battery limits Similarly, battery power variations are limited by their power reserves. Moreover, recalling that the system states correspond to the exceed of energy stored in the batteries with respect to the scheduled energy profile, the states are bounded by the so-called energy reserves, defined in (2.1.12). As discussed, this constraint corresponds to require the SOC trajectories not to violate the minimum

and maximum SOCs prescribed by the microgrids themselves and therefore it is an hard constraint.

$$\bar{r}_b^{\downarrow}(\tau) \leq u_b(\tau) \leq \bar{r}_b^{\uparrow}(\tau) \qquad \forall \tau \in [t, t_N - 1] \tag{3.2.19a}$$

$$\bar{r}_e^{\downarrow}(\tau) \leq x(\tau) \leq \bar{r}_e^{\uparrow}(\tau) \qquad \forall \tau \in [t+1, t_N] \tag{3.2.19b}$$

Final state Within the end of the prediction horizon, the batteries SOCs must be brought back to their scheduled values. This requirement can be translated in a constraint on the final state of the system. It not only ensures that at any time instant a control sequence able to recharge or discharge the batteries back to their nominal values does exist, but in the last hour of the day it progressively enforces the restoration of the declared states of charge, owing to the FRH principle.

$$x(t_N) = \emptyset_{n_M,1} \tag{3.2.20}$$

Net power mismatch bound To attain the primary goal of the cluster controller, i.e. maintaining the cluster net power sufficiently close to the day-ahead scheduling, a bound on the mismatch is prescribed. The extent of this bound is determined by the desired performances of the controller: a narrower bound guarantees a better tracking of the scheduled net power, but implies a lower control moderation. Of course, the closer $y_1(t)$ is to $\bar{P}^{net}(t)$ for each cluster, the closer the actual power imported from the transmission grid is to the declared power profile, which is the ultimate goal of the whole control architecture.

$$-\rho \leq y_1(\tau) - \bar{P}^{net}(\tau) \leq \rho \qquad \forall \tau \in [t, t_N - 1] \tag{3.2.21}$$

Albeit this constraint could seem so strict to compromise the optimization problem's feasibility, owing to the independence of y_1 from the system states and to its instantaneous dependency on the input vector u, the only case in which the feasibility is a concern is that in which both generators' and batteries' reserves are too small to provide the desired output value. In this scenario, however, DC power can be requested to the supervisor in order to preserve the problem feasibility. Actually u_{dc} is a slack variable, since it is a strongly costly lever to change y_1 in such a way to fulfill constraint (3.2.21).

DC slack variable Ideally, the slack control action u_{dc} should be adequately weighted to ensure that, if a feasible solution exists, the optimal one has $u_{dc} = 0$. Due to the numerical optimization routines, however, this ideal behavior is never achieved and optimal solutions show small non-null values of u_{dc}. Such numerical issues, in light of the structure of the supervisor, might compromise its feasibility and therefore need to be addressed at this stage. In operational research the typical strategy to cope with these problems is to introduce binary variables that force u_{dc} to be exactly zero unless non-zero values are required to attain feasibility.

Let us denote by $\mathbb{B}^n$ the set of possible combinations of n Boolean variables, i.e. $\mathbb{B}^n = \{x_1, .., x_n | x_i = 0 \vee x_i = 1\}$. Indicating by $s_{dc} \in \mathbb{B}^N$ the vector of Boolean variables enabling, at any time instant of the prediction horizon, the slack variable

activation, the following constraint - which is contextually accounting the AC/DC interface capabilities, i.e. (2.2.15) - can be introduced.

$$(P_k^{dc,min} - \bar{P}_k^{dc}(\tau)) s_{dc}(\tau) \leq u_{dc}(\tau) \leq (P_k^{dc,max} - \bar{P}_k^{dc}(\tau)) s_{dc}(\tau) \qquad \forall \tau \in [t, t_N - 1] \quad (3.2.22)$$

To properly work the activation variables must be adequately weighted in the cost function.

The introduction of Boolean variables transform the QP problem into a *Binary Quadratic Programming* (BQP) problem, which entails a significantly higher computational complexity. To relieve this complexity it should be observed that, in view of the Flexible Receding Horizon principle, at each step only the first control action of the sequence is applied. A single Boolean variable can be used to bound $u_{dc}(t)$ only, as the numerical approximations of the successive u_{dc} of the control sequence are not a matter of concern, since they are not issued to the supervisor. Reducing the dimensionality of s_{dc} and, consequently, the number of possible sequences, the computational load is relieved.

$$\begin{aligned} &(P_k^{dc,min} - \bar{P}_k^{dc}(t))\ s_{dc} \leq u_{dc}(t) \leq (P_k^{dc,max} - \bar{P}_k^{dc}(t))\ s_{dc} \\ &P_k^{dc,min} - \bar{P}_k^{dc}(\tau) \leq u_{dc}(\tau) \leq P_k^{dc,max} - \bar{P}_k^{dc}(\tau) \qquad \forall \tau \in [t+1, t_N - 1] \end{aligned} \quad (3.2.23)$$

Cost function

As mentioned above, owing to the flexibility of the optimization problem formulation, different control objectives can be pursued at the same time. Hence, to attain the desired control performances, it is crucial to properly define the cost function. In fact, since at each step the optimal solution is the one minimizing the cost function while fulfilling all the constraints, an improper selection might not only lead to inadequate performances, but even to completely wrong solutions, for example when constraints relaxation is not sufficiently penalized with respect to the other objectives.

Let us denote by $J(\cdot)$ the cost function $J(\underline{y}_1(t), \underline{u}(t), s_{dc})$. As previously mentioned, $J(\cdot)$ is quadratic, which ensures the existence of a minimum. It should in fact be noted that selecting the cost function in the form of (3.2.24) guarantees that it is lower bounded, i.e. $J(\cdot) \in [0, +\infty)$.

$$J(\cdot) = \sum_{\tau=t}^{t_N-1} \left[(y_1(\tau) - \bar{P}^{net}(\tau))^T Q (y_1(\tau) - \bar{P}^{net}(\tau)) + u(\tau)^T R u(\tau) \right] \quad (3.2.24)$$

Where Q and R must be positive-definite diagonal matrices, customarily selected diagonal[21], i.e. $Q = diag(q_1, q_2, ...)$ and $R = diag(r_1, r_2, ...)$ with $q_i > 0$ and $r_i > 0$.

In the following, the short notation $\|x\|_Q$ is used to denote the quadratic form of matrix Q along vector x, which - owing to the particular structure of Q - corresponds to the weighted sum of the squared elements of the vector, see (3.2.25).

$$\|x\|_Q = x^T Q x = \sum_i q_i x_i^2 \tag{3.2.25}$$

The different terms appearing in the implemented cost function are now be presented in detail.

Output error Not only the deviation of the predicted output trajectory from the scheduled one is bounded by the constraint (3.2.21), but it also penalized in the cost function in order to avoid unmotivated collisions of the output with such bounds.

$$\omega_y \sum_{\tau=t}^{t_N-1} \|y_1(\tau) - \bar{P}^{net}(\tau)\|_I$$

Generated power Recalling that the elements of the control variable u_g are the power variations dispatched to microgrids' aggregated generators, it would be desirable that $u_g(t) = \emptyset_{n_M,1}$ at any time instant. This would indeed mean that no ancillary service is requested to microgrids' generators, so that they can work in their optimal working condition, corresponding to power profiles declared by microgrids' scheduler on the day-ahead.

For the sake of simplicity, since intra-day ancillary services must be remunerated regardless they imply an increase or a decrease of the produced power, a quadratic cost is assumed. A more advanced approach could consist in the adoption of a piecewise quadratic cost, penalizing power increases more than power decreases[21].

$$\omega_g \sum_{\tau=t}^{t_N-1} \|u_g(\tau)\|_{R_g}$$

Generated power variation rate Another desirable behavior of the control variable u_g is to be as constant as possible, avoiding continuous adjustments of the generators' set-points. This requirement also entails a better usage of the batteries, which are the most adequate to cope with the disturbance's high-frequency components.

In terms of cost function, the corresponding contribution is the penalization of all the variations of u_g within the prediction horizon, as reported below. It is worth noting that $u_g(t-1)$ is the control action applied at the previous time instant, which is not an optimization variable, but rather the control action applied at the previous time instant.

$$\omega_\delta \sum_{\tau=t}^{t_N-1} \|u_g(\tau) - u_g(\tau-1)\|_{R_\delta}$$

[21] Although the reduction of the produced power with respect to the optimal value implies a lower efficiency, less fuel is used. Conversely, an increase of the produced power implies both the efficiency reduction and the fuel consumption increase. This asymmetry can be captured by means of a piecewise quadratic cost, but it is out of the scope of this work.

Battery power The penalty related to the batteries' usage is twofold. The explicit contribution to the cost function is associated to the small reduction, due to the control action u_b, of batteries' residual life. Indeed, as a power variation is dispatched to a battery, the resulting energy deviation marginally reduces the amount of remaining discharge cycles before its end-of-life. Albeit this cost is difficult to quantify, a slight penalty factor is required to avoid unmotivated charge-discharge cycles.

$$\omega_b \sum_{\tau=t}^{t_N-1} \|u_b(\tau)\|_{R_b}$$

The implicit contribution is instead associated to the constraint on final states previously discussed, which - at least in the MPC predictions - forces to use the generators power dispatches to restore the SOCs to their scheduled values within the prediction horizon. In other words, the utilization of batteries' power in the current time instant entails a future cost for their recharge. This fact is implicitly captured by the predictive capabilities of the controller and does not require any additional term in the cost function.

DC power As widely explained, the control variable u_{dc}, corresponding to a request of variation of the power injected into the cluster by the MVDC interface, should be considered as a slack variable. It is, in fact, a strongly penalized lever to fulfill the bound on the output error.

There are multiple reasons for such a penalization:

- In a decentralized control system, the interactions among controlled areas - like requesting power via the DC transmission - shall be as small as possible.
- The actual DC power variations, controlled by the clusters supervisor, are not communicated to the C-MPCs. Unrequested variations are in fact compensated by the cluster controllers as they were loads' fluctuations. As for the previous point, these mutual interactions must be avoided.
- If multiple DC power requests are simultaneously issued by different clusters, the satisfaction of all of them might be complex or even impossible. It is in fact reminded that, as discussed in Chapter 2.3, the power flows through the interfaces are not free variables, but need to be conciliated in order to satisfy the constraint (2.3.12). See Chapter 3.3 for more details.

The corresponding term in the cost function is reported below. Both the DC power variation request u_{dc} and the auxiliary binary variable s_{dc}, introduced to avoid numerical approximations, are penalized.

$$\omega_{dc} \sum_{\tau=t}^{t_N-1} \|u_{dc}(\tau)\|_{R_{dc}} + \omega_s \; s_{dc}$$

The full cost function is reported in (3.2.26).

$$
\begin{aligned}
J(\underline{y}(t), \underline{u}(t), s_{dc}) = \omega_y & \sum_{\tau=t}^{t_N-1} \|y_1(\tau) - \bar{P}^{net}(\tau)\|_I \\
& + \omega_g \sum_{\tau=t}^{t_N-1} \|u_g(\tau)\|_{R_g} \\
& + \omega_\delta \sum_{\tau=t}^{t_N-1} \|u_g(\tau) - u_g(\tau-1)\|_{R_\delta} \\
& + \omega_b \sum_{\tau=t}^{t_N-1} \|u_b(\tau)\|_{R_b} \\
& + \omega_{dc} \sum_{\tau=t}^{t_N-1} \|u_{dc}(\tau)\|_I \\
& + \omega_s \; s_{dc}
\end{aligned}
\tag{3.2.26}
$$

Notice that the diagonal elements of the $R_\cdot$ matrices shall determine how the control action is partitioned among the microgrids, while the priorities of the control system objectives should be uniquely determined by the choice of the positive weights $\omega_y, ..., \omega_s$. Reminding that $R_\cdot$ are positive definite matrices, this can be formalized as in (3.2.27), where $tr(\cdot)$ corresponds to the trace operator.

$$
tr(R_g) = tr(R_b) = tr(R_\delta) = 1 \tag{3.2.27}
$$

Furthermore, in light of the considerations made for each penalization term, the guideline for the selection of the weights $\omega_\cdot$ reported below can be adopted.

$$
\omega_s, \omega_{dc} \gg \omega_\delta > \omega_y > \omega_g \gg \omega_b \tag{3.2.28}
$$

In the following page the full MPC optimization step has been reported.

$$
\begin{aligned}
\min_{\underline{u}(t),s_{dc}} \quad & \omega_y \sum_{\tau=t}^{t_N-1} \|y_1(\tau) - \bar{P}^{net}(\tau)\|_I + \omega_g \sum_{\tau=t}^{t_N-1} \|u_g(\tau)\|_{R_g} \\
& + \omega_\delta \sum_{\tau=t}^{t_N-1} \|u_g(\tau) - u_g(\tau-1)\|_{R_\delta} + \omega_b \sum_{\tau=t}^{t_N-1} \|u_b(\tau)\|_{R_b} \\
& + \omega_{dc} \sum_{\tau=t}^{t_N-1} \|u_{dc}(\tau)\|_I + \omega_s \; s_{dc}
\end{aligned}
$$

$$
\begin{aligned}
s.t. \quad & \underline{x}(t) = A_c \; x(t) + B_c \; \underline{u}(t) \\
& \underline{y}_1(t) = D_{c1} \; \underline{u}(t) + M_{c1} \; \underline{h}(t) + \underline{\tilde{d}}(t) \\
& \bar{r}_g^{\downarrow}(\tau) \leq u_g(\tau) \leq \bar{r}_g^{\uparrow}(\tau) && \forall \tau \in [t, t_N - 1] \\
& \bar{r}_b^{\downarrow}(\tau) \leq u_b(\tau) \leq \bar{r}_b^{\uparrow}(\tau) && \forall \tau \in [t, t_N - 1] \\
& \bar{r}_e^{\downarrow}(\tau) \leq x(\tau) \leq \bar{r}_e^{\uparrow}(\tau) && \forall \tau \in [t+1, t_N] \\
& x(t_N) = \emptyset_{n_M,1} \\
& -\rho \leq y_1(\tau) - \bar{P}^{net}(\tau) \leq \rho && \forall \tau \in [t, t_N - 1] \\
& (P_k^{dc,min} - \bar{P}_k^{dc}(t)) \; s_{dc} \leq u_{dc}(t) \leq (P_k^{dc,max} - \bar{P}_k^{dc}(t)) \; s_{dc} \\
& P_k^{dc,min} - \bar{P}_k^{dc}(\tau) \leq u_{dc}(\tau) \leq P_k^{dc,max} - \bar{P}_k^{dc}(\tau) && \forall \tau \in [t+1, t_N - 1]
\end{aligned}
$$

$$
\begin{aligned}
where \quad & t_N = min \left(\left(\left\lfloor \frac{t}{M_s} \right\rfloor + M_p \right) M_s, \left(\left\lfloor \frac{t}{M_d} \right\rfloor + 1 \right) M_d \right) \\
& M_s = 10 \quad M_p = 4 \quad M_d = 960
\end{aligned}
$$

3.2.6 Cluster reserves

Once the optimization problem is solved and the microgrids' power variations are dispatched, each C-MPC communicates to the supervisor both the predicted trajectory of the output $\underline{y}_2(t)$ and its DC power request $u_{dc}(t)$. Indeed, the former is required for system monitoring, while the latter is conciliated with other power requests and then actuated by the supervisor.

Let us introduce two more quantities to be issued to the supervisor for control purposes, namely the *cluster reserves*, defined as the residual operative margins for the aggregated power dispatches of the cluster at the current time instant. The upwards cluster reserve $R^{C\uparrow}$ thus corresponds to the residual power which could be supplied by the cluster's microgrids, while the downwards cluster reserve $R^{C\downarrow}$ represents how much it could be possible to decrease the dispatched power.

$$R^{C\uparrow}(t) = \sum_{j=1}^{n_M} R_j^{G\uparrow}(t) + \sum_{j=1}^{n_M} min\left(R_j^{B\uparrow}(t), -\frac{R_j^{E\downarrow}(t+1)}{\tau}\right) - u_{dc}(t) \tag{3.2.29a}$$

$$R^{C\downarrow}(t) = \sum_{j=1}^{n_M} R_j^{G\downarrow}(t) + \sum_{j=1}^{n_M} max\left(R_j^{B\downarrow}(t), -\frac{R_j^{E\uparrow}(t+1)}{\tau}\right) - u_{dc}(t) \tag{3.2.29b}$$

Notice that the actual microgrids' reserves appearing in (3.2.29) are those defined in (2.1.31). Replacing the actual microgrid reserves in (3.2.29) with scheduled ones, the day-ahead schedules of cluster reserves can be retrieved.

Although due to the non-linear minimum and maximum operators it is not possible to model $R^{C\uparrow}$ and $R^{C\downarrow}$ in the state-space cluster model, these quantities can be a-posteriori computed and communicated to the supervisor.

3.2.7 Brief summary

In this part of the chapter, a Model Predictive Control strategy based on the new concept of Flexible Receding Horizon principle has been introduced for the decentralized cluster control. After the reformulation of the system model in its predictive form, the problem of estimating the future disturbance trajectory using available measurement has been coped. Eventually, the optimization problem corresponding to an MPC step has been formalized. The constraints fulfilling the requirements and a cost function attaining the desired performances have thus been discussed in detail, along with some hints for the choice of the weights. In the following part of the chapter, the Cluster Supervisor is presented.

3.3 Clusters Supervisor

On top of cluster controllers, a centralized supervisor is now designed to amend and actuate the DC power requests possibly issued by each C-MPC. As a matter of fact, due to the decentralized architecture of cluster controllers, these requests are not result of any consensus among the clusters: by design, C-MPCs are granted no information about the status of other clusters, e.g. whether they are running out of reserves or not. Therefore, not only it might be impossible to satisfy all the requests at once, but the power variation granted to a cluster must be adequately compensated by others, in view of the conservation of power. The primary objective of the supervisor is therefore to exploit its knowledge of the available reserves of each cluster to optimally actuate the conciliated requests. Besides, the secondary goal is to balance the cluster reserves, pro-actively sustaining the most hindered ones.

This control layer can be easily formulated as a static optimization problem, executed - at each time-step - after the C-MPCs. A predictive supervisor, unfortunately, cannot be implemented due to impossibility to explicitly formulate a predictive closed-loop[22] model for each cluster. Indeed, as the supervisor adjusts power flows through the DC interfaces, it does not directly control the clusters' microgrids to compensate those variations. This compensation is actually delegated to the C-MPCs, which perceive the DC power flows' variations as disturbances to be rejected, in the exact same way of loads' fluctuations[23]. Therefore, unless this control action is somehow embedded in the cluster model, there is now way in which the supervisor can predict the states' trajectories. Despite the choice of a static supervisor could seem quite inadequate for such a system, a proper formulation of the optimization problem ensures the compliance to the control objectives and avoids undesired destabilizing effects on the lower control levels.

As previously mentioned in Chapter 2.3, MVDC interfaces are supposed to be ideal and dc-voltage-controlled. The former assumption means that the active power injected by each interface into the connected AC bus equals the power absorbed from the corresponding DC node. For the sake of compactness, we will refer to this active power flowing through the interface as *DC power*. The latter assumption implies that each interface tracks the DC voltage set-point provided by the supervisor itself. The supervisor shall dispatch the voltage set-points which, in view of DC power flow equations (2.3.11), entail the desired active power injection in the clusters. Hence, we might introduce an instantaneous model of the system in which the DC voltage references are the control variables and the DC powers through the interfaces are the (constrained) outputs. The input-output relationship consists in the non-linear and non-convex set of power flow equations of the DC transmission grid.

[22]Here the word *closed-loop* is used with a stretch of its original meaning, hinting to the requirement of a model which shall explicitly account the control action of the C-MPCs.

[23]Let us, for example, suppose that the supervisor commands a MVDC interface to decrease the power injected in the corresponding cluster. The C-MPC of that cluster senses this reduction as an internal disturbance, thus committing a power increase to its microgrids in order to adequately track the scheduled net power.

The non-convexity of the model, unfortunately, has several implications:

- The convergence of the optimization problem cannot be guaranteed.
- If the optimization procedure is interrupted, the partial solution is neither guaranteed to be feasible nor close to the optimal solution.
- Given a solution of the optimization problem, it is not guaranteed to be the global optimum.

These considerations make a non-convex optimization problem not suitable for safety-critical environments. Despite in the literature an exact convexification technique has been presented, see [23], the hypothesis under which the exactness of the relaxation holds are too strict to fit our purposes. A novel multi-stage supervisor is therefore devised to guarantee the availability of - at least - a sub-optimal set of voltage references.

The reminder of this chapter is organized as follows: after a brief introduction to the adopted notation, a non-convex supervisor is introduced; then, to face the mentioned safety concerns, a multi-stage solution providing optimality guarantees is presented.

Notation In order to model the DC transmission, the notation reported in Table 2.4 has been conciliated with the notation adopted for C-MPC. In particular, assuming for simplicity that the i-th interface is connected to cluster i and dropping the time dependence for the sake of compactness[24], it holds that:

$$p_i^{dc} = \bar{P}_i^{dc} + \Delta P_i^{dc}$$

Let us denote by subscript $_{(i)}$ a quantity referred to the i-th cluster and, for the multi-stage supervisor, by superscript $^{(i)}$ an output quantity of the i-th stage. Notice that $u_{dc,(i)}$ is the DC power request issued by the C-MPC of the i-th cluster, while ΔP_i^{dc} is the actual DC power variation; n_c is the number of clusters, which is also equal to the number of AC/DC converters, N_i. Furthermore, we denote by $\mathring{v}_i^{dc}$ the voltage set-points dispatched to the interfaces, corresponding to all and only voltages of the DC nodes connected to an interface.

$$\mathring{v}_i^{dc} = v_i^{dc} \qquad \forall i \in [1..N_d] : S_{dc}(i) \neq \emptyset \tag{3.3.1}$$

[24]Indeed, as the supervisor is static, all the quantities are intended to be relative to the current time instant.

3.3.1 Non-convex supervisor

As mentioned, the supervisor consists in a static optimization problem which shall determine the optimal DC voltage set-points $\mathring{v}_i^{dc}$ attaining the desired control objectives, i.e. the power requests satisfaction and the reserves' balance. Despite the non-convexity of this formulation entails no theoretical guarantee, its simplicity allows a better understanding of the problem and constitutes a solid ground towards the multi-stage supervisor.

The former control objective can be easily enforced constraining the actual DC power variations to be greater (with the correct sign) than the requires issued by the C-MPCs, if any.

$$\sigma_i \ \Delta P_i^{dc} \geq \sigma_i \ u_{dc,(i)} \quad \sigma_i = sign(u_{dc,(i)}) \qquad \forall i \in [1, n_c] \tag{3.3.2}$$

It should be noted that:

- The auxiliary variables σ_i are known, since $u_{dc,(i)}$ are not optimization variables, but rather exogenous inputs.
- If no DC power variation has been requested by cluster i, the corresponding sign variable is $\sigma_i = 0$ and constraint (3.3.2) is satisfied for any ΔP_i^{dc}.
- In view of (2.3.12) at most $n_c - 1$ non-null $u_{dc,(i)}$ can be satisfied.

Although the hardness of this constraint could undermine the optimization problem's feasibility, being the $u_{dc,(i)}$ rarely non-null as they are slack variables, the relaxation of this constraint has proved to be unnecessary[25].

As far as the second control objective is concerned, i.e. the balancing of clusters' reserves, a fundamental premise needs to be explained. Let us consider, for example, the case in which the DC power injected in cluster i is increased by ΔP_i^{dc}. Owing to its disturbance rejection capabilities, this increase is automatically compensated by the C-MPC dispatching a power reduction to the microgrids, which ultimately leads to the increase of the actual cluster reserves. In other words, controlling the DC power flows it is possible to manipulate the actual cluster reserves.

Intuitively, the goal of balancing the cluster reserves can be pursued maintaining them *sufficiently close* to their scheduled value: in this case, indeed, microgrids' generators and batteries would be operating close to their day-ahead schedules, which correspond to the declared optimal working condition. A straightforward way to accomplish such result is enforcing the sum between the DC power variation and the upwards (downwards) cluster reserves to be greater (lower, respectively) than a fixed fraction φ of the scheduled cluster reserves.

$$0 \leq \varphi < 1 \tag{3.3.3a}$$

$$R_{(i)}^{C\uparrow} + \Delta P_i^{dc} \geq \varphi \ \bar{R}_{(i)}^{C\uparrow} \qquad \forall i \in [1, n_c] \tag{3.3.3b}$$

$$R_{(i)}^{C\downarrow} + \Delta P_i^{dc} \leq \varphi \ \bar{R}_{(i)}^{C\downarrow} \qquad \forall i \in [1, n_c] \tag{3.3.3c}$$

[25] Constraint could be relaxed by introducing a slack variable $\epsilon \geq 0$ and modifying (3.3.2) to:

$$\sigma_i \ \left(\Delta P_i^{dc} + \epsilon\right) \geq \sigma_i \ u_{dc,(i)}$$

To avoid unfeasibility problems it is however advisable to relax constraints (3.3.3) introducing a slack variable λ. Specifically, the effect of this variable is that, when no feasible solution would exist, a lower fraction of the scheduled cluster reserve is accepted.

$$R_{(i)}^{C\uparrow} + \Delta P_i^{dc} \geq (\varphi - \lambda)\ \bar{R}_{(i)}^{C\uparrow} \qquad \forall i \in [1, n_c] \tag{3.3.4a}$$

$$R_{(i)}^{C\downarrow} + \Delta P_i^{dc} \leq (\varphi - \lambda)\ \bar{R}_{(i)}^{C\downarrow} \qquad \forall i \in [1, n_c] \tag{3.3.4b}$$

$$0 \leq \lambda \leq \varphi \tag{3.3.4c}$$

Furthermore, the power variations through the interfaces are determined by the DC voltages according to power flow equations reported below, where the slack voltage prescribed by the slack interface i^* is accounted by constraint (3.3.6)[26].

$$-\sum_{h \in S_{dc}(i)} (\bar{P}_h^{dc} + \Delta P_h^{dc}) = v_i^{dc} \sum_{k \in S_{io}^{dc}(i)} \frac{v_i^{dc} - v_k^{dc}}{r_{ik}^{dc}} \qquad \forall i \in [1, N_d] \tag{3.3.5}$$

$$v_{i*}^{dc} = 1 \tag{3.3.6}$$

The MVDC operative limits, such as the minimum and maximum power and voltage, need of course to be properly enforced by means of hard constraints.

$$P_i^{dc,min} \leq \bar{P}_i^{dc} + \Delta P_i^{dc} \leq P^{dc,max} \qquad \forall i \in [1, n_c] \tag{3.3.7}$$

$$v^{dc,min} \leq v_i^{dc} \leq v^{dc,max} \qquad \forall i \in [1, N_d] \tag{3.3.8}$$

The quadratic lower-bounded cost function, reported in (3.3.9), is constituted by three terms respectively penalizing:

- The weighted actual DC power variations, since all of them shall be null unless non-null values are required to fulfill the constraints.
- The ΔP^{dc} variation with respect to the previous time instant (denoted by ΔP_i^{dc-}), to enhance its smoothness and avoid an unnecessary flickering of the disturbances measured by the clusters[27].
- The slack variable λ.

$$J(\cdot) = \gamma_1 \sum_{i=1}^{n_c} c_i (\Delta P_i^{dc})^2 + \gamma_2 \sum_{i=1}^{n_c} c_i (\Delta P_i^{dc} - \Delta P_i^{dc-})^2 + \gamma_3\ \lambda \tag{3.3.9}$$

Notice that the weights γ_j shall determine the penalization strength, while the weights c_i shall normalize the power variations with respect to clusters' capabilities.

$$c_i = \frac{1}{\bar{R}_{(i)}^{C\uparrow} - \bar{R}_{(i)}^{C\downarrow}} \tag{3.3.10}$$

[26]Recall that quantities are expressed in per units, therefore 1 p.u. is the DC nominal voltage.
[27]Recall that ΔP^{dc} acts as a disturbance measured and compensated by the C-MPC.

Below, the full non-convex supervisor optimization problem has been reported. Albeit it has been implemented in the simulation environment without any convergence problem and it proved to properly work, in Chapter 3.3.2 the optimization problem has been reformulated as a multi-stage optimization routine providing convergence guarantees and comparable performances. This latest formulation is hence more suitable to be implemented in a real system.

$$
\begin{aligned}
\min_{\mathring{v}^{dc}_{1..N_i}} \quad & \gamma_1 \sum_{i=1}^{n_c} c_i (\Delta P_i^{dc})^2 + \gamma_2 \sum_{i=1}^{n_c} c_i (\Delta P_i^{dc} - \Delta P_i^{dc-})^2 + \gamma_3 \ \lambda \\
s.t. \quad & \sigma_i \ \Delta P_i^{dc} \geq \sigma_i \ u_{dc,(i)} && \forall i \in [1, n_c] \\
& R_{(i)}^{C\uparrow} + \Delta P_i^{dc} \geq (\varphi - \lambda) \ \bar{R}_{(i)}^{C\uparrow} && \forall i \in [1, n_c] \\
& R_{(i)}^{C\downarrow} + \Delta P_i^{dc} \leq (\varphi - \lambda) \ \bar{R}_{(i)}^{C\downarrow} && \forall i \in [1, n_c] \\
& P_i^{dc,min} \leq \bar{P}_i^{dc} + \Delta P_i^{dc} \leq P^{dc,max} && \forall i \in [1, n_c] \\
& - \sum_{h \in S_{dc}(i)} (\bar{P}_h^{dc} + \Delta P_h^{dc}) = v_i^{dc} \sum_{k \in S_{io}^{dc}(i)} \frac{v_i^{dc} - v_k^{dc}}{r_{ik}^{dc}} && \forall i \in [1, N_d] \\
& v^{dc,min} \leq v_i^{dc} \leq v^{dc,max} && \forall i \in [1, N_d] \\
& v_{i*}^{dc} = 1 \\
& 0 \leq \lambda \leq \varphi
\end{aligned}
$$

3.3.2 Multi-stage supervisor

The proposed solution attaining convergence and optimality guarantees consists in a three-stage optimization routine, as sketched in figure 3.7.

The first stage determines reference values for the DC power variations, namely $\Delta P_{1..n_c}^{dc,(1)}$, solving a convex optimization problem based on a relaxed model. Although approximated, these reference values proved to be sufficiently close to the exact optimal quantities. Successively, the second stage determines a set of DC voltages $v_{1..N_d}^{dc,(2)}$ realizing the DC power variations calculated at the previous step, by solving adequately relaxed power flow equations. Eventually, in the third stage the approximated DC power variations and the corresponding voltage set-points are used to initialize an exact non-convex optimization problem in a neighborhood the global optimum, facilitating its convergence. In case of non-convergence, the approximated voltage set-points $\mathring{v}_{1..n_c}^{dc,(2)}$ can be dispatched to the MVDC interfaces with a marginal performance degradation.

In the following part of the chapter, the three stages are discussed in detail and formalized.

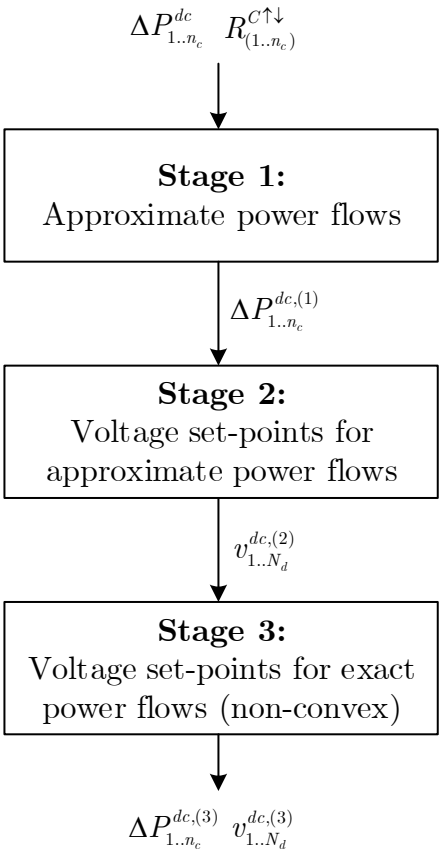

Figure 3.7: Scheme of the multi-stage Clusters Supervisor.

First stage

The rationale of supervisor's first stage is performing a model relaxation and convexification to restore the theoretical guarantees of convergence to the global optimum. Ascertained the impossibility to apply the convex relaxation technique proposed in [23] due to the strict assumptions and to the incompatible cost function which should be used to ensure the relaxed model's exactness, a tailored convexification strategy has been developed exploiting the peculiarities of our system.

The first observation is that power flow equations introduced in (3.3.5) are only required to account a fundamental relationship among the power flowing through the MVDC interfaces: the conservation of power prescribed by the Tellegen theorem. In (2.3.12) this relationship has been made explicit, while the non-convex dependency on DC voltages has been *hidden* in the power loss term. Under the reasonable assumption that the day-ahead power profiles $\bar{P}^{dc}_{1..n_c}$ have been provided by any centralized scheduler ensuring the feasibility of the mentioned values, such as an OPF[28], the expected power losses can be computed isolating the corresponding term $\bar{p}^{\,dc,loss}$ in equation (2.3.12).

[28]In other words, we suppose the existence of a set of scheduled DC voltages $\bar{v}^{dc}_{1..N_d}$ such that $\bar{P}^{dc}_{1..n_c}$ and $\bar{p}^{\,dc,loss}$ are the corresponding solutions to the power flow equations.

$$\bar{p}^{\,dc,loss} = -\sum_{i=1}^{n_c} \bar{P}_i^{dc} \geq 0 \tag{3.3.11}$$

These power losses are generally very small owing to the high efficiency of MVDC transmission. Let us now replace the actual powers appearing in (2.3.12) with the sum of their scheduled values and the corresponding variation.

$$\sum_{i=1}^{n_c} \left(\bar{P}_i^{dc} + \Delta P_i^{dc,(1)} \right) + \bar{p}^{\,dc,loss} + \Delta p^{dc,loss} = 0 \tag{3.3.12}$$

Replacing (3.3.11) in (3.3.12) we reformulate the power conservation constraints in terms of DC power variations.

$$\sum_{i=1}^{n_c} \Delta P_i^{dc,(1)} + \Delta p^{dc,loss} = 0 \tag{3.3.13}$$

Albeit $\Delta p^{dc,loss}$ still depends on the DC voltages through the non-convex power flow equations, this formulation paves the way for model relaxation. As the power flowing through each interface is operated around its scheduled working point, the actual power losses are close to their expected value. Indeed, from practical tests (Chapter 4.4.2) the mismatch $\Delta p^{dc,loss}$ turned out to be at most in the order of $10^{-2} p.u.$, rather marginal with respect to DC power variations in the order of $1 p.u.$

Simply by neglecting $\Delta p^{dc,loss}$, the non-convex power flow constraint introduced in (2.3.12) is replaced by a trivial balance of the DC power variations, which is both linear and convex.

$$\sum_{i=1}^{n_c} \Delta P_i^{dc,(1)} = 0 \tag{3.3.14}$$

Hence, the non-convex supervisor presented in Chapter 3.3.1 can be reformulated as a QP problem substituting constraints (3.3.5) with the power variations' balance (3.3.14) and dropping the DC voltage optimization variables, which are no more present in the model. The first stage optimization problem is reported below.

$$\begin{aligned}
\min_{\Delta P_{1..n_c}^{dc,(1)}} \quad & \gamma_1 \sum_{i=1}^{n_c} c_i \left(\Delta P_i^{dc,(1)} \right)^2 + \gamma_2 \sum_{i=1}^{n_c} c_i \left(\Delta P_i^{dc,(1)} - \Delta P_i^{dc-} \right)^2 + \gamma_3 \ \lambda \\
s.t. \quad & \sum_{i=1}^{n_c} \Delta P_i^{dc,(1)} = 0 \\
& \sigma_i \ \Delta P_i^{dc,(1)} \geq \sigma_i \ u_{dc,(i)} && \forall i \in [1, n_c] \\
& R_{(i)}^{C\uparrow} + \Delta P_i^{dc,(1)} \geq (\varphi - \lambda) \ \bar{R}_{(i)}^{C\uparrow} && \forall i \in [1, n_c] \\
& R_{(i)}^{C\downarrow} + \Delta P_i^{dc,(1)} \leq (\varphi - \lambda) \ \bar{R}_{(i)}^{C\downarrow} && \forall i \in [1, n_c] \\
& P_i^{dc,min} \leq \bar{P}_i^{dc} + \Delta P_i^{dc,(1)} \leq P_i^{dc,max} && \forall i \in [1, n_c] \\
& 0 \leq \lambda \leq \varphi
\end{aligned}$$

Second stage

Once the approximate optimal power variations $\Delta P^{dc,(1)}_{1..n_c}$ are computed, the corresponding DC voltage references must be retrieved. As aforementioned, in fact, the interfaces are supposed to be voltage-controlled.

The non-linear equations must be therefore solved for the nodal voltages by substituting the known power variation references, computed at the first stage. In view of the approximated model previously adopted, the equations need to be relaxed by introducing the slack variable ϵ_{i^*} in the power flow equation associated to the slack node i^*. With such an expedient, the slack variable *absorbs* the approximation committed neglecting $\Delta p^{dc,loss}$ by adjusting the power flow through the slack interface, restoring the solvability of equations (3.3.15).

$$v^{dc}_{i^*} = 1 \tag{3.3.15a}$$

$$-\sum_{h\in S_{dc}(i^*)} (\bar{P}^{dc}_h + \Delta P^{dc,(1)}_h) + \epsilon_{i^*} = v^{dc,(2)}_{i^*} \sum_{k\in S^{dc}_{io}(i^*)} \frac{v^{dc,(2)}_{i^*} - v^{dc,(2)}_k}{r^{dc}_{ik}} \tag{3.3.15b}$$

$$-\sum_{h\in S_{dc}(i)} (\bar{P}^{dc}_h + \Delta P^{dc,(1)}_h) = v^{dc,(2)}_i \sum_{k\in S^{dc}_{io}(i)} \frac{v^{dc,(2)}_i - v^{dc,(2)}_k}{r^{dc}_{ik}} \qquad \forall i \in [1, N_d] \setminus i^* \tag{3.3.15c}$$

Notice that the set of equations reported above has N_d unknowns, corresponding to ϵ_{i^*} and $v^{dc}_{i\neq i^*}$, and N_d equations. Despite the multivariate quadratic system of equations (3.3.15) may have multiple solutions, it has been proved that under mild conditions, adequately bounding the DC voltages within the operative limits and the slack variable within a range of reasonable values, a unique admissible solution exists, see [24] and [25]. Such uniqueness has been further confirmed by experimental results.

$$\begin{aligned} v^{dc,min}_i \leq v^{dc,(2)}_i \leq v^{dc,max}_i \\ -\epsilon^{max} \leq \epsilon_{i^*} \leq \epsilon^{max} \\ \epsilon^{max} = \max_i \left(P^{dc,max}_i\right) - \min_i \left(P^{dc,min}_i\right) \end{aligned} \tag{3.3.16}$$

Therefore, the DC voltage set-points $\mathring{v}^{dc,(2)}_{1..N_d}$, computed solving the power flow equations (3.3.15) subject to the bounds (3.3.16) and applying (3.3.1), are then exploited to initialize the third-stage optimization problem in a neighborhood of the optimal solution.

Third stage

Due to the formulation of the supervisor's second stage, if the aforementioned voltage references $\mathring{v}^{dc,(2)}_{1..N_d}$ are dispatched to the interfaces, the neglected power losses variations are entirely compensated by the slack interface. To overcome this undesired effect, a non-convex third stage redistributing the compensation efforts among the interfaces is implemented. Below the corresponding optimization problem has

been formalized. In addition to the traditional power flow equations and operative limits constraints, a cost function penalizing the weighted[29] deviation from the DC power reference computed at the first step has been implemented.

$$
\begin{aligned}
\min_{v_{1..N_d}^{dc,(3)}} \quad & \sum_{i=1}^{n_c} c_i \left(\Delta P_i^{dc,(3)} - \Delta P_i^{dc,(1)}\right)^2 \\
s.t. \quad & -\sum_{h \in S_{dc}(i)} (\bar{P}_h^{dc} + \Delta P_h^{dc,(3)}) = v_i^{dc,(3)} \sum_{k \in S_{io}^{dc}(i)} \frac{v_i^{dc,(3)} - v_k^{dc,(3)}}{r_{ik}^{dc}} && \forall i \in [1, N_d] \\
& \sigma_i \ \Delta P_i^{dc,(3)} \geq \sigma_i \ u_{dc,(i)} && \forall i \in [1, n_c] \\
& P_i^{dc,min} \leq \bar{P}_i^{dc} + \Delta P_i^{dc,(3)} \leq P_i^{dc,max} && \forall i \in [1, n_c] \\
& v_i^{dc,min} \leq v_i^{dc,(3)} \leq v_i^{dc,max} && \forall i \in [1, N_d] \\
& v_{i^*}^{dc,(3)} = 1
\end{aligned}
$$

Once the optimization problem is solved, in view of (3.3.1) the DC voltage set-points to be dispatched to the interfaces are extracted from the set of DC voltages.

$$\mathring{v}_i^{dc} = v_i^{dc,(3)} \qquad \forall i \in [1..N_d] : S_{dc}(i) \neq \emptyset$$

Notice that, despite this stage - owing to an almost exact initialization - has proven to be computationally effortless and to converge in few iterations, in the worse scenario of convergence problems it is always possible to commit the voltage set-points computed at the previous stage:

$$\mathring{v}_i^{dc} = v_i^{dc,(2)} \qquad \forall i \in [1..N_d] : S_{dc}(i) \neq \emptyset$$

This *rollback* capability of the multi-stage supervisor therefore guarantees the existence of, at least, a sub-optimal solution fulfilling the constraints.

3.3.3 Brief summary

In this chapter the supervisor's control objectives and a strategy to attain them by means of static optimization problems have been presented. Two architectures with comparable performances have been formalized: first a simple non-convex supervisor with no guarantee of convergence to the global optimum, then a multi-stage supervisor guaranteeing the availability of, at least, a sub-optimal solution have been described in detail.

[29] Weights c_i are computed as in (3.3.10), so that a smaller cluster capability implies a stronger penalization.

3.4 Optimal Reactive Power Flow

In the previous control layers, the nodal voltages have been conveniently disregarded, supposing them to lie within the operative limits regardless of the applied control action. In the C-MPC this assumption was fundamental to avoid both the introduction of power flow equations in the system model - which would have entailed a noteworthy complication in the controller design - and the dependency, at each time-step, on all the component of the disturbance vector $\underline{d}(t)$. The supervisor, instead, completely neglected the clusters' topology and internal components, determining the control action only based on their requests and reserves. A centralized *Optimal Reactive Power Flow* (ORPF) is hence periodically executed to minimize the power losses and adjust the nodal voltages, keeping them within the regulatory limits and sufficiently close to their nominal values.

ORPF is a well-known formulation of the Optimal Power Flow problem (see [11]), in which the real power generation is fixed a-priori[30], while the reactive power generation and - possibly - the FACTS devices are controlled to achieve the control objectives. Notice that this control layer is completely decoupled from the others, since it operates on reactive powers only, while the active power generation is supposed to perfectly balance loads, which is indeed true when both C-MPCs and CS work adequately.

It is worth noting that to execute an ORPF problem it is necessary to assume the exact knowledge of the disturbances acting on the system, i.e. the $\tilde{P}_{\cdot}^{L}$ and $P_{\cdot}^{L}$ variables, at the time instant immediately anticipating the optimization routine's execution. Let us assume that these quantities are available once every 15 minutes, coinciding with the chosen ORPF time step. Furthermore, let us adopt the notation described in Table 2.4, reminding the reader of the simplifying assumptions declared in Chapter 2.3.

The known exogenous inputs of the optimization problem, grouped in (3.4.1a), corresponds to the following quantities:

- The scheduled net powers supplied by the microgrids.
- The active power variations dispatched to generators and batteries.
- The actual active and reactive power absorbed by grid loads.
- The DC voltage set-points dispatched by the supervisor.
- The scheduled position of OLTCs.

$$h = (\bar{p}^{mg}_{1..N_m}, \Delta p^{G}_{1..N_m}, \Delta p^{B}_{1..N_m}, \hat{\tilde{p}}^{L}_{1..N_n}, \Delta\tilde{p}^{L}_{1..N_n}, \bar{q}^{mg}_{1..N_m}, \tilde{q}^{L}_{1..N_m}, \hat{v}^{dc}_{1..N_i}, \bar{\tau}_{S_s}) \tag{3.4.1a}$$

$$u = (\Delta q^{G}_{1..N_m}, q^{dc}_{1..N_i}, \tau_{S_s}) \tag{3.4.1b}$$

$$x = (v_{1..N_n}, \delta_{1...N_n}, p_{i..N_n}, q_{i..N_n}, v^{dc}_{1..N_d}, p^{dc}_{1..N_i}, p_{loss}) \tag{3.4.1c}$$

The goal of the optimization problem is to minimize the cost function dispatching the reactive powers and controlling the FACT devices, which correspond

[30] In this work the real power generation is fixed by C-MPCs, while the CS fixes the DC voltages.

to the input optimization variables reported in (3.4.1b). The dependent optimization variables, represented in (3.4.1c), are the nodal voltage amplitudes and phases, the net nodal powers, the DC power flows realized by the DC voltage references and the total power losses.

In the following page the full optimization problem, based on the model presented in Chapter 2.3, is formalized. For the sake of convenience, the constraints have been divided in four groups: the first two correspond to the power flow equations and to the prescription of slack voltages by primary substations; the third group of constraints corresponds to the voltage regulatory limits and to the maximum currents flowing through the transmission lines; the last group accounts the control variables' capabilities.

In this regard, is worth stressing that - owing to the assumption of square operative regions for both microgrids and AC/DC interfaces - reactive powers are bounded by constant capabilities, regardless of active powers. As discussed in [6], despite this assumption may imply a restricted operative region, it ensures the independence of the ORPF layer from C-MPCs and CS, which is indeed necessary to guarantee the feasibility of the optimal reactive power dispatches[31].

To attain the desired performances, the cost function needs to be carefully designed and the different control objectives to be properly balanced. Consider, for example, the goal of minimizing power losses. Such control objective could be undoubtedly achieved increasing the nodal voltages, which would reduce the currents flowing through the branches and consequently the Joule losses along transmission lines. The mentioned strategy conflicts with another control objective, i.e. the upkeep of nodal voltages as close as possible to the feeder's nominal voltage, in order to ensure a robust fulfillment of the voltage regulatory limits with respect to unexpected load variations.

The implemented cost function is composed by five quadratic terms, weighted by the coefficients $\kappa_{1..5}$, and is therefore lower-bounded. In addition to the aforementioned penalization of both squared power losses and squared voltage deviations from the nominal value, the control variables are slightly penalized to avoid unmotivated requirements of ancillary services.

3.4.1 Brief summary

In this part of the chapter an Optimal Reactive Power Flow control layer has been introduced to reduce both the power losses of the system and the nodal voltage deviations, ensuring their compliance with the regulatory limits. These objectives are fulfilled exploiting the microgrids' ancillary services, the reactive power generation capabilities of the MVDC interfaces and the OLTC devices.

[31] Consider a generic element, supplying both active and reactive power, characterized by larger operative region such as a bound on the apparent power. In this case, it holds that:

$$\sqrt{P^2 + Q^2} \leq S_{max} \iff -\sqrt{S_{max}^2 - P^2} \leq Q \leq \sqrt{S_{max}^2 - P^2}$$

Reactive power is therefore bounded by a function of the active power: in the successive time instants, an adjustment of P - dispatched by other control layers - might compromise the feasibility of the reactive power committed by the ORPF.

$$\min_{u} \quad \kappa_1\, p_{loss}^2 + \kappa_2 \sum_{j=1}^{N_n} \left(v_j - v_j^{nom}\right)^2 + \kappa_3 \sum_{j \in S_s} \left(\tau_j - \bar{\tau}_j\right)^2 +$$
$$+ \kappa_4 \sum_{j=1}^{N_m} \left(\Delta q_j^G\right)^2 + \kappa_5 \sum_{j=1}^{N_i} \left(q_j^{dc}\right)^2$$

$$s.t. \quad p_j = \sum_{h \in S_m(j)} \left(\bar{p}_h^{mg} + \Delta p_h^G + \Delta p_h^B\right) - \left(\hat{\tilde{p}}_j^L + \Delta \tilde{p}_j^L\right) + \sum_{h \in S_{ac}(j)} p_h^{dc} \qquad \forall j \notin S_s$$

$$q_j = \sum_{h \in S_m(j)} \left(\bar{q}_h^{mg} + \Delta q_h^G\right) - \tilde{q}_j^L + \sum_{h \in S_{ac}(j)} q_h^{dc} \qquad \forall j \notin S_s$$

$$p_j = v_j \sum_{k \in S_{io}(j)} v_k \left(G_{jk} \cos\left(\delta_j - \delta_k\right) + B_{jk} \sin\left(\delta_j - \delta_k\right)\right) + G_{jj} v_j^2 \qquad \forall j \in [1, N_n]$$

$$q_j = v_j \sum_{k \in S_{io}(j)} v_k \left(G_{jk} \sin\left(\delta_j - \delta_k\right) - B_{jk} \cos\left(\delta_j - \delta_k\right)\right) - B_{jj} v_j^2 \qquad \forall j \in [1, N_n]$$

$$- \sum_{h \in S_{dc}(j)} p_h^{dc} = v_j^{dc} \sum_{k \in S_{io}^{dc}(j)} \frac{v_j^{dc} - v_k^{dc}}{r_{jk}^{dc}} \qquad \forall j \in [1, N_d]$$

$$v_i^{dc} = \mathring{v}_i^{dc} \qquad \forall i : S_{dc}(i) \neq \emptyset$$

$$p_{loss} = \sum_{j=1}^{N_n} p_j$$

$$\delta_j = 0 \qquad \forall j \in S_s$$

$$v_j = \tau_j\, v_j^{nom} \qquad \forall j \in S_s$$

$$v_j^{min} \leq v_j \leq v_j^{max} \qquad \forall j \in [1, N_n]$$

$$-\delta_j^{max} \leq \delta_j \leq \delta_j^{max} \qquad \forall j \in [1, N_n]$$

$$\left(v_j \cos\delta_j - v_k \cos\delta_k\right)^2 y_{jk}^2 + \left(v_j \sin\delta_j - v_k \sin\delta_k\right)^2 y_{jk}^2 \leq \left(c_{jk}^{max}\right)^2 \qquad \forall (i,k) \in S_b$$

$$q_j^{mg,min} \leq \bar{q}_j^{mg} + \Delta q_j^G \leq q_j^{mg,max} \qquad \forall j \in [1, N_m]$$

$$q_j^{dc,min} \leq q_j^{dc} \leq q_j^{dc,max} \qquad \forall j \in [1, N_i]$$

$$\tau^{min} \leq \tau_j \leq \tau^{max} \qquad \forall j \in S_s$$

Chapter 4

Simulation results

In this chapter the multi-layer control system previously introduced is tested on a simulated benchmark grid, whose topology and parameters have been retrieved from IEEE Test Feeders[26].

Both the control system and the simulated grid have been implemented in MATLAB R2018a[32] exploiting Yalmip[33][27], an open source toolbox which allows a symbolic formulation of optimization problems. Hence, the QP/BQP optimization problems have been solved with IBM ILOG CPLEX 12.8.0[34], while non-convex ones have been solved with MATLAB's *fmincon* function. In addition, the Symbolic Toolbox[35] has been used to implement the second stage of the multi-stage Cluster Supervisor.

This chapter is organized as follows. First and foremost, the benchmark grid's topology and parameters are introduced. After a brief overview on the adopted power profiles and the mechanism for day-ahead schedules' generation, it is shown that the uncontrolled system behaves inadequately. Eventually, the control system is implemented and its effectiveness is demonstrated, as well as the fulfillment of both operative and regulatory limits.

4.1 Benchmark grid

In order to test the designed Control System on a realistic grid, the IEEE 13-bus and IEEE 37-bus test feeders from [26] have been adopted to derive the benchmark grid's topology and parameters. The two mentioned feeders are supposed to be remote and unconnected by AC transmission lines, hence there are two distinct slack buses by which the two corresponding isolated areas[36] are connected to the transmission stage. Notice that, despite the different nominal line-to-line voltage of the two areas ($v_{50}^{nom} = 4.8kV$ and $v_{7}^{nom} = 4.16kV$), for the sake of simplicity a unique base voltage v_{base}, coinciding with v_{50}^{nom}, has been defined.

[32] `https://it.mathworks.com`
[33] `https://yalmip.github.io`
[34] `https://www.ibm.com/analytics/cplex-optimizer`
[35] `https://it.mathworks.com/products/symbolic.html`
[36] Note that Area 1 correspond to the IEEE 37-bus feeder, while Area 2 to the IEEE 13-bus.

$$v_{base} = 4.8\ kV$$

It is worth reminding the reader that, in view of the assumptions introduced in Chapter 2.3, the benchmark grid shall a balanced three-phase feeder. Some adjustments were thus required to perform the per-unit normalization introduced in Appendix A:

- The single-phase, two-phase and unbalanced three-phase links have been substituted by balanced three-phase links.
- Transformers have been neglected and replaced by simple impedances, while circuit breakers have been short-circuited.

The three-phase base power is conveniently selected to be $1MVA$, thus the base current and impedance are uniquely defined.

Table 4.1: AC base quantities

v_{base}	s_{base}	c_{base}	z_{base}
4.8 kV	1 MVA	120.3 A	23 Ω

Eight microgrids have been distributed - almost uniformly - across the benchmark grid, while load positions are the ones specified in [26]. For simplicity, microgrids' internal loads are supposed to be aggregated to grid's loads.

Further adjustments of the IEEE 37-bus feeder were required to highlight three main geographical regions, providing a guideline for the cluster selection. To this regard, let us remind the reader that geographical-based grid partitioning principle entails a local uncertainty compensation and all the consequent advantages previously discussed. It is also reminded that each cluster must include at least one microgrid and exactly one MVDC interface. In light of these considerations the length of branches $(15, 26)$ and $(22, 36)$ have been increased, leading to the cluster selection represented in figure 4.1.

A simple radial MVDC transmission connecting the four clusters' interfaces has been eventually introduced. This configuration was in fact selected to allow the exchange of power between any pair of interfaces and to enhance the robustness of the DC transmission system. Line parameters such as lines' resistance and maximum current have been selected from data-sheets[37], assuming a unipolar circuit with a DC nominal voltage of $12kV$[38]. For the sake of simplicity the interfaces are supposed to be ideal[39] and with a square operative region[40].

[37] `http://www.nexans.co.uk/UK/files/Underground%20Power%20Cables%20Catalogue%2003-2010.pdf`

[38] Actually, MVDC are typically bipolar, in order to achieve higher voltages with lower XLPE's voltage classes, see [1]. From an implementation point of view, there is no difference between the two configurations.

[39] Interfaces non-ideality could be restored introducing additional series resistances between each interface and the connected DC node. This would indeed involve an additional joule loss proportional to the power flowing through the interfaces themselves.

[40] Reasonable power limits have been deduced from [1] and [4].

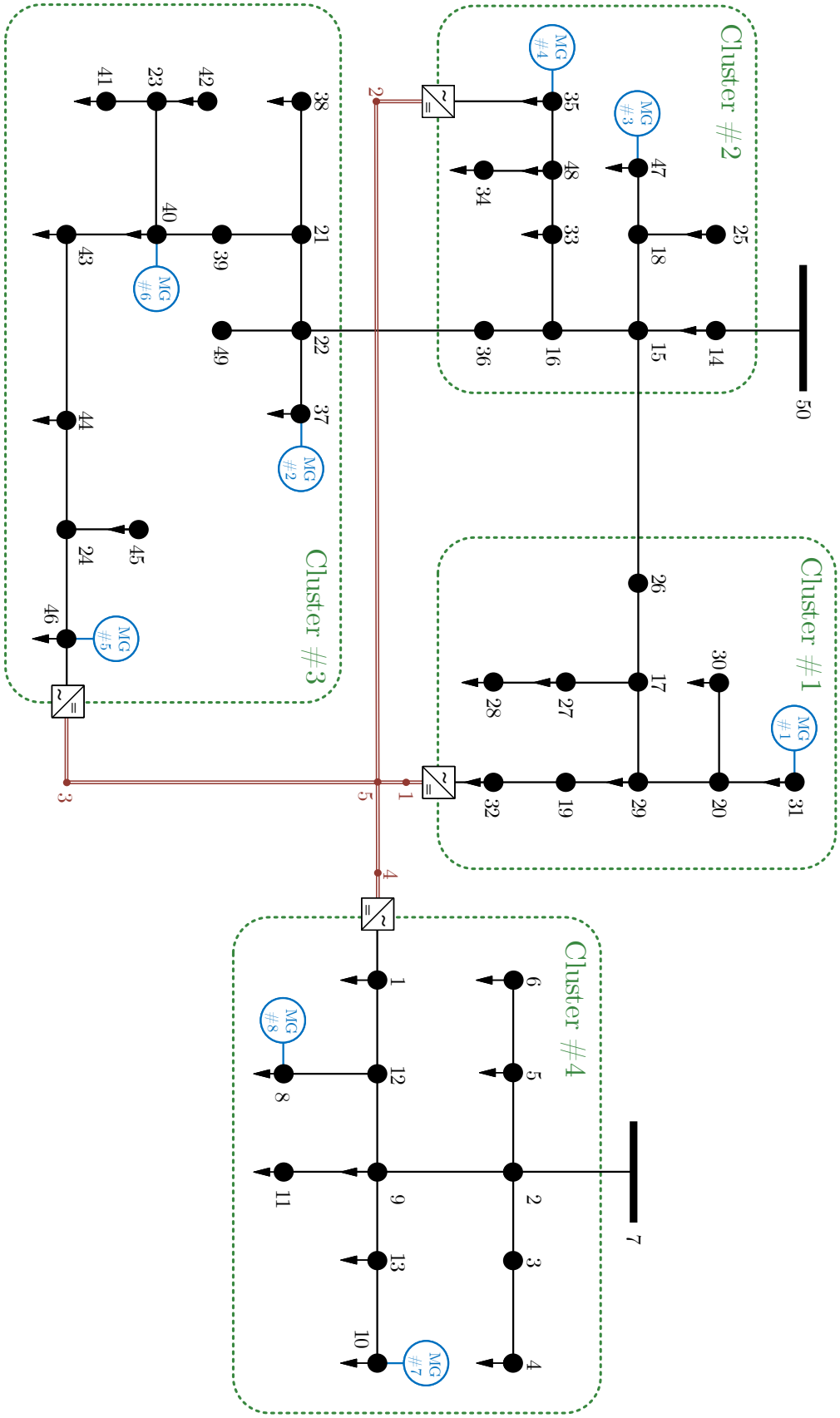

Figure 4.1: Benchmark grid topology and selected clusters.

Notice that, as mentioned earlier in this work, the DC base power shall be selected exactly equal to the three-phase power, i.e. 1 MW. This in fact allows to avoid cumbersome base conversions in the formulated models. The consequent DC base quantities are reported in table 4.2.

Table 4.2: DC base quantities

v_{base}^{dc}	p_{base}^{dc}	c_{base}^{dc}	r_{base}^{dc}
12 kV	1 MW	83.3 A	144 Ω

In Appendix B the parameters of the benchmark grid have been reported.

4.2 Power profiles

As the benchmark grid's topology and parameters are well defined, it is required - for both simulation and control purposes - to retrieve actual and expected (realistic) power profiles for both loads and non-dispatchable microgrids' generators. Furthermore, day-ahead schedules are required for the construction of all the control-oriented system models previously presented.

Actually, retrieving such a large number of consistent power profiles for each load of the grid has proven to be very hard, as only few profiles for some primary substations are freely available on the Internet. Nevertheless, thanks to the fruitful collaboration with RSE S.p.a., a set of power profiles sampled with a 15-minutes resolution from a real distribution grid[41] have been used.

Despite the availability of an adequate set of power profiles, the associated day-ahead and intra-day forecasts need to be somehow extracted from data. As discussed in Chapter 2.1.4, one option could be to identify a SARIMA model for each load and PV from the dataset and to exploit those models to generate forecasts: this solution, however, not only is out of the scope of this work, but would also require a considerably larger dataset to capture power profiles' seasonality.

The much simpler solution adopted in this work makes use of MATLAB's Curve Fitting Toolbox[42] to determine the forecasts as *cubic splines* fittings of the actual power profiles: by tuning splines' roughness it is possible to generate forecasts with different accuracies. This technique is of course meaningful only for off-line simulations. In figures 4.2 and 4.3 some resulting forecasts are reported.

Notice that, since only active powers were provided, loads' reactive power profiles have been computed by randomly generating time-varying power factors, while their forecasts have been estimated as discussed above.

[41] Specifically, loads power profiles were sampled from some secondary substation of Milan's feeder, while PV power profiles have been extracted from a couple of PV plants, also located in Milan.

[42] `https://www.mathworks.com/products/curvefitting.html`

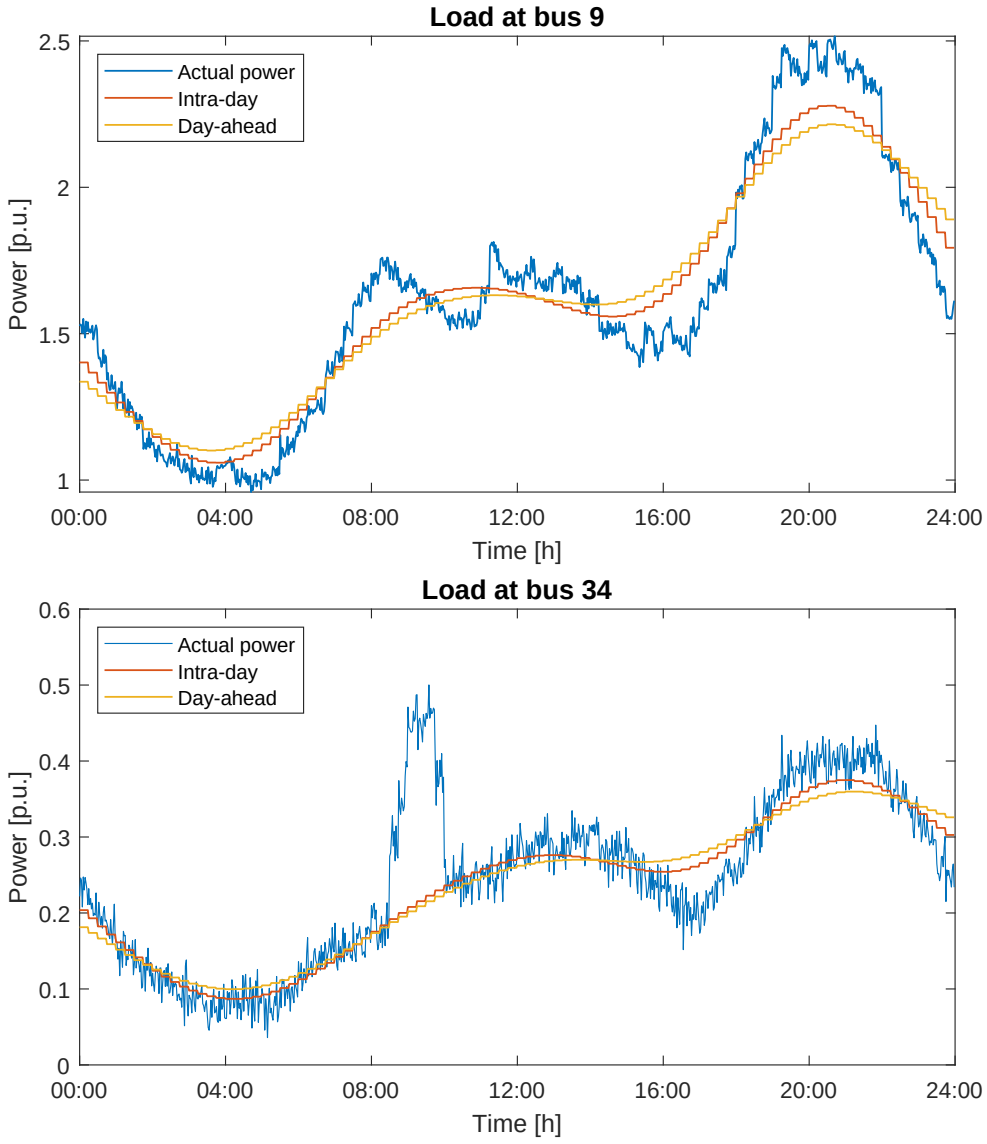

Figure 4.2: Forecasts of the loads connected to AC buses 9 and 34 respectively. Intra-day forecast are generally more precise than the day-ahead ones. Notice that poor loads' forecasts have been intentionally selected to test the control system performances.

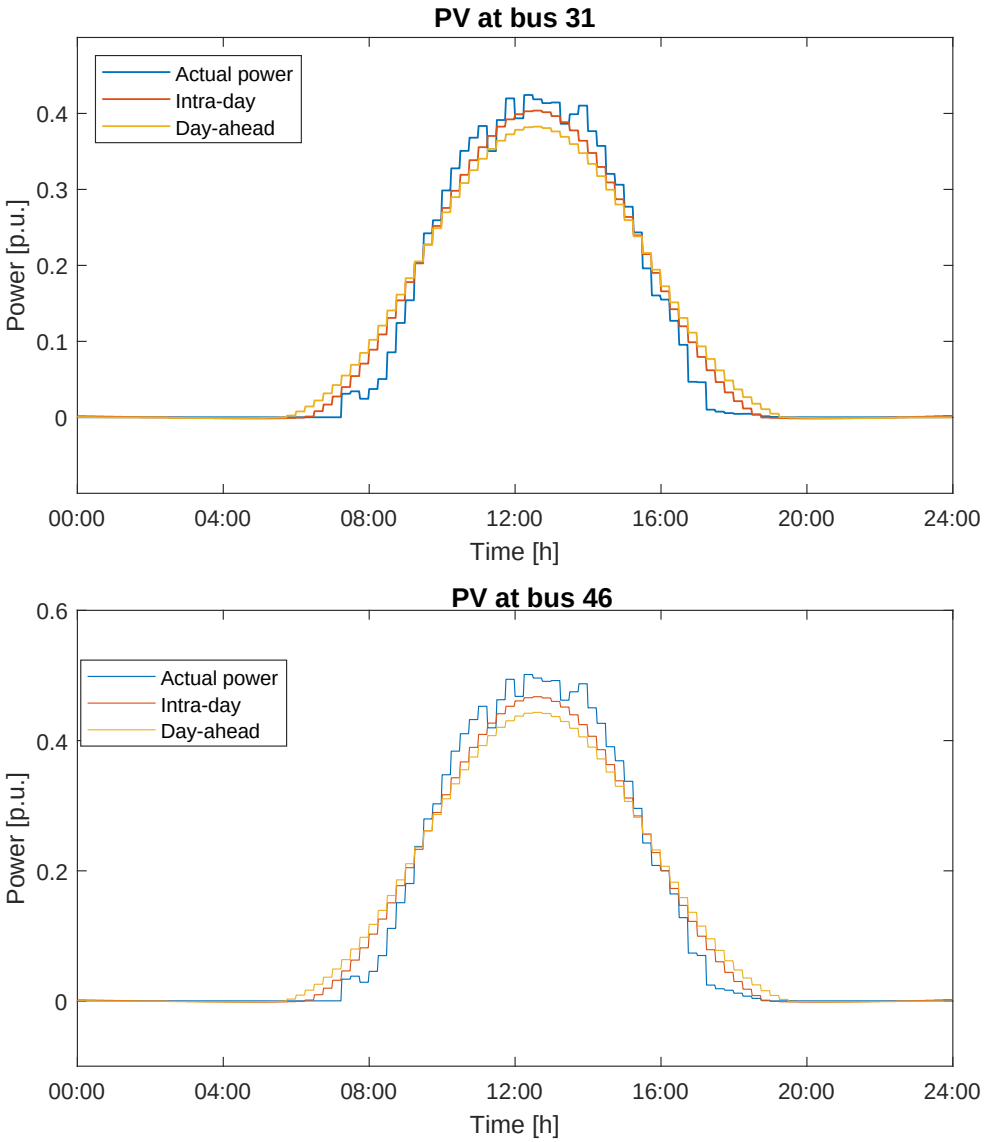

Figure 4.3: Forecasts of microgrids' aggregated PV connected to AC buses 31 and 41 respectively. Intra-day forecast are generally more precise than the day-ahead ones.

Similarly, the scheduled power profiles of microgrids' aggregated generators and batteries - which, as mentioned in Chapter 2.1, should be communicated by the microgrids' schedulers - have been retrieved adequately scaling the outputs of previous works on microgrids scheduling algorithms, [10]. An example of these power profiles is reported in figure 4.4.

As microgrids' and loads' active power profiles and forecasts are entirely available at this point, the day-ahead optimization exerted by the Grid Operator can be emulated running a traditional Optimal Power Flow problem [11] for each 15-minutes step, which we remind to be the profiles' resolution. This day-ahead optimization routine provides all the required scheduled quantities, some of which are depicted in figures 4.5 and 4.6:

- Power flows through the MVDC interfaces.
- Voltage amplitude and phase of each AC node.
- OLTCs positions.
- Clusters' net powers.
- Declared power profiles at primary substations.
- DC voltages and currents.
- Clusters' and microgrids' scheduled reserves.

The day-ahead schedules, the forecasts and the actual power profiles have thus been retrieved: it is now possible to simulate the system with and without the designed control architecture, hence assessing its performances.

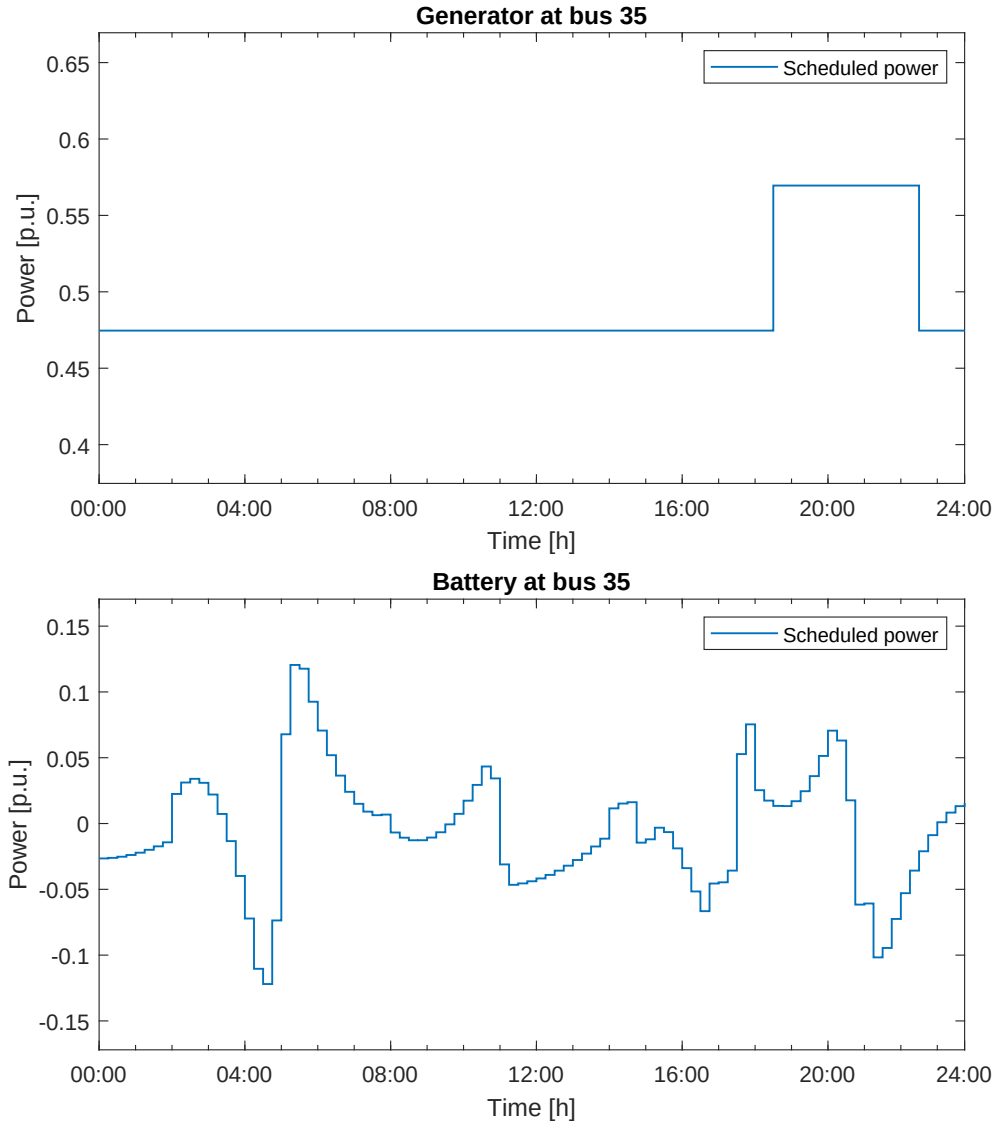

Figure 4.4: Scheduled active power supplied by the aggregated generator and battery of the microgrid connected to bus 35.

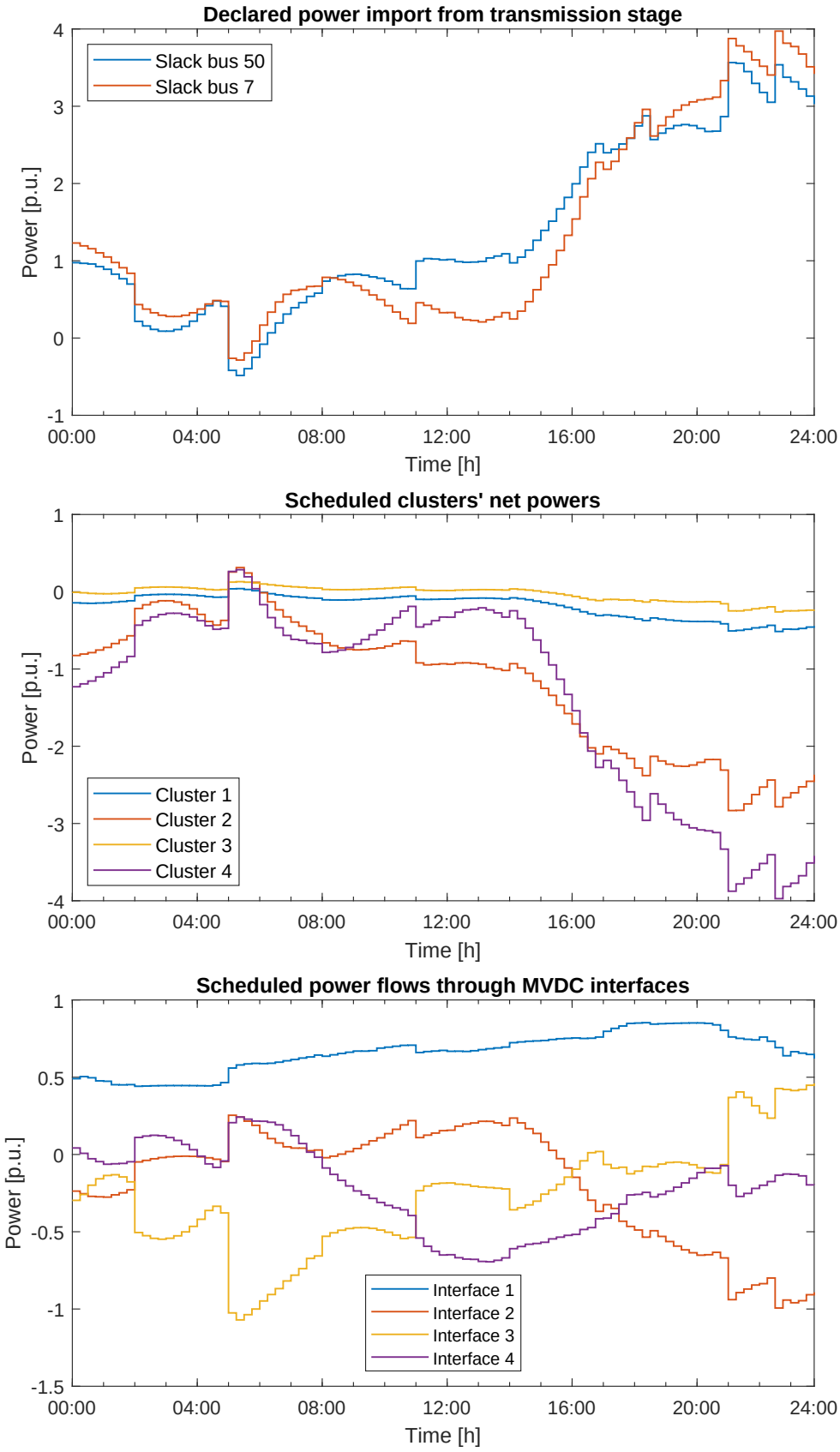

Figure 4.5: Power schedules retrieved from the day-ahead optimization routine.

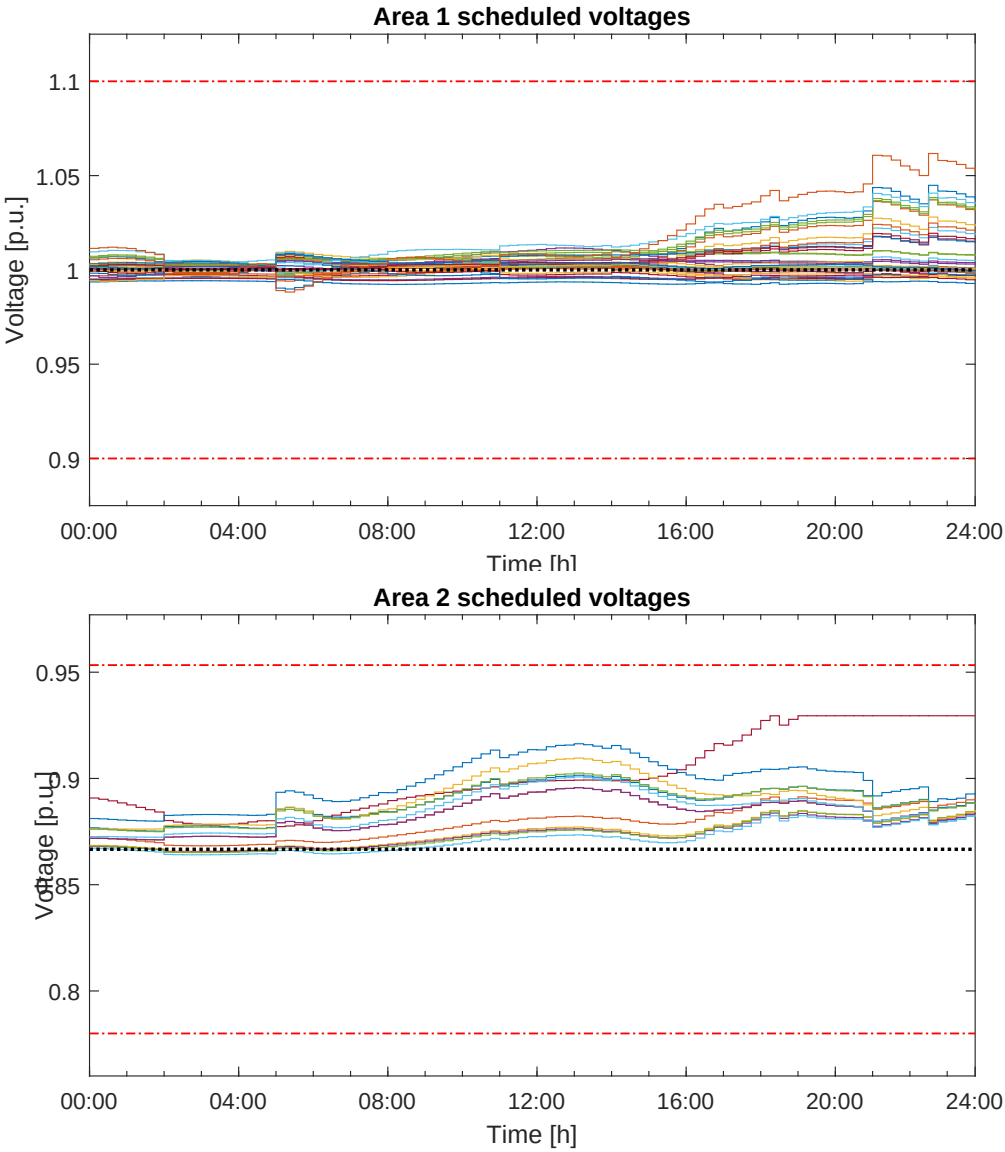

Figure 4.6: Scheduled nodal voltages. The dotted black lines represent the areas nominal voltage in per units, red dashed-dotted lines correspond to regulatory limits.

4.3 Uncontrolled system

Given the benchmark grid introduced in the previous part of the Chapter, the actual power profiles for loads and non-dispatchable generators and the day-ahead schedules, it is necessary to assess the behavior of the grid when no control system is implemented, ascertaining the requirements violation. It is indeed reminded that the nodal voltages shall meet the regulatory limits and that the active power absorbed from the transmission stage shall be *close enough* to the declared profile.

To simulate the response of the system, at each time step a so-called *Power Flow* problem needs to be defined and solved. Power Flow is a feasibility problem in which the state quantities (nodal voltages, nodal net powers, currents, power losses, etc.) associated to a given set of fixed independent quantities (power variation dispatches, OLTC positions and interfaces' voltage set-points) are sought. This can be done substituting the known independent quantities in the grids' power flow equations - corresponding to the first two groups of constraints introduced in the optimization problem reported in Chapter 3.4 - and solving them for the missing variables, which are those reported in (3.4.1c).

Specifically, in case of an uncontrolled system, owing to the absence of control action, the dispatched power variations are null and the interfaces' voltage references match the day-ahead schedules.

$$\begin{gathered} \Delta p^{G}_{1..N_m} = 0 \quad \Delta p^{B}_{1..N_m} = 0 \\ q^{dc}_{1..N_i} = \bar{q}^{dc}_{1..N_i} \quad \Delta q^{G}_{1..N_m} = 0 \\ \mathring{v}^{dc}_{1..N_i} = \bar{\mathring{v}}^{dc}_{1..N_i} \\ \tau_{j \in S_s} = \bar{\tau}_{j \in S_s} \end{gathered} \tag{4.3.1}$$

The simulated uncontrolled system turned out to violate both operative and regulatory constraints. From figure 4.7 it is indeed evident that there are time instants in which some nodal voltages violate such limits. The buses involved in this breach are confined in Cluster 3, that is the most geographically far from the primary substation: due to the absence of a Control System, loads' fluctuations are not locally compensated. Instead, the exceed of loads' demands is sustained importing more power from the transmission stage, which causes higher currents in the AC branches and consequently larger voltage drops. Similarly, due to the excess of power production, some buses of Cluster 4 violate the upper regulatory limit. Not surprisingly the deviation of grid power from the day-ahead declared profile is also significant, as shown in figure 4.8.

A control system, hence, is necessary to attain the desired performances, fulfill the mentioned constraints, and possibly reduce the power losses. The evaluation of control action's fitness will be based on five *Key Performances Indicators* (KPI): ε_{p1} and ε_{p2}, which are the RMS mismatches between the actual powers imported from primary substations and their nominal profiles; ε_{v1} and ε_{v2}, which are the RMS of voltage deviations from nominal values; ε_l, which is the RMS value of the power losses.

These can be easily computed as in 4.3.2, where N_t denotes the number of time-steps per day, i.e. 960, $S_a(i)$ is the set of AC buses in the i-th area and $|S_a(i)|$ its cardinality, i.e. the number of buses in that area.

$$\varepsilon_{p1} = \sqrt{\frac{1}{N_t} \sum_t \left(p_{50}(t) - \bar{p}_{50}(t)\right)^2} \tag{4.3.2a}$$

$$\varepsilon_{p2} = \sqrt{\frac{1}{N_t} \sum_t \left(p_7(t) - \bar{p}_7(t)\right)^2} \tag{4.3.2b}$$

$$\varepsilon_{v1} = \sqrt{\frac{1}{N_t \cdot |S_a(1)|} \sum_t \sum_{j \in S_a(1)} \left(v_j - v_j^{nom}\right)^2} \tag{4.3.2c}$$

$$\varepsilon_{v2} = \sqrt{\frac{1}{N_t \cdot |S_a(2)|} \sum_t \sum_{j \in S_a(2)} \left(v_j - v_j^{nom}\right)^2} \tag{4.3.2d}$$

$$\varepsilon_l = \sqrt{\sum_t \left(p_{loss}(t)\right)^2} \tag{4.3.2e}$$

Table 4.3: Uncontrolled system KPIs

ε_{p1}	ε_{p2}	ε_{v1}	ε_{v2}	ε_l
0.613 p.u.	0.533 p.u.	0.029 p.u.	0.034 p.u.	0.189 p.u.

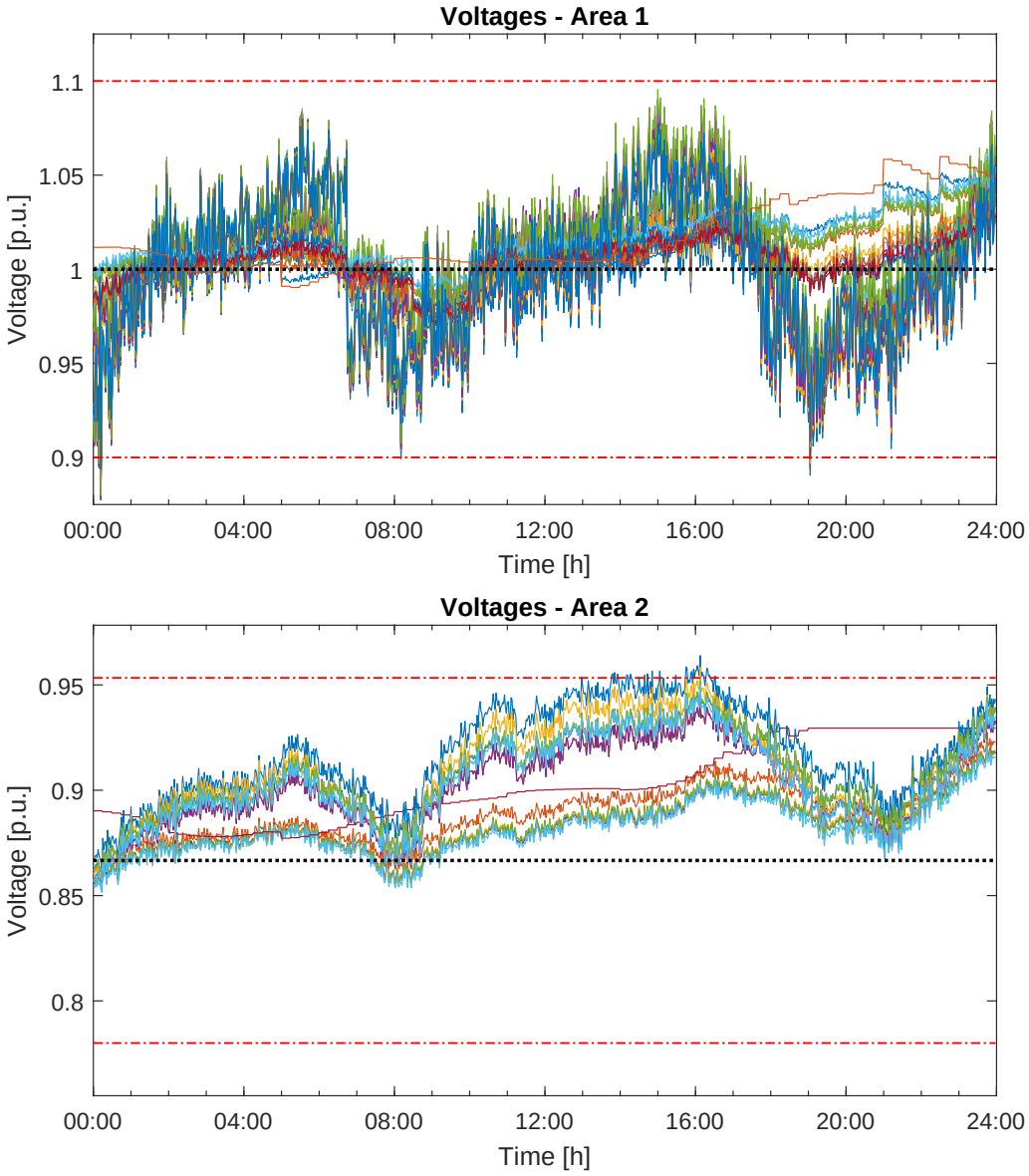

Figure 4.7: Nodal voltages of the uncontrolled system.

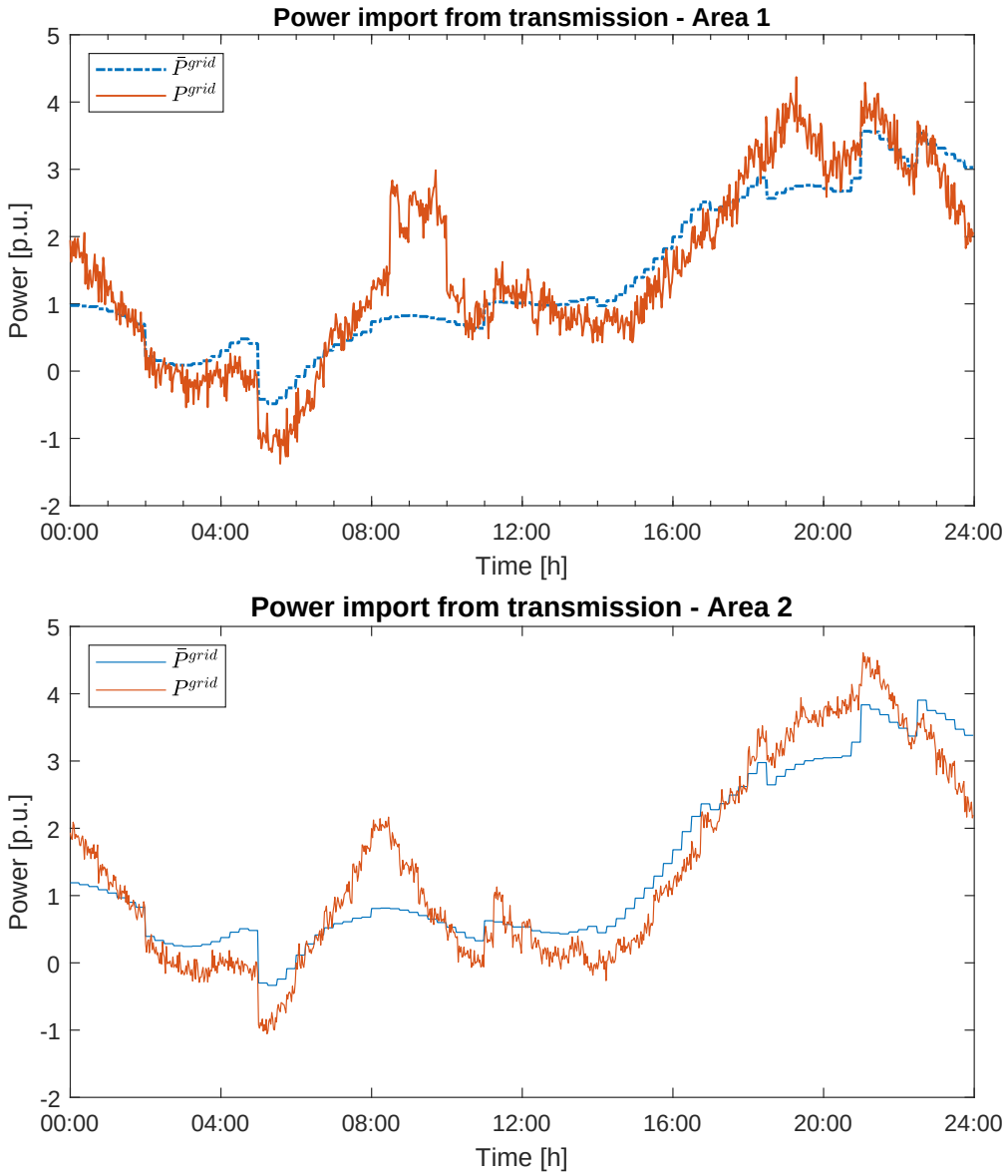

Figure 4.8: Comparison between the actual powers imported from transmission stage and the declared ones.

4.4 Controlled system

Ascertained the necessity of a controller, the multi-layer control architecture presented in Chapter 3 is now implemented and the closed-loop system is simulated.

Despite the single layers of the Control System and their interactions have been already widely discussed, a fundamental premise shall be made for a correct implementation. As the entire system has been realized in MATLAB, which is indeed a sequential programming language, the order in which signals are evaluated and exchanged is important for truthful simulation results. If, for example, the disturbance is measured by cluster controllers even before it is applied to the system itself, the resulting control action will be anticipative. These errors must be avoided, because they can lead to misleading conclusions.

The correct sequence of operations to be executed at each 90-seconds time-step is the following:

1. For each cluster the aggregated disturbance $\tilde{d}(t)$ is estimated from the data measured at the end of the previous time step.
2. Based on the estimated disturbance trajectory $\underline{\tilde{d}}(t)$, the vector of known exogenous quantities $\underline{h}(t)$, and the measured states $x(t)$, the C-MPC step is executed for all the clusters[43]. Optimal power variation dispatches for microgrids' generators and batteries are hence applied.
3. DC power requests and cluster reserves are issued to the Clusters Supervisor, which conciliates them and actuates the interfaces' DC voltage set-points.
4. Before executing the Power Flow to compute the grid's nodal voltages, DC power flows and power losses, the loads' and renewable resources' current disturbances[44] are applied.
5. Once every 15 minutes, at the end of the time-step, an ORPF problem is executed based on a snapshot of the grid, adjusting the OLTC positions and the reactive power generation for the successive 15 minutes.

Notice that the controllers' computational time is assumed to be negligible and disturbances are supposed constant across the time-step.

The control system, whose parameters have been reported in Appendix C, attains more than satisfactory results on the benchmark grid. Notice that for the sake of simplicity[45], in spite of (3.2.27), the chosen weight matrices are:

[43] Notice that, as each C-MPC problem is independent from the others, hence the execution order is irrelevant.

[44] Both active and reactive power disturbances are considered

[45] A more adequate choice would indeed be

$$R_g = R_b = R_\delta = I \cdot \frac{1}{N_m}$$

which respects (3.2.27). Nevertheless, given the small number of microgrids in each cluster, the solution doesn't change significantly. It should also be noted that, selecting equal diagonal elements, the power requests are equally split among microgrids, regardless of their size.

$$R_g = R_b = R_\delta = I$$

In the reminder of this chapter, the performances of each layer are discussed and the resulting KPIs are presented.

4.4.1 C-MPC performances

To assess the C-MPC control layer's performances, the behavior of a single cluster controller is herein analyzed. In particular, Cluster 2 is under scope, since the considerations formulated below are significantly visible, owing to the aggregated disturbance's magnitude.

The main characteristics expected from this control layer are:

- A strong rejection of the disturbance acting on cluster net power.
- A proper usage of the batteries, which should be exploited to cope with fast variations of the disturbance and then charged/discharged back to their scheduled SOC.
- Soft variations of the generators' dispatches.
- A DC power request only when all the cluster's generators and batteries are saturated.

From figures 4.9 and 4.10 it is evident how these specifications are fulfilled by the C-MPC. First and foremost, notice that, owing to the hard bound introduced in the C-MPC formulation, the cluster net power accurately tracks its scheduled profile. Indeed, the residual tracking error is mainly due to the unforeseeable disturbance acting on the cluster successively to the control action commitment.

Batteries are also exploited as expected: in the time windows 00:00-02:00 and 10:00-12:00, for example, they are used to compensate sudden disturbance variations, leaving to the generators power enough time to vary in a soft fashion. Around 10:00 the disturbance rapidly decreases but, rather than performing a quick reduction of the power committed to generators, using the temporarily exceeding power to recharge the batteries a slower contraction is preferred. This smoothness of the control action, enforced by the cost function, is fundamental to avoid fast and large variations of generators set-points. Towards the end of the day, batteries' scheduled SOCs are progressively restored, hence fulfilling the final state constraint.

It is furthermore worth noting that in the time interval ranging from 08:30 to 10:00 a large disturbance has been injected into the system[46] to test the C-MPC behavior in saturation conditions. Due to the disturbance magnitude, in fact, generators suddenly saturate: the only way to compensate the extra load, hence attaining problem feasibility, is by issuing a DC power request to the supervisor.

[46] As depicted in Figure 4.2, disturbance can be injected by introducing unexpected load peaks.

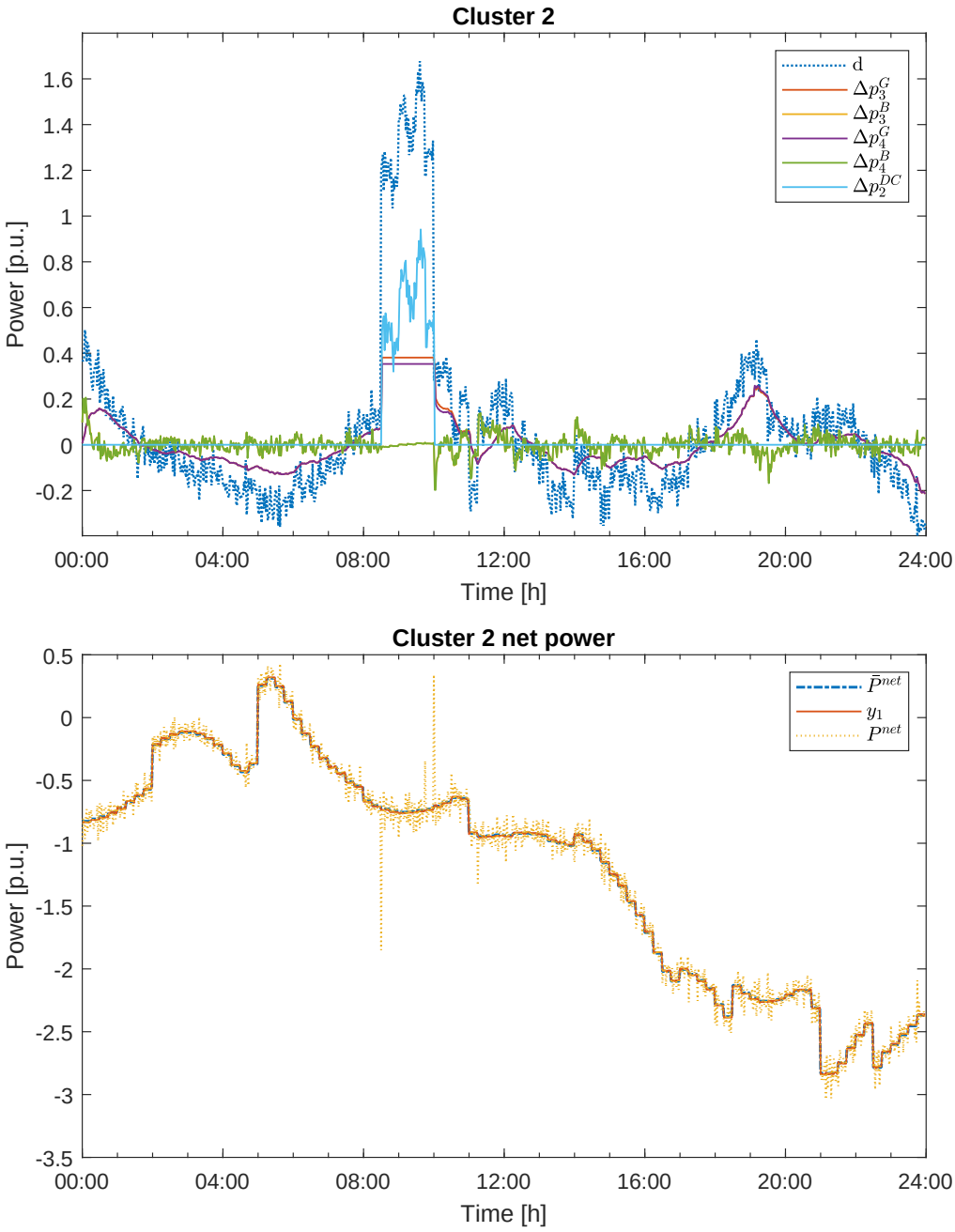

Figure 4.9: Insight of Cluster 2 aggregated disturbance and control variables. Actual versus scheduled net power. Notice that microgrids' batteries and generators power profiles are almost always coinciding, owing to the choice of R..

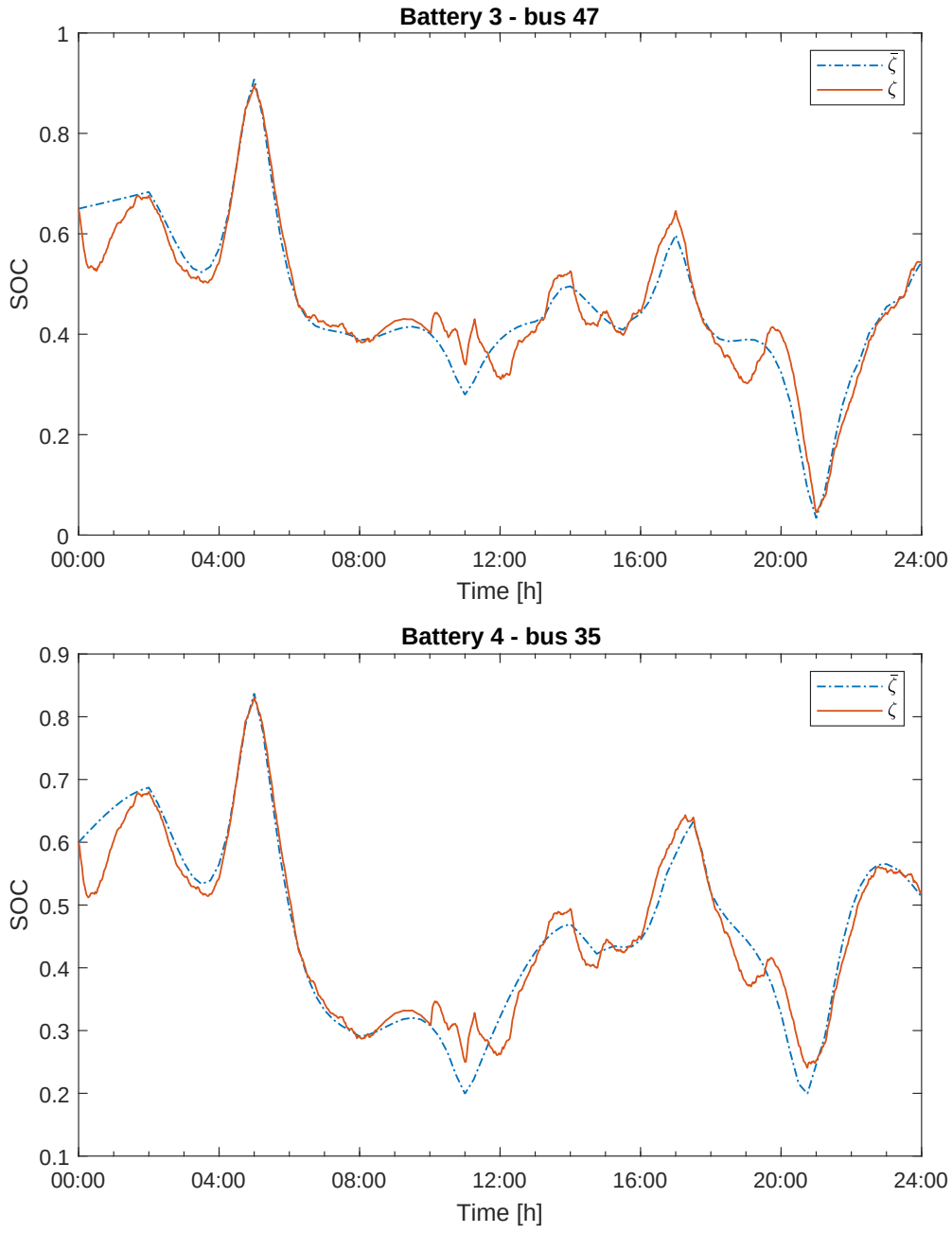

Figure 4.10: Insight of the State of Charge of Cluster 2's batteries. Notice that the final SOC matches the scheduled value, i.e. the final state is null in both cases.

4.4.2 Clusters Supervisor performances

The performances of Clusters Supervisor match the expectations as well. Consider, in fact, the DC power variations depicted in Figure 4.11, where both the issued requests - $u_{dc,(\cdot)}$, denoted by point markers - and the power variations actuated by the supervisor - denoted by continuous lines - are represented. One can easily notice not only that all requests have been satisfied, but power variations have also been amended, i.e. the extra power provided to one cluster is supplied by the others according to their capabilities.

As mentioned, since at the beginning of the day Cluster 2 is overloaded, its C-MPC requires a large amount of power, which is in turn allocated to other clusters by the supervisor. Cluster 1, analogously, faces unexpected load fluctuations towards the end of the day and is hence forced to issue DC power requests to the supervisor. It is worth reminding the reader, however, that not only the supervisor must fulfill clusters' requests, but it should also keep their upwards and downwards reserves greater than a fixed fraction, namely φ, of their nominal values. The supervisor is in fact designed to sustain clusters' reserves by committing DC power variations in such a way to fulfill the aforementioned bounds, see Chapter 3.3.

In figures 4.12-4.15 the amended reserves (red continuous lines) are compared to the C-MPC declared reserves (green dotted lines), to the day-ahead nominal reserves (blue dashed-dotted lines) and to the margins (black dashed lines).

Let us reference, in particular, to figure 4.13, reminding the reader that in the time window 08:30-10:00 Cluster 2 requests DC power to cope with the disturbance. The effect of DC power requests is first and foremost to decrease the actual upwards reserve to negative values. The supervisor satisfies this inquiry drawing power from Clusters 3 and 4, restoring $R_{(2)}^{C\uparrow}$ to its minimum value, i.e. $\varphi R_{(2)}^{C\uparrow}$. Once the extra power is no more required, the power variations are brought back to zero in a smooth fashion, hence avoiding clusters' destabilization.

Similarly, as depicted in figure 4.12, towards the end of the day, the downwards reserve of Cluster 1 is maintained within the desired bound by the supervisor.

The last comment regards the assumption of negligible DC power losses variations, introduced in the formulation of the Multi-Stage Supervisor, see (3.3.14). In figure 4.16 the order of magnitude of $\Delta p^{dc,loss}$ is assessed to be at most $10^{-2} p.u.$, which is by far negligible with respect to the power flowing through the DC transmission, in the order of $1 p.u.$. The assumption is hence confirmed and DC power losses can be safely considered constants.

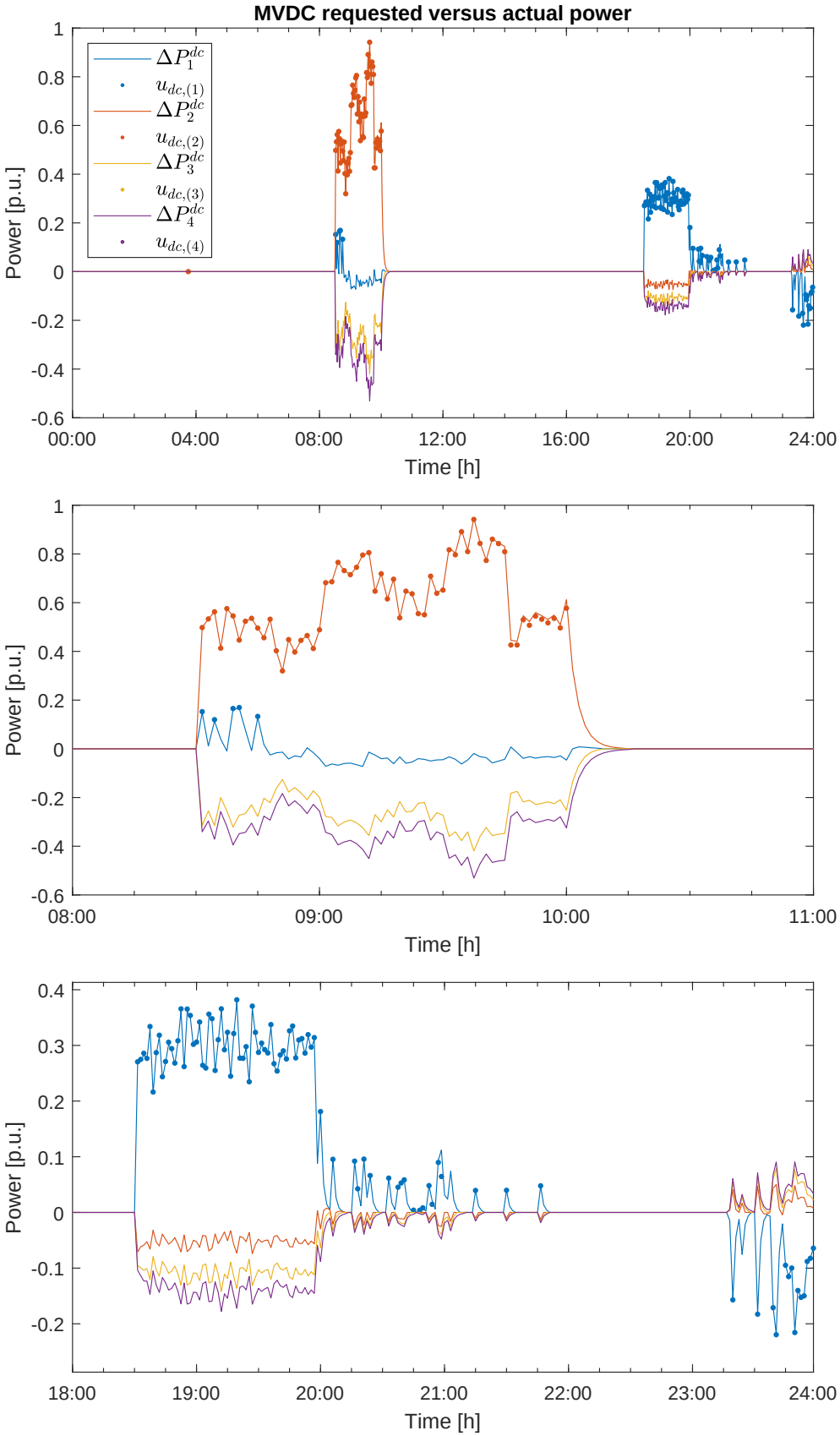

Figure 4.11: Actual DC power variations, represented by continuous lines, versus required variations, marked with points. Power variations actuated by the supervisor are always greater than the requests.

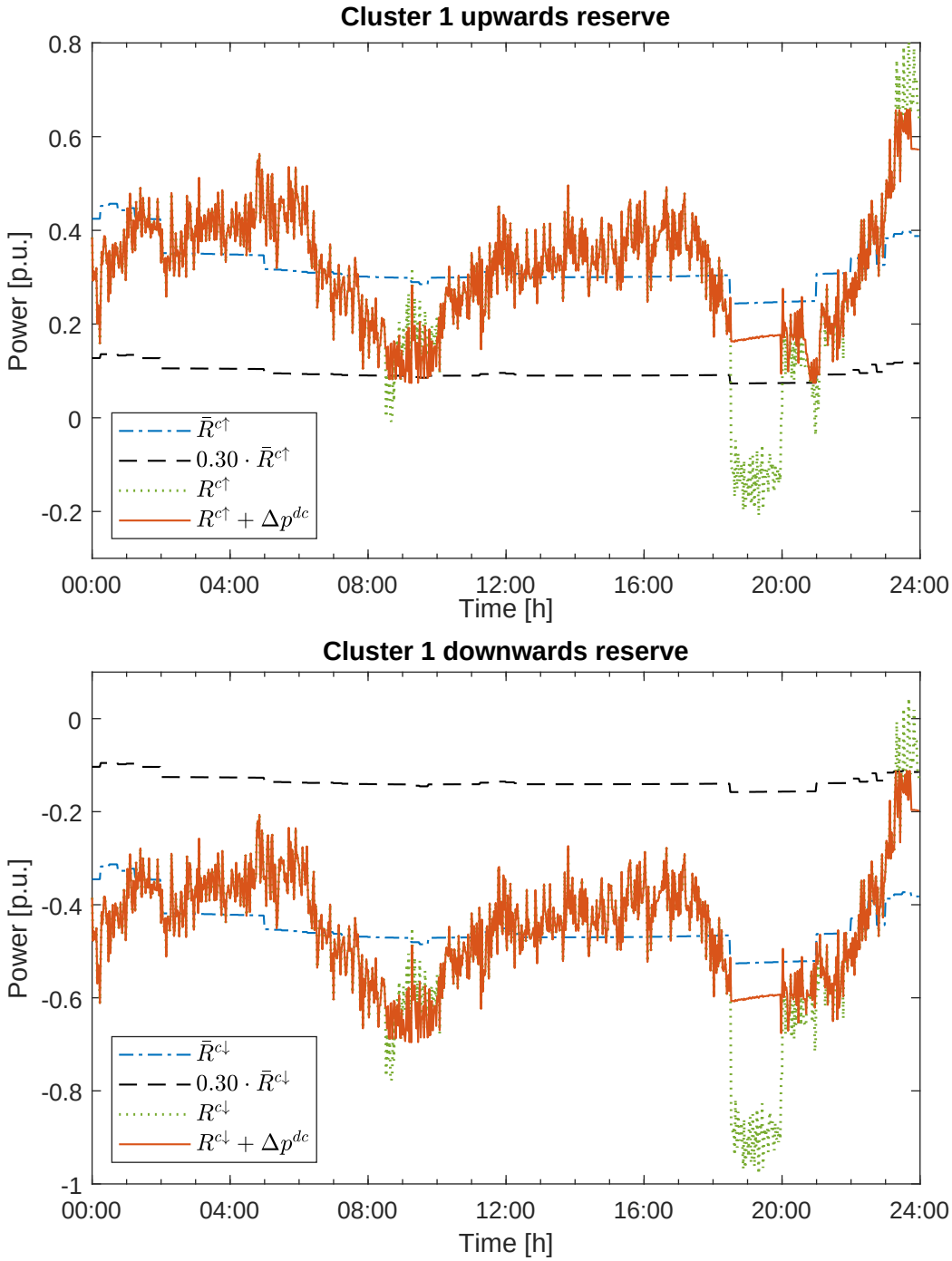

Figure 4.12: Cluster 1 reserves before (dotted line) and after (continuous line) amendment by the supervisor. The dashed line correspond to the lower (upper, resp.) margin.

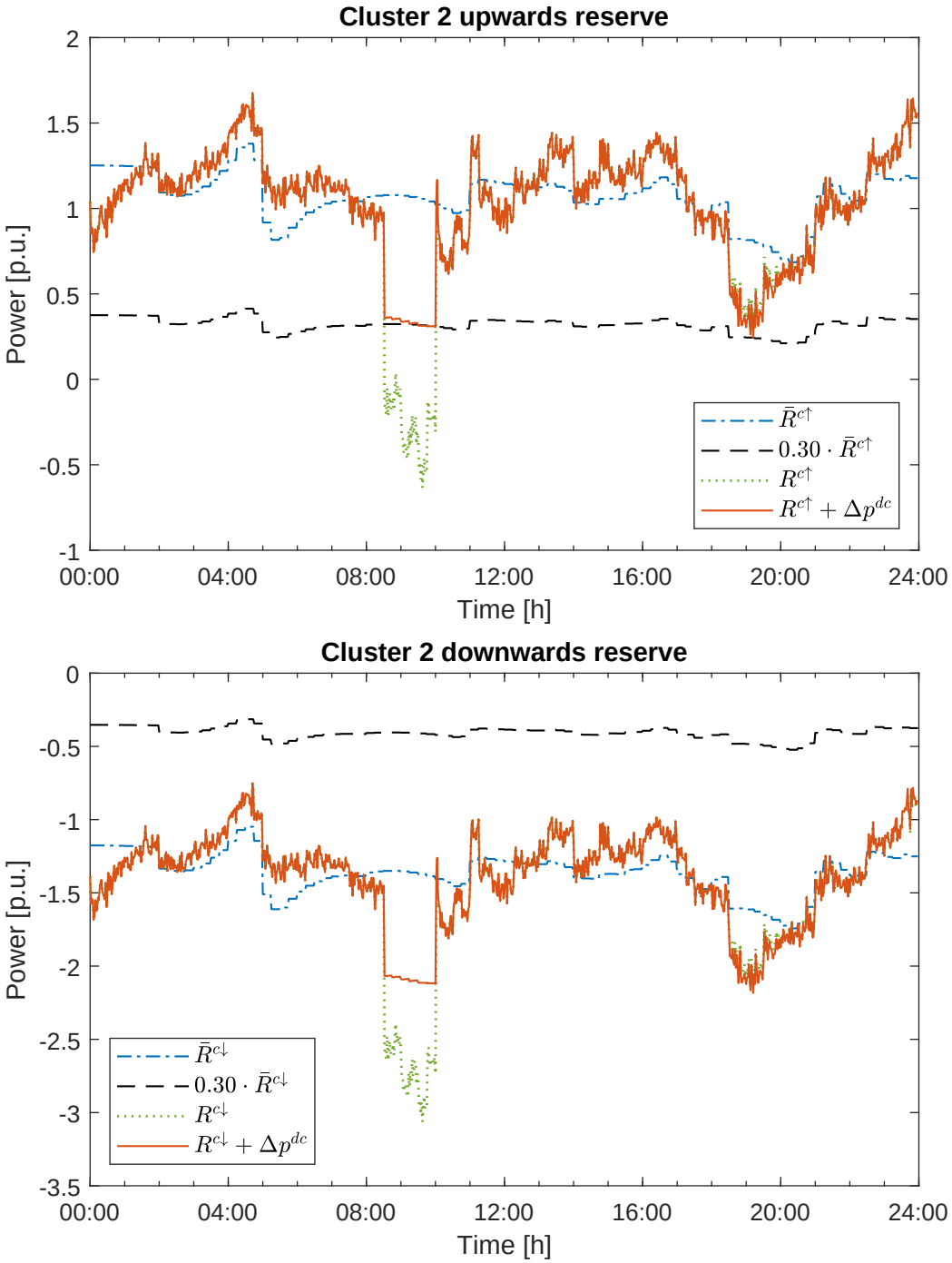

Figure 4.13: Cluster 2 reserves before (dotted line) and after (continuous line) amendment by the supervisor. The dashed line correspond to the lower (upper, resp.) margin.

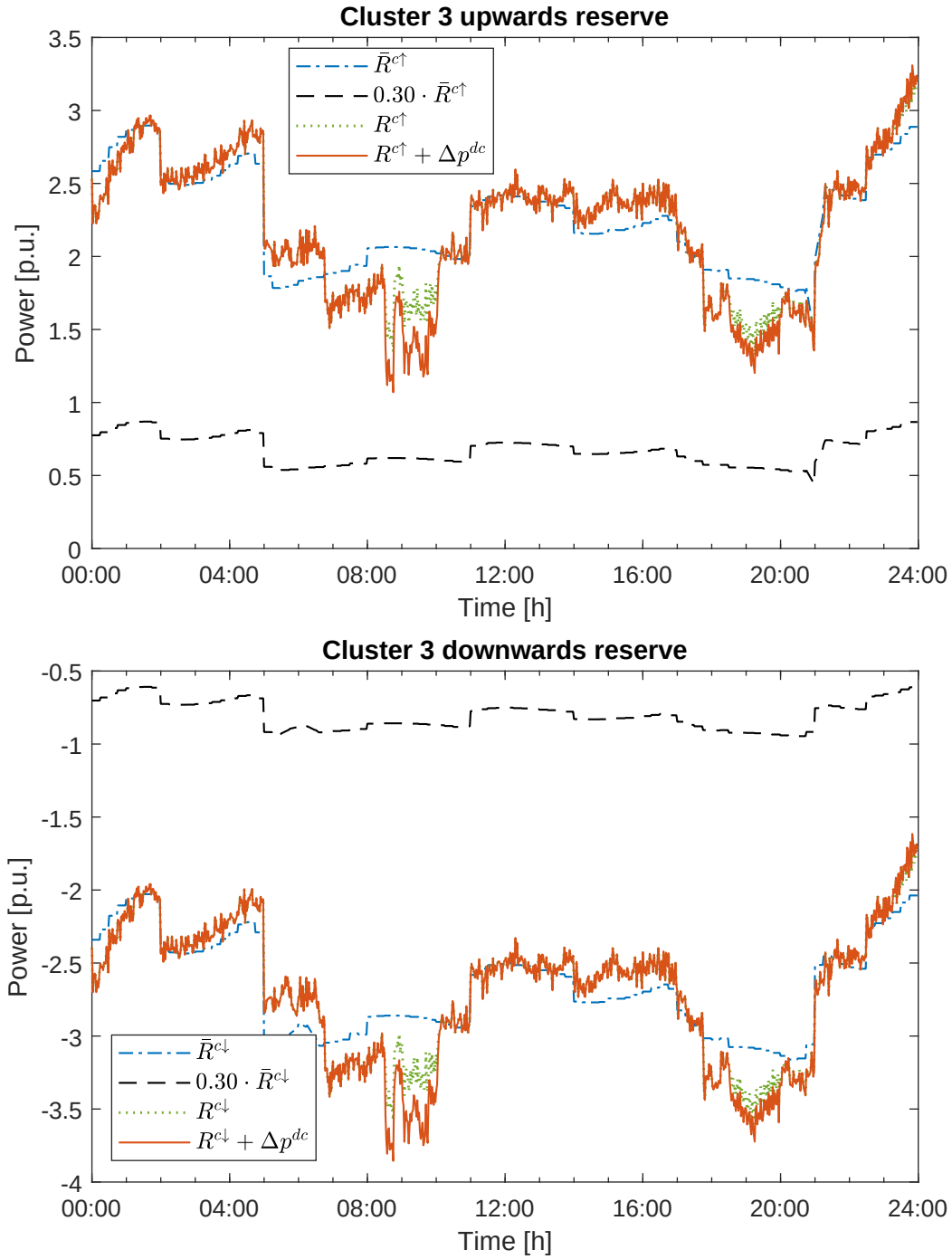

Figure 4.14: Cluster 3 reserves before (dotted line) and after (continuous line) amendment by the supervisor. The dashed line correspond to the lower (upper, resp.) margin.

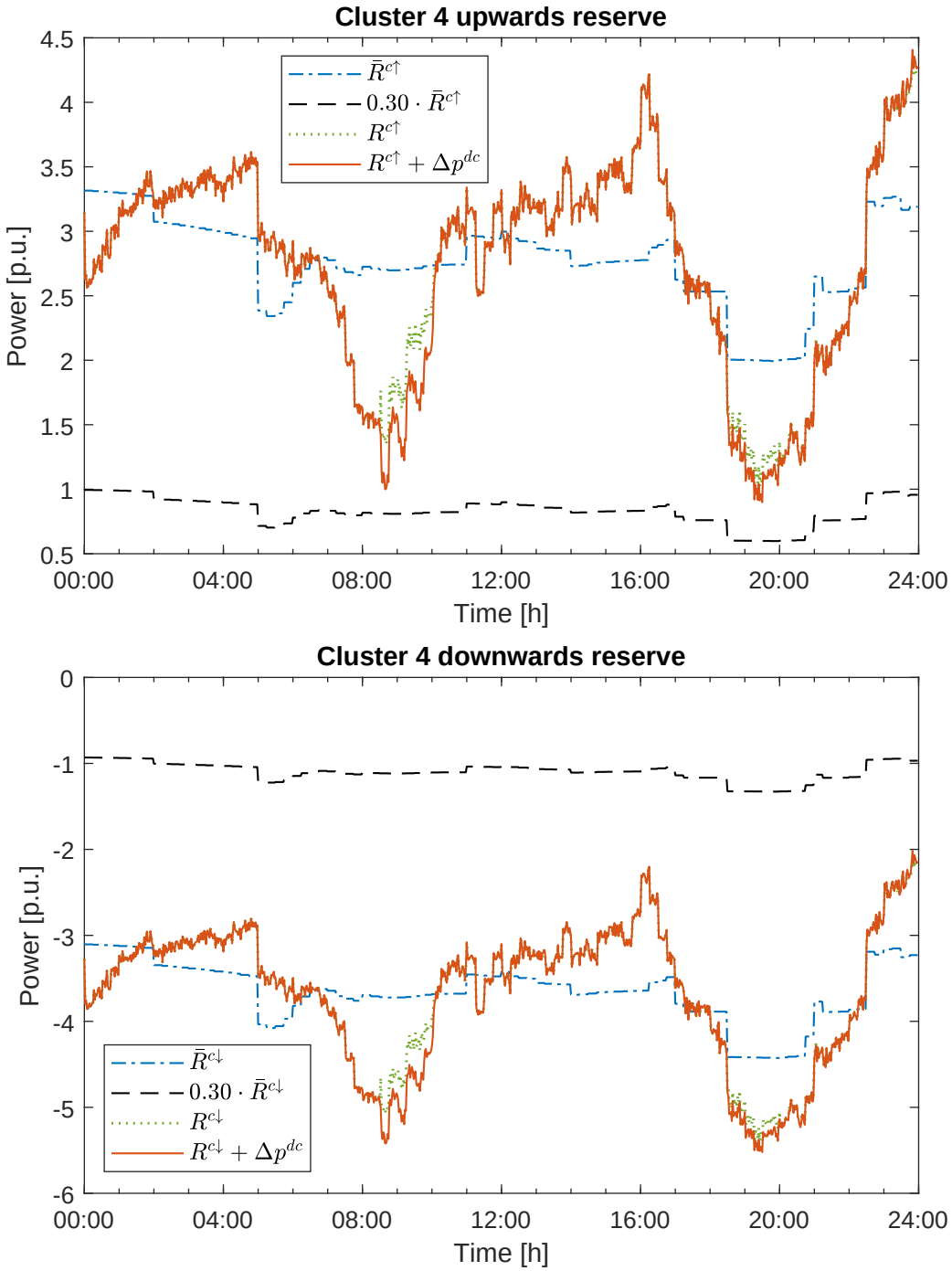

Figure 4.15: Cluster 4 reserves before (dotted line) and after (continuous line) amendment by the supervisor. The dashed line correspond to the lower (upper, resp.) margin.

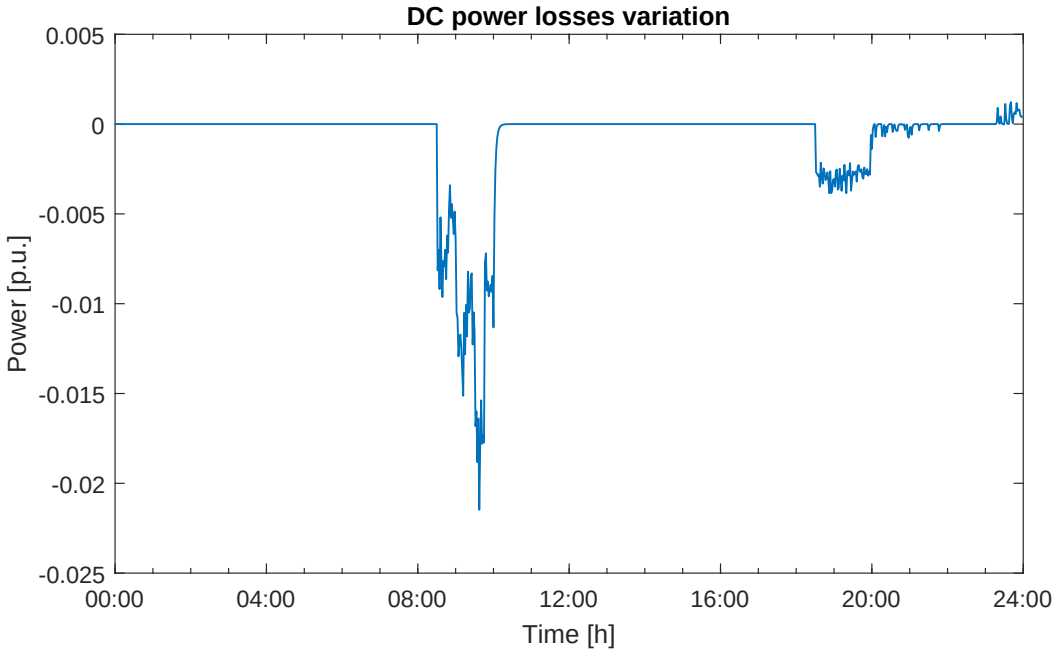

Figure 4.16: DC power losses variations.

4.4.3 ORPF performances

In figure 4.17 the nodal voltages of the controlled system are reported. It should be noted that the local compensation of disturbances, performed by cluster controllers, allows to drastically attenuate voltage deviations. This is, indeed, one of the main reasons for which the clusters were introduced.

Voltages are also adjusted by the execution of a periodic ORPF, which regulates the OLTCs' positions and the reactive power dispatches' so as to compress the voltages' towards their nominal voltage. This confinement has a twofold advantage: it enhance the robustness of voltage regulation fulfillment and it reduces the current flowing through grid branches, which also entails the decrease of power losses. The reader is in fact reminded that the reduction of power losses is another control objective of ORPF.

Albeit this improvement is numerically quantified in the next part of the chapter, from the mentioned figure 4.17 one can straightforwardly notice not only that the voltage baselines are closer to the nominal value, indicated by the black dotted lines, but the spread is also dramatically reduced.

4.4.4 Control system performances

The implemented multi-layer control system, owing to the compensation capabilities of cluster controllers, ensures a good tracking of the declared power absorption from the primary substations. As depicted in figure 4.19, the actual power drawn from slack nodes mimics the scheduled profile, exception made for an high-frequency component of the noise, which is however ineradicable. Any unexpected increase of a load, in fact, is not compensated until the successive C-MPC time step. In the meanwhile, the missing extra power is supplied by the transmission stage, resulting in a spike of p^{grid}. It should be noted that the closeness of p^{grid} to $\bar{p}^{grid}$ is ultimately determined by the ρ parameter of cluster controller, see (3.2.21).

This improvement is indeed captured by the corresponding KPIs, namely ε_{p1} and ε_{p2}, which are reduced by a factor of 5 with respect to the uncontrolled system. As aforementioned, nodal voltages are also bounded to their nominal values, which leads to a significant reduction of ε_{v1} and ε_{v2}. Power losses are also marginally reduced, as they RMS is decreased by $0.03 p.u.$, corresponding to $30 kW$.

Table 4.4: Controlled system KPI

Case	ε_{p1}	ε_{p2}	ε_{v1}	ε_{v2}	ε_{l}
Controlled	0.148 p.u.	0.097 p.u.	0.013 p.u.	0.019 p.u.	0.16 p.u.
Uncontrolled	0.613 p.u.	0.533 p.u.	0.029 p.u.	0.034 p.u.	0.189 p.u.
Scheduled	-	-	0.009 p.u.	0.022 p.u.	0.16 p.u.

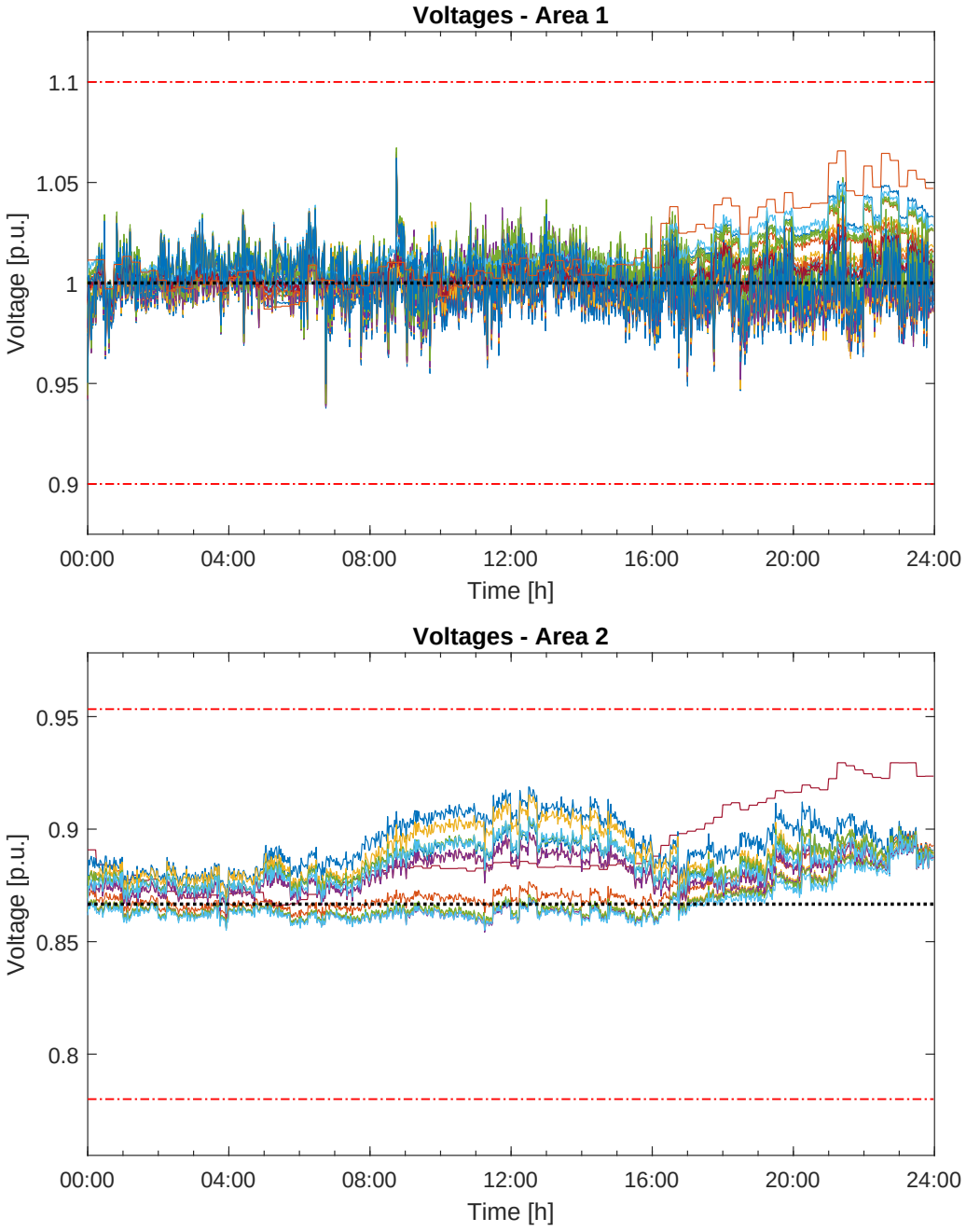

Figure 4.17: Nodal voltages are centered to the nominal voltage of the respective areas and lie within the regulatory limits.

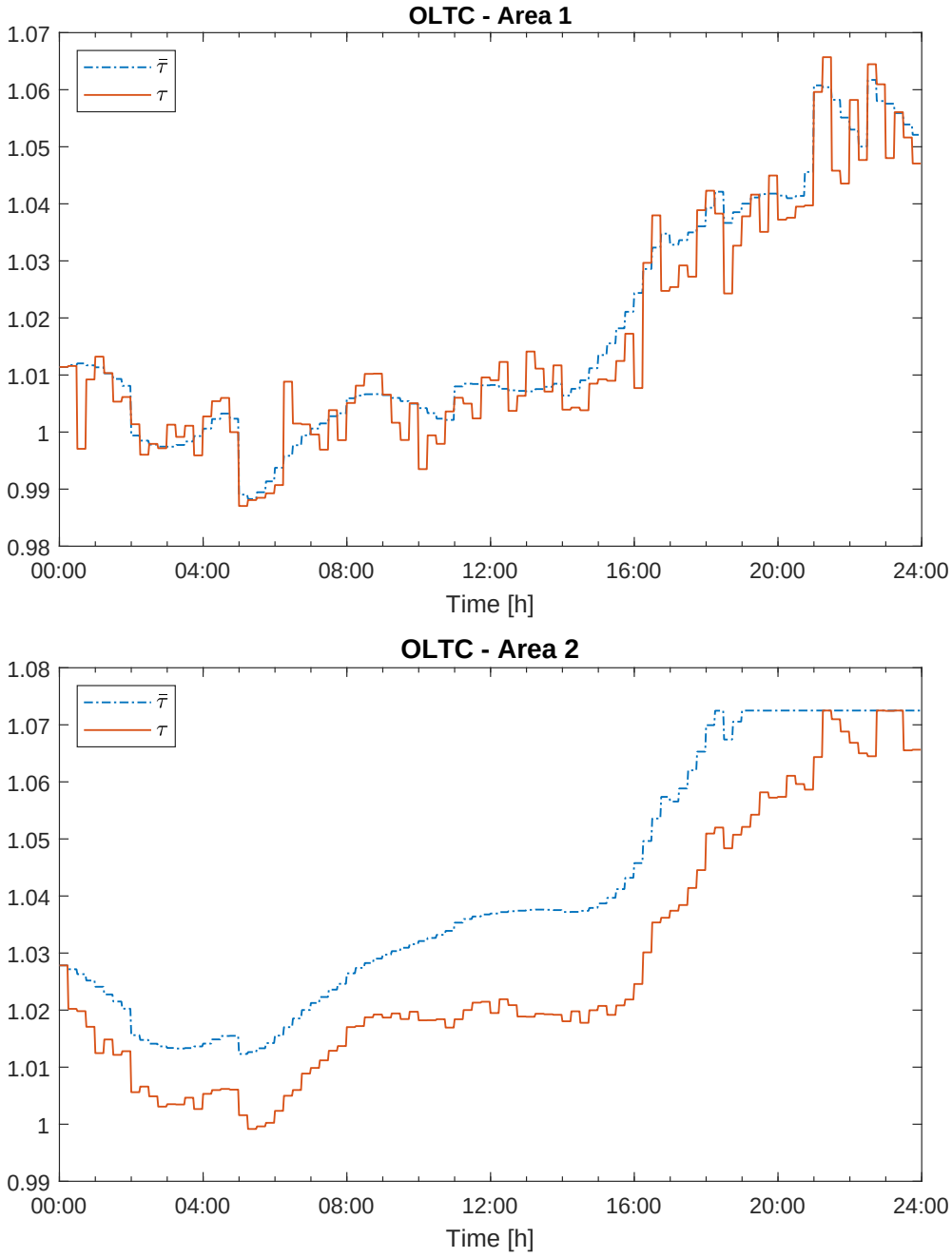

Figure 4.18: OLTCs' positions are adjusted by the ORPF control layer.

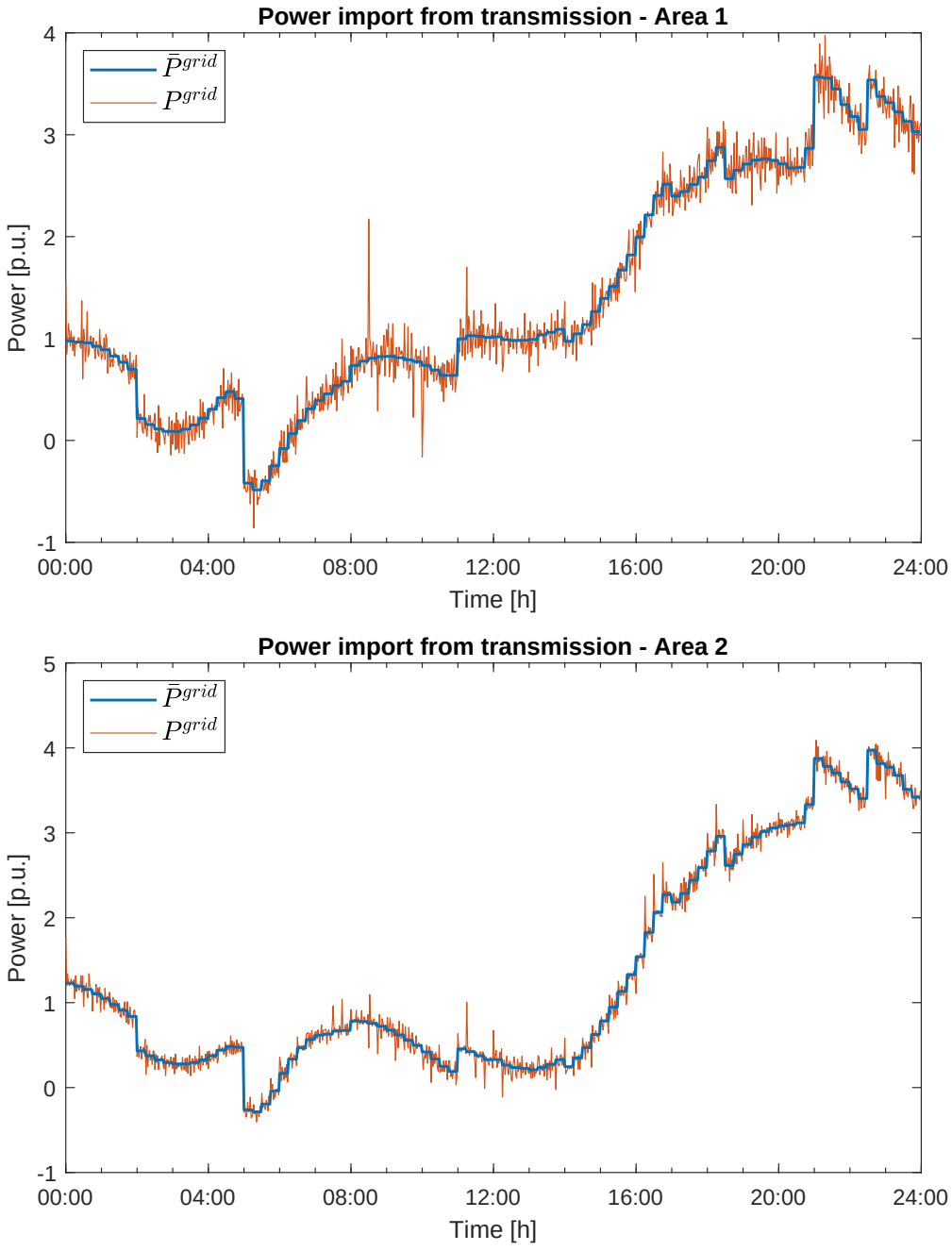

Figure 4.19: Exception made for high-frequency noise due to the non-instantaneous compensation, the power absorbed from primary substations almost perfectly matches the declared profiles.

4.5 Brief summary

In this chapter a realistic grid model has been introduced to test the Control System performances. This model is based on the combination of two well-known test feeders by IEEE, slightly modified to match the assumptions previously made. The adopted loads' and RES' power profiles have been instead provided by RSE S.p.a. An OPF has been implemented to retrieve the day-ahead scheduled profiles required by the Control System, where forecasts have been generated adequately fitting the available data.

Eventually, both the uncontrolled and the controlled system have been simulated. The former turned out not to absorb the declared power from transmission and to violate the regulatory limits. The latter, instead, proved to behave as well as expected, attaining all the control objectives formulated in the previous chapters.

Chapter 5

Scenario-based cluster control

In Chapter 3, an MPC-based cluster controller has been designed to locally compensate the cluster's net power deviations caused by loads' and RES' uncertainty. Once the predictive model had been formulated, we highlighted the dependency of the future outputs' trajectories on the future values of the disturbance. To cope with this problem, as customary in industrial applications, the disturbance was supposed constant and equal to the current estimated value, which could be calculated with few measurements only, namely the power flows through the cluster's AC ports.

Albeit, as shown in Chapter 4, this approach provides satisfactory results, in the last part of this research work, the possibility to improve the control action exploiting a set of historical data is explored. The desirable outcome would actually be to anticipate the future disturbance trajectory, enhancing the resources' planning. In this chapter, a first attempt to design such a data-driven control strategy, named *Cluster Scenario-based Model Predictive Control* (C-SCMPC), is presented, based on the so-called *Scenario Approach* (SA).

The SA is a recent research topic for the data-driven robust optimization of convex systems subject to uncertainty, see [28], [29]. Basically, a scenario-based optimization problem, also called *Scenario Program*, allows to exploit *scenarios*, i.e. sampled realizations of the uncertainty, to guarantee the constraints satisfaction with a given confidence, ultimately depending on the number of scenarios employed, for any possible realization of the uncertain variables. Differently from traditional robust optimization techniques, however, no knowledge of the uncertainty's support set or its probability distribution is required. The key concept is that, if a given optimal solution is feasible for a sufficiently large number of scenarios, it is likely feasible for all the other unknown realizations of the uncertainty.

The drafted C-SCMPC has been inspired by [30], in which a Scenario-based MPC resembles a Stochastic MPC by exploiting the available scenarios to approximate the unknown probability distribution of the uncertain variables. Theoretical guarantees for such a controller have been provided in [31]. In light of these considerations, before introducing the C-SCMPC optimization problem, it is necessary to determine which are the uncertain variables of our system and explain how their realizations can be sampled.

As mentioned in the previous chapters, grid's uncertainty is associated with loads' and RES' fluctuations, i.e. their deviations from forecasts. More specifically, in the cluster energetic model defined in Chapter 2.2, the uncertain elements have been collected in the vector of disturbances $d(t)$. Then, in the cluster predictive model introduced in Chapter 3.2.3, future disturbance trajectories have been grouped in the vector $\underline{d}(t)$, defined in (3.2.8). To this regard, it is worth noting that:

- The last element of $d(t)$, namely $\Delta P^{loss}(t)$, is not uncertain, but it rather depends on an unknown function of other quantities, e.g. the power flows variations and voltages. Let us, for the sake of simplicity, ignore this term.
- In Chapter 2.1, the uncertainty of non-dispatchable generators has been aggregated to loads' variations, see equation (2.1.20). Unfortunately, due to the very different nature of those uncertainties, in order to retrieve adequate scenarios the two components should be separated.
- For the sake of simplicity, microgrid loads' fluctuations can be aggregated to those of the corresponding grid load.

Let us therefore denote by $\Delta P_j^{NG}(t)$ the component of $\Delta P_j^L(t)$ associated to microgrids aggregated RES' deviation, while microgrids' loads uncertainty is instead incorporated into the variation of the corresponding grid load, denoted by $\Delta \tilde{P}_i^L(t)$.

Thus, at each MPC time-step, a scenario $\delta^{\{k\}}$ corresponds to a realization of $\left(\Delta P_1^{NG}, .., \Delta P_{n_M}^{NG}, \Delta \tilde{P}_1^L, .., \Delta \tilde{P}_{n_L}^L\right)$ throughout the control horizon. Having introduced the structure of a scenario, it now necessary to explain how they can be retrieved and exploited for control purposes.

5.1 Scenarios generation

As mentioned, in order to complete a multi-step Scenario Program, such as the Cluster SCMPC, a sufficient amount of scenarios is required. Actually, before explaining the possible approaches to retrieve these scenarios, let us introduce a simple yet meaningful classification for such a context:

- **Indirect methods** consist in determining - offline - any component of the scenario as the mismatch between the actual realization of the uncertain power profile and its forecasts:

$$\begin{aligned} \Delta P_j^{NG}(t) &= P_j^{NG}(t) - \hat{P}_j^{NG}(t) \quad \forall t \\ \Delta \tilde{P}_i^L(t) &= \tilde{P}_i^L(t) - \hat{\tilde{P}}_i^L(t) \quad \forall t \end{aligned} \tag{5.1.1}$$

- **Direct methods** consist, instead, in determining - online - the realization of each uncertain variable, e.g. $\Delta P_j^{NG}(t)$, based on its previous values.

In the former approach, adopted for example in [32], [33], retrieving a scenario means to generate a power profile for each quantity subject to uncertainty, a-posteriori determining the realization of each component of $\delta^{(k)}$ according to (5.1.1). The latter approach, adopted for example in [34], implies instead a model-based on-line scenario generation technique, which is out of the scope of this work.

Using an indirect method we hence shift the problem from generating a realization of the uncertainty itself to the generation of realistic power profiles for the uncertain elements, i.e. loads and PVs. Once more, this can be performed in several ways:

- **Historical data**: A first attempt could indeed be resorting to the historical measures of the system under scope. Although naive, this would guarantee both the scenarios' independence and the spatial correlation, i.e. the coherence of the power profiles to the geographic position of the corresponding elements. For example, the power profile of two neighbor PVs are typically characterized by similar shapes. The problem of this approach is that it generally requires years of data for each uncertain element, which is usually impractical.
- **Copula estimation**: Considering a power profile as a vector of correlated random variables, its probability density function - namely *copula* - can be estimated from data and used to generate new profiles by means of sampling techniques, see [33]. The main limitation of this method is, however, that the spatial correlation of the generated scenarios is lost.
- **Neural networks**: In [32] a novel scenario generation technique based on neural networks has been introduced. This method, discussed in Appendix D, allows the generation of a large number of power profiles resembling the training data, in terms of shape and frequency content. If adequately trained, the neural network can also capture the spatial correlation of power profiles. This approach has been widely tested in this research work, but, despite its potential, it requires further efforts to ensure the adequacy of generated scenarios.

In light of these considerations, in the remaining part of the chapter historical power profiles are used as scenarios, although the control system is later tested also with the scenarios generated by the aforementioned technique based on Neural Networks.

5.2 Cluster SCMPC

As mentioned at the beginning of this chapter, Cluster Scenario-based MPC is a slight modification of the C-MPC presented in Chapter 3.2, inspired by [30]. This formulation should hence exploit scenarios to implement future disturbance trajectories more plausible than the previously assumed constant one. At this point we suppose to have K scenarios, namely $\delta^{\{1\}}, .., \delta^{\{K\}}$, where - as discussed - each scenario corresponds to a realization of loads' and RES' uncertainty.

It is worth reminding the reader that, in order to exploit a generic scenario $\delta^{\{k\}}$ in the control problem formulation, it is first necessary to retrieve the consequent disturbance realization, since in the predictive model introduced in Chapter 3.2.5 the fluctuations of uncertain elements have been aggregated in the disturbance trajectory $\underline{\tilde{d}}(t)$.

Let us consider a generic cluster. Let $\underline{\tilde{d}}^{\{k\}}(t)$ be the aggregated disturbance corresponding to the k-th scenario for that cluster and $t_N(t)$ be the end-of-horizon, specified later in this chapter. For compactness, the explicit dependency of t_N from time t is dropped. Generically, $\underline{\tilde{d}}^{\{k\}}(t)$ can be structured as (5.2.1), where $\tilde{d}^{\{k\}}(\tau|t)$ corresponds to the aggregated disturbance at time τ in the k-th scenario.

$$\underline{\tilde{d}}^{\{k\}}(t) = \begin{bmatrix} \tilde{d}(t) \\ \tilde{d}^{\{k\}}(t+1|t) \\ \vdots \\ \tilde{d}^{\{k\}}(t_N|t) \end{bmatrix} \tag{5.2.1}$$

It should be noted that, since $\tilde{d}(t)$ can be estimated as in (3.2.13), it does not depend on the scenario. As far as future values are concerned, in light of (3.2.9), for any cluster they can be computed, according to (5.2.2), from the scenario components.

$$\tilde{d}^{\{k\}}(\tau|t) = \sum_{j=1}^{n_M} \Delta P_j^{NG\ \{k\}}(\tau) - \sum_{j=1}^{n_L} \Delta \tilde{P}_j^{L\ \{k\}}(\tau) \tag{5.2.2}$$

Let us informally use the word *scenario* to refer to the realization of the aggregated disturbance, instead of the uncertain variables' themselves. Since in the predictive model presented in Chapter 3.2.3 the aggregated disturbance directly acts on the output trajectory, K scenarios will determine exactly K different output trajectories, each denoted by $\underline{y}_1^{\{k\}}(t)$. The predictive model adopted for C-SCMPC is hence reported in (5.2.3).

$$\begin{cases} \underline{x}(t) = A_c \cdot x(t) + B_c \cdot \underline{u}(t) \\ \underline{y}_1^{\{1\}}(t) = D_{c1} \cdot \underline{u}(t) + M_{c1} \cdot \underline{h}(t) + \underline{\tilde{d}}^{\{1\}}(t) \\ \quad \vdots \\ \underline{y}_1^{\{K\}}(t) = D_{c1} \cdot \underline{u}(t) + M_{c1} \cdot \underline{h}(t) + \underline{\tilde{d}}^{\{K\}}(t) \end{cases} \tag{5.2.3}$$

In view of the potentially large number of variables involved in such an optimization problem, a larger time-step of $150s$ has been selected to relieve the computational complexity. The corresponding FRH parameters are:

- $M_s = 6$, since in a 15-minutes time window there are 6 MPC steps.
- $M_p = 4$, for the reasons discussed in Chapter 3.2.2.
- $M_d = 576$, as in a day there are exactly 576 time-steps.

Analogously to [30], the selected cost function consists in the sum of C-MPC cost functions under all the scenarios. Indeed, if they are independently sampled,

this formulation resembles the expected value of the cost function over the unknown uncertainty's probability distribution.

A reformulation of the constraint (3.2.21) on the output trajectory is also required. One could be tempted to replace this constraint with the following one:

$$-\rho \leq y_1^{\{k\}}(\tau) - \bar{P}^{net}(\tau) \leq \rho \qquad \forall k \in [1,K], \forall \tau \in [t, t_N - 1] \tag{5.2.4}$$

Such a constraint, unfortunately, would make the optimization problem unfeasible. This bound is indeed desirably strict, while the controlled system is non-strictly proper and the scenario acts directly on the output. The proposed solution is to bound, instead, the expected output trajectory, which indeed attains the optimization problem feasibility:

$$-\rho \leq \frac{1}{K}\sum_{k=1}^{K} y_1^{\{k\}}(\tau) - \bar{P}^{net}(\tau) \leq \rho \qquad \forall \tau \in [t, t_N - 1] \tag{5.2.5}$$

Below the C-SCMPC optimization problem for a generic time step t is reported.

$$\begin{aligned}
\min_{\underline{u}(t), s_{dc}} \quad & \sum_{k=1}^{K} \Bigg[\omega_y \sum_{\tau=t}^{t_N-1} \|y_1^{\{k\}}(\tau) - \bar{P}^{net}(\tau)\|_I + \omega_g \sum_{\tau=t}^{t_N-1} \|u_g(\tau)\|_{R_g} \\
& + \omega_\delta \sum_{\tau=t}^{t_N-1} \|u_g(\tau) - u_g(\tau-1)\|_{R_\delta} + \omega_b \sum_{\tau=t}^{t_N-1} \|u_b(\tau)\|_{R_b} \\
& + \omega_{dc} \sum_{\tau=t}^{t_N-1} \|u_{dc}(\tau)\|_I + \omega_s \; s_{dc} \Bigg] \\
s.t. \quad & \underline{x}(t) = A_c \; x(t) + B_c \; \underline{u}(t) \\
& \underline{y}_1^{\{k\}}(t) = D_{c1} \; \underline{u}(t) + M_{c1} \; \underline{h}(t) + \underline{\tilde{d}}^{\,(k)}(t) && \forall k \in [1,K] \\
& \bar{r}_g^{\downarrow}(\tau) \leq u_g(\tau) \leq \bar{r}_g^{\uparrow}(\tau) && \forall \tau \in [t, t_N - 1] \\
& \bar{r}_b^{\downarrow}(\tau) \leq u_b(\tau) \leq \bar{r}_b^{\uparrow}(\tau) && \forall \tau \in [t, t_N - 1] \\
& \bar{r}_e^{\downarrow}(\tau) \leq x(\tau) \leq \bar{r}_e^{\uparrow}(\tau) && \forall \tau \in [t+1, t_N] \\
& x(t_N) = \emptyset_{n_M,1} \\
& -\rho \leq \frac{1}{K}\sum_{k=1}^{K} y_1^{\{k\}}(\tau) - \bar{P}^{net}(\tau) \leq \rho && \forall \tau \in [t, t_N - 1] \\
& (P_k^{dc,min} - \bar{P}_k^{dc}(t)) \; s_{dc} \leq u_{dc}(t) \leq (P_k^{dc,max} - \bar{P}_k^{dc}(t)) \; s_{dc} \\
& P_k^{dc,min} - \bar{P}_k^{dc}(\tau) \leq u_{dc}(\tau) \leq P_k^{dc,max} - \bar{P}_k^{dc}(\tau) && \forall \tau \in [t+1, t_N - 1]
\end{aligned}$$

$$\begin{aligned}
where \quad & t_N = min\left(\left(\left\lfloor \frac{t}{M_s} \right\rfloor + M_p\right) M_s, \left(\left\lfloor \frac{t}{M_d} \right\rfloor + 1\right) M_d\right) \\
& M_s = 6 \quad M_p = 4 \quad M_d = 576
\end{aligned}$$

5.3 Results

As the C-SCMPC optimization problem has been formalized, it can be tested on the defined benchmark grid, comparing the resulting performances to the ones attained by the previous control structure based on C-MPC. For this test, the forecasts and the actual power profiles of loads have been extracted from a dataset provided by RSE S.p.a., while those of PV have been retrieved from the *NREL Solar Integration Dataset*[47], specifically from the historical data of October. The adopted scenarios correspond, instead, to the other power profiles of the datasets for the months of September, October and November. It should be noted that this choice entails $K = 90$ scenarios, which is still low for practical applications. Later in this chapter, the control scheme is tested also with the scenarios retrieved from the GAN presented in Appendix D.

In figure 5.1 the resulting actual realization of the disturbance is compared to the region *covered* by scenarios' trajectories. Not only it lies within such region, but it also turns out to be close to the average scenario's trajectory. In light of this consideration, a good behavior of the C-SCMPC control system would be expected, despite the small number of scenarios, at least for the selected power profiles.

The resulting KPIs associated to grid power's mismatch are reported in Table 5.1 for both the uncontrolled and the controlled system, while other KPIs have been omitted as they are not meaningful in this context.

Table 5.1: Scenario KPIs - grid power mismatches

Case	ε_{p1}	ε_{p2}
C-SCMPC	0.069 p.u.	0.072 p.u.
C-MPC	0.064 p.u.	0.072 p.u.
Uncontrolled	0.250 p.u.	0.490 p.u.

The reader should, however, not be misled by the marginal variations of these performance indicators: at this point we are, in fact, interested in determining whether such a control strategy allows to score a lower cost function, i.e. if it achieves a better planning of the resources or not. To assess this property, let us define a cost function $l(\cdot)$, which resembles the optimization problem's cost function, except for the replacement of the DC power request with the actuated DC power variation and the substitution of the actual cluster net power in place of the controller's output trajectory. By comparing $l(\cdot)$ for the two cluster control strategies, it is hence possible to verify whether or not the usage of scenarios leads to the desired cost reduction.

[47] `https://www.nrel.gov/grid/solar-power-data.html`

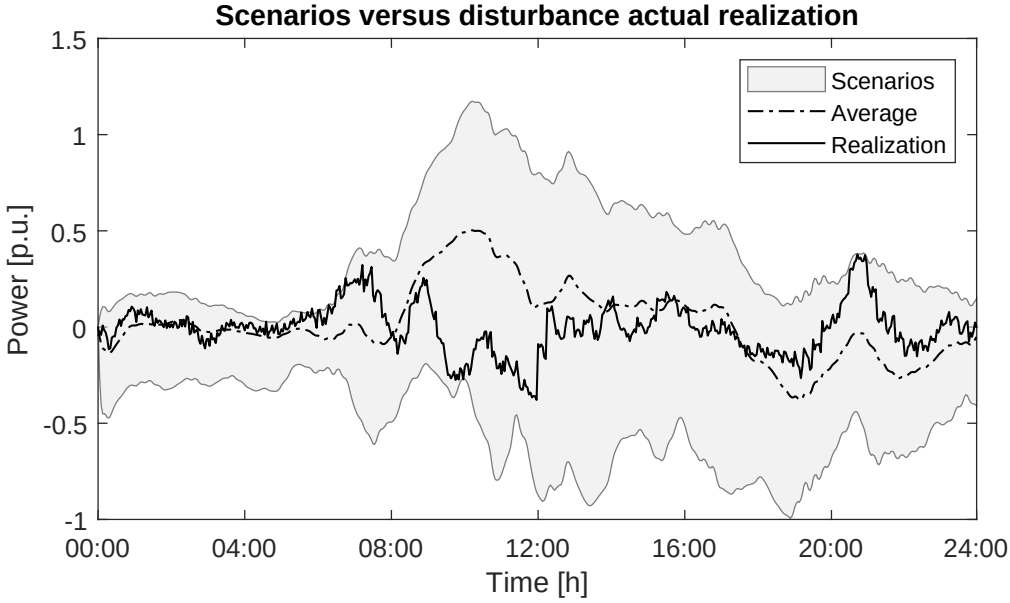

Figure 5.1: Actual disturbance realization acting on Cluster 2, compared to the region covered by the scenarios' trajectories.

$$l(\cdot) = \frac{1}{10^6}\left[\omega_y \sum_{i=1}^{n_c}\left(P_{(i)}^{net}(t) - \bar{P}_{(i)}^{net}(t)\right)^2 + \omega_b \sum_{i=1}^{N_m}\left(\Delta p_i^B(t)\right)^2 + \omega_g \sum_{i=1}^{N_m}\left(\Delta p_i^G(t)\right)^2 + \omega_\delta \sum_{i=1}^{N_m}\left(\Delta p_i^G(t) - \Delta p_i^G(t-1)\right)^2 + \omega_d \sum_{i=1}^{N_i}\left(\Delta P_i^{DC}(t)\right)^2\right] \tag{5.3.1}$$

In figure 5.2 the cumulative cost functions of the two controllers are compared: unfortunately, it is possible to notice that - throughout the entire day - the C-SCMPC cost function is higher than the one scored by C-MPC. Despite this implies that the designed data-driven control strategy does not attain a lower cost function - as desired -, it is convenient to analyze the reasons of such a behavior, to devise possible future developments of this strategy.

In figure 5.3 the average mismatch between the actual disturbance trajectories and the ones assumed by the control system is depicted for Cluster 2. Specifically, the blue line corresponds to the mean error committed by the controller when assuming a disturbance trajectory coinciding with the average scenario, which is denoted by ϵ_s, while the red line corresponds to the mean mismatch when a constant disturbance is instead assumed, denoted by ϵ_c. Such quantities can be respectively computed as in (5.3.2) and (5.3.3), where $N = N(t)$ is the length of the prediction horizon.

$$\epsilon_s(t) = \frac{1}{N}\sum_{\tau=t}^{t_N}\left|\frac{1}{K}\sum_{k=1}^{K} d^{\{k\}}(\tau|t) - d(\tau)\right| \tag{5.3.2}$$

$$\epsilon_c(t) = \frac{1}{N}\sum_{\tau=t}^{t_N}|d(t) - d(\tau)| \tag{5.3.3}$$

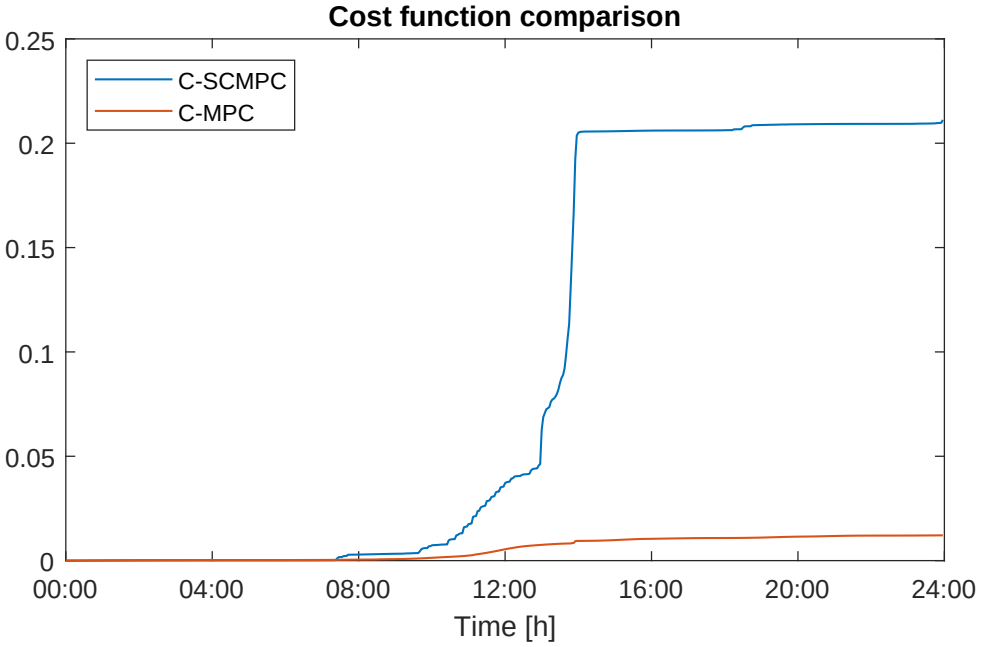

Figure 5.2: Comparison of C-SCMPC and C-MPC cumulative cost functions: the C-SCMPC scores an higher cost.

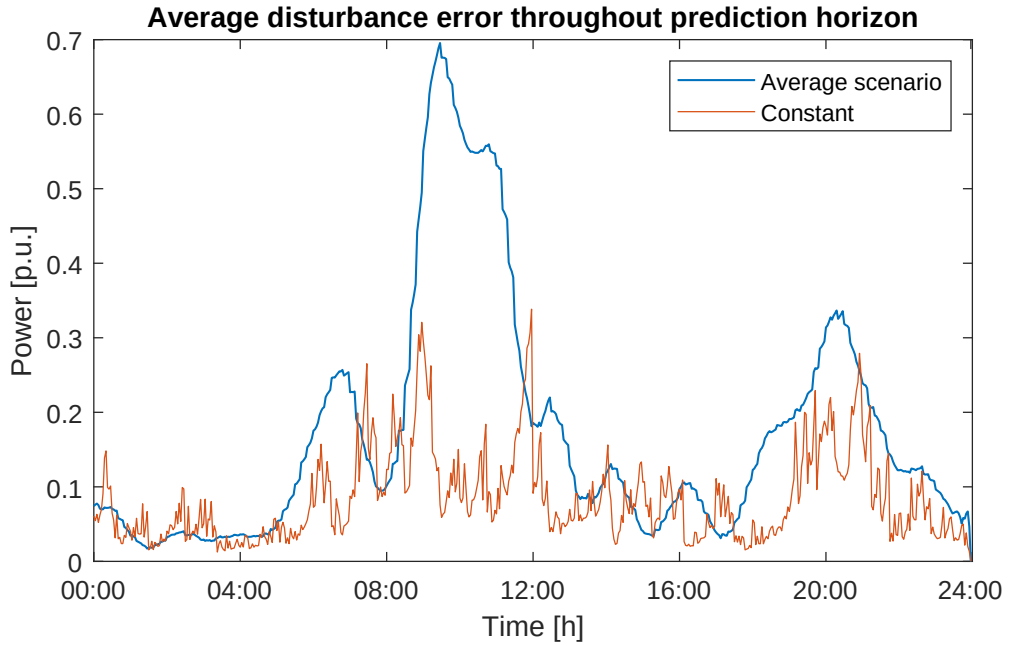

Figure 5.3: Average mismatch between the assumed and actual disturbance trajectories throughout the prediction horizon for Cluster 2. In particular, the blue line corresponds to the mean mismatch of the disturbance with respect to the average scenario trajectory, whereas the red line is the mean error when the disturbance is supposed constant throughout the control horizon.

From figure 5.3 it is evident that trusting the scenarios leads to an average error larger than supposing a constant disturbance, which is the ultimate reason for the aforementioned cost function increase: C-SCMPC actually plans the resource usage based on future disturbance trajectories significantly different from the real ones. This behavior has been verified also adopting $K = 900$ scenarios generated by the GAN presented in Appendix D achieving similar results, see figures 5.4 and 5.5.

To overcome these problems, a future research work should explore the following possibilities:

- Based on the latest measurements of the actual disturbance realization, the outliers scenarios could be removed and higher weights could be assigned to those mostly compatible with the measurements. Most likely scenarios would be more weighted in the C-SCMPC cost function and in constraint (5.2.5).
- A direct on-line scenario generation method could be adopted, as devised in [34], which would allow to only generate scenarios coherent with the pasts measurements, avoiding outliers.

5.4 Brief summary

In this chapter a first attempt to design a data-driven cluster controller, inspired by the well-known Scenario-based Model Predictive Control, has been devised.

Scenarios have been retrieved both from the historical data and adopting an approach based on Generative Adversarial Network, recently proposed in the literature. The latter technique seems, however, to require more research work to enhance the generated scenarios.

The mentioned C-SCMPC problem has then been formalized and its results have been compared to those of the previous C-MPC controller, showing a worsening of the control system performances, likely associated to the inaccuracy of the adopted scenarios. Eventually, some hints for future research have been introduced to cope with this issue.

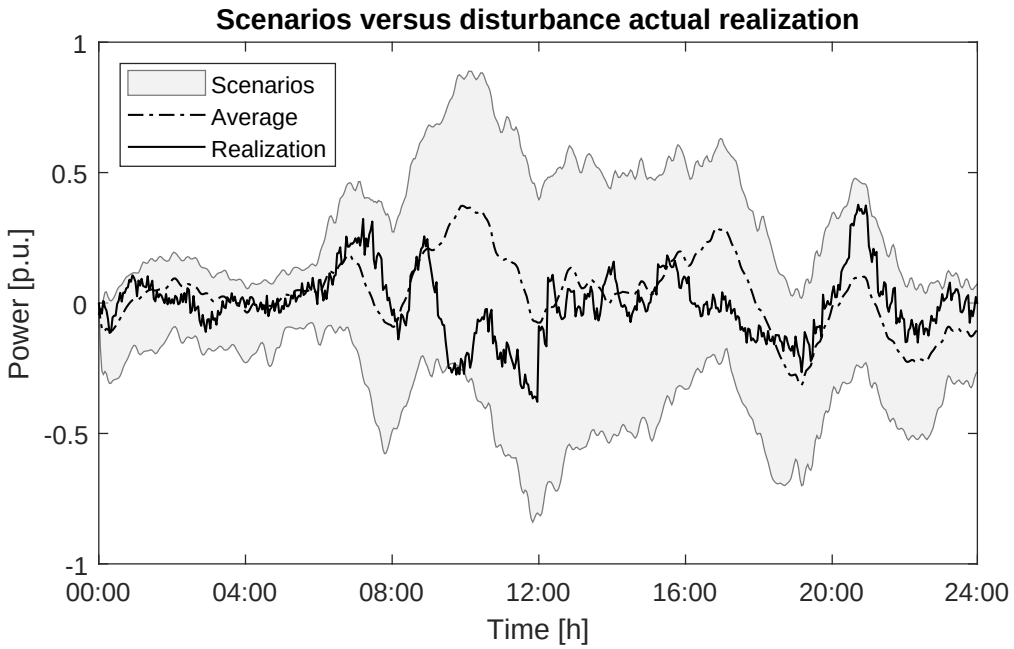

Figure 5.4: Actual disturbance realization acting on Cluster 2, compared to the region covered by the trajectories of scenarios generated by the GAN presented in Appendix D.

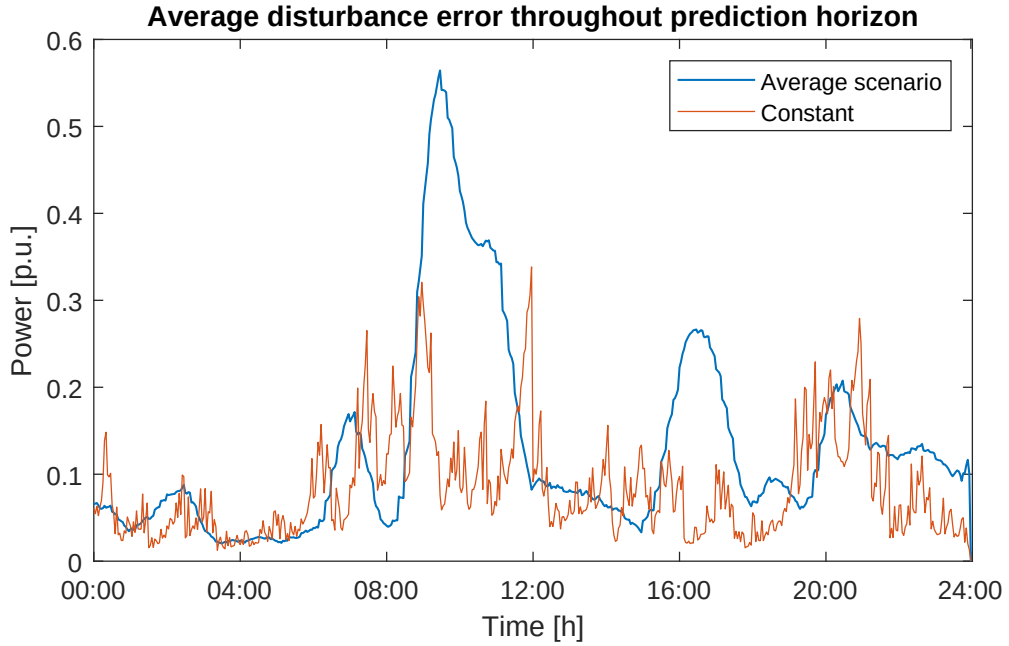

Figure 5.5: Average mismatch between the assumed and actual disturbance trajectories throughout the prediction horizon for Cluster 2, adopting the scenarios generated by the GAN.

Chapter 6

Conclusions and future developments

In the first chapter a brief overview of the electric power system has been provided, illustrating the main problems of the current infrastructure and the future challenges to be coped. As a matter of fact, the necessary transition towards systems with distributed energy resources requires a change in the actual paradigm of the electric grid, which is mostly inadequate to manage bidirectional power flows and distributed generation. Furthermore, the intrinsic uncertainty of RES and the increasing power demand undermine grid predictability, complicating the operation planning, which is still at the basis of the power system management. After a survey of the electric grid's structure, motivations are given for the introduction of a MVDC transmission system connecting multiple points of existing distribution grids, which has recently been subject to increasing research interests by the main companies operating in the field. Actually, in addition to the reinforcement of feeders' AC backbones, MVDC allows controllable and efficient power transfers. Further flexibility is granted by the progressive diffusion of microgrids, providing precious ancillary services which can be exploited by the grid control system to attain its objectives. Thanks to these services it is in fact possible to enhance the usage of available resources and to mitigate the aforementioned loads' and RES' uncertainty, which has been identified as the main goal of this Thesis.

The proposed solution consists in partitioning the grid in multiple clusters, which self-compensate the internal fluctuations exploiting microgrids' ancillary services. Each cluster is selected in such a way that it includes an AC/DC converter, thus enabling the possibility to balance clusters reserves and sustain the most hindered ones.

In the second chapter, three different models have been introduced. In particular, considering microgrids composed by dispatchable and non-dispatchable generators, batteries and non-deterministic loads, an energetic model of this component has first been formulated. This model neglects the internal microgrid topology and, exploiting the power profiles scheduled by the MG scheduler, defines the aggregated power and energy reserves of the microgrid, i.e. the operative margins for the ancillary services that can be provided to the grid. It should be noted that

the extent of these reserves is ultimately established by the microgrids themselves, based on the amount of ancillary services they are willing to provide. The mentioned model has then been simplified by aggregating generators, batteries and loads respectively, since ancillary services are not requested to the single elements of the microgrid but rather to its scheduler, which is in turn supposed to commit these requests to the individual generators and batteries.

Having defined a model for microgrids, a control-oriented energetic cluster model has been provided. Specifically, to formalize the state-space model, the state, input and output variables and the corresponding transformation matrices have been specified.

Eventually, the model of a mixed AC-DC grid, which is necessary for both simulation and control purposes, have been formulated under rather general simplifying assumptions, based on power flow equations.

In the third chapter, the multi-layer control architecture has been presented. In the proposed solution each cluster is controlled by a decentralized Model Predictive Control system, namely C-MPC, which dispatches the microgrids' aggregated batteries and generators to locally compensate internal disturbance, associated to loads' and RES' uncertainty. By design, C-MPC works with few measurements only, as it exploits the measured active powers outgoing from cluster's AC ports to estimate the current disturbance, whose future trajectory is customarily assumed to be constant. Moreover, the new concept of Flexible Receding Horizon principle has been devised to achieve a better usage of the available forecasts and to cope with the peculiarities of our system. C-MPC has thus been formalized by defining the predictive model and the optimization problem's cost function and constraints. The control objective is to maintain the cluster net power close enough to the day-ahead schedule: this allows, indeed, to attain the primary goal of the entire control structure, which is to maintain the power absorbed from the transmission stage close enough to the day-ahead declared profile. Owing to the presence of an MVDC interface in each cluster, in case of overload, C-MPC can also issue DC power requests to attain the requirements.

Such requests, possibly amended by a centralized Cluster Supervisor, are then actuated committing the adequate DC voltage set-points to the MVDC interfaces. For this purpose, a non-convex supervisor has been first formulated, where the non-convexity is actually entailed by the DC power flow equations. A multi-stage supervisor guaranteeing the existence of, at least, a sub-optimal solution has then been devised, which is indeed more suitable for such a safety-critical environment.

Eventually, an Optimal Reactive Power Flow, periodically executed to adjust the nodal voltages and reduce power losses, has been presented. These objectives can be attained controlling the OLTCs and dispatching requests of reactive power ancillary services to microgrids and MVDC interfaces.

In the fourth chapter, the aforementioned control system has been tested. First and foremost, a benchmark grid has been defined, adopting the IEEE 37-bus and IEEE 13-bus test feeders and introducing a radial MVDC transmission grid which connects multiple buses of the feeders. Some microgrids have also been distributed almost uniformly across the benchmark grid. The power profiles of loads' and non-

dispatchable generators' have been provided by RSE S.p.a., whereas their forecasts have been retrieved, for simplicity, by means of smooth cubic splines fittings. The scheduled quantities have then been computed by means of a multi-step OPF, resembling the day-ahead optimization procedures.

To assess the fitness of the designed control system, both the uncontrolled and controlled systems have been tested on the benchmark grid with the same power profiles. In the former case, loads' and RES' fluctuations lead not only to the violation of voltage regulatory limits, but also to a significant deviation of the power imported from the transmission stage with respect to the day-ahead plan and to a conspicuous increase of power losses. The controlled system has instead proven to work as expected: not only, in fact, the local uncertainty compensation allows an adequate tracking of the declared power import, but voltage deviations are limited and power losses reduced. Moreover, the designed multi-stage cluster supervisor has also proved to successfully reconcile the incoming power requests, dispatching accurate DC voltage references.

In the fifth and last chapter, a cluster data-driven control strategy - namely C-SCMPC - has been proposed, with the goal of employing the available historical data to better guess the future disturbance trajectory, previously assumed constant. This strategy, inspired by the widely known Scenario-based Model Predictive Control available in the literature, actually requires a large amount of scenarios, i.e. sampled realizations of the uncertain variables, such as the deviations of loads' and RES' power profiles from their forecasts. Thus, a brief overview of the techniques that could be used to retrieve the required scenarios have been proposed. Due to the unsatisfactory results of the implemented approach based on Generative Adversarial neural Networks, the scenarios have been retrieved from historical measurements. The C-SCMPC control strategy has been formalized with a small reformulation of the previously defined C-MPC optimization problem, and its results have been illustrated, turning out to be unsatisfactory due to the increased control cost. Finally, a possible reason for such a behavior has been explored, proposing possible solutions for future research works.

To summarize, the proposed multi-layer control strategy is characterized by:

- A decentralized cluster control which, based on few measurements only, is able to locally compensate the disturbance associated to uncertain elements. Furthermore, thanks to cluster controllers' predictive capabilities and to the FRH principle, intra-day forecasts are fully exploited and the operative constraints on batteries are fulfilled.
- A supervisor which, owing to the proposed multi-stage architecture, is able to satisfy the power requests issued by cluster controllers. Once more, this control layer is designed to require the lowest possible number of signals from cluster controllers, i.e. their power reserves and requests themselves.
- An ORPF routine minimizing power losses and voltage deviations.

Although the results achieved by the proposed control architecture are satisfactory, there are several topics which would be worth investigating in future activities.

Distributed C-MPC Rather than implementing a centralized supervisor, the DC power variations could be object of a consensus among purely-distributed cluster controllers. It is indeed worth noting that, despite such a control strategy would involve an iterative optimization procedure, the strong advantage would be an agreed long-term planning of power transfers through the MVDC transmission. Conversely, in this work - due to the static supervisor implemented - neither the DC power transfers are planned, nor the clusters have knowledge of the actual power transfered through the DC port: the supervisor only satisfies instantaneous requests and balances powers when reserves are excessively low.

Improved scenario generation The generation of independent and realistic scenarios is surely fundamental for the illustrated Scenario-based control strategy. To this regard, enlarging the training dataset and improving the tuning of GAN's hyper-parameters could improve the generated power profiles. Moreover, it would be extremely interesting to produce weather-conditioned scenarios, which is possible but still not implemented. Further developments attaining indirect scenario generation could consist in the implementation of copula-based methods, comparing the generated profiles to those of GAN. Direct scenario generation methods should also be explored, as they would allow to exploit the past measurements to produce coherent scenarios.

Scenario-based control Although promising, the proposed C-SCMPC needs to be further studied to attain adequate and uniform performances. Substantial improvements could be achieved by means of a proper scenario removal algorithm, where the outliers selection could be based on the last few samples of the measured disturbance, assigning higher weights to the scenarios most compatible with such measurements. In other words, this approach would consist in assigning - at each time-step - to each scenario a likelihood based on the past realization of the disturbance itself, discarding those with the lowest probability and trusting more the ones with the highest likelihood.

Bibliography

[1] "Mvdc plus, Medium voltage direct current managing the future grid," Siemens. [Online]. Available: http://www.siemens.com/global/en/home/products/energy/medium-voltage/solutions/mvdc.html.

[2] R. Marconato, *Electric Power Systems*, Second Edition, I. E. Committee, Ed. 2004.

[3] N. Flourentzou, V. G. Agelidis, and G. D. Demetriades, "Vsc-based hvdc power transmission systems: An overview," *IEEE Transactions on Power Electronics*, vol. 24, no. 3, pp. 592–602, Mar. 2009, ISSN: 0885-8993. DOI: 10.1109/TPEL.2008.2008441.

[4] F. Mura and R. W. De Doncker, "Design aspects of a medium-voltage direct current (mvdc) grid for a university campus," in *Power Electronics and ECCE Asia (ICPE & ECCE), 2011 IEEE 8th International Conference on*, IEEE, 2011, pp. 2359–2366.

[5] L. Piegari and P. Tricoli, "A control algorithm of power converters in smartgrids for providing uninterruptible ancillary services," in *Harmonics and Quality of Power (ICHQP), 2010 14th International Conference on*, IEEE, 2010, pp. 1–7.

[6] A. L. Bella, S. R. Cominesi, C. Sandroni, and R. Scattolini, "Hierarchical predictive control of microgrids in islanded operation," *IEEE Transactions on Automation Science and Engineering*, vol. 14, no. 2, pp. 536–546, Apr. 2017, ISSN: 1545-5955. DOI: 10.1109/TASE.2016.2633397.

[7] S. R. Cominesi, M. Farina, L. Giulioni, B. Picasso, and R. Scattolini, "A two-layer stochastic model predictive control scheme for microgrids," *IEEE Transactions on Control Systems Technology*, vol. 26, no. 1, pp. 1–13, Jan. 2018, ISSN: 1063-6536. DOI: 10.1109/TCST.2017.2657606.

[8] B. Li, J. Shen, X. Wang, and C. Jiang, "From controllable loads to generalized demand-side resources: A review on developments of demand-side resources," *Renewable and Sustainable Energy Reviews*, vol. 53, pp. 936–944, 2016, ISSN: 1364-0321. DOI: https://doi.org/10.1016/j.rser.2015.09.064. [Online]. Available: http://www.sciencedirect.com/science/article/pii/S1364032115010345.

[9] D. E. Olivares, A. Mehrizi-Sani, A. H. Etemadi, C. A. Cañizares, R. Iravani, M. Kazerani, A. H. Hajimiragha, O. Gomis-Bellmunt, M. Saeedifard, R. Palma-Behnke, *et al.*, "Trends in microgrid control," *IEEE Transactions on smart grid*, vol. 5, no. 4, pp. 1905–1919, 2014.

[10] A. La Bella, M. Farina, C. Sandroni, and R. Scattolini, "On the design of aggregators for microgrids providing active and reactive power services," *arXiv preprint arXiv:1804.02195*, 2018.

[11] S. Frank and S. Rebennack, "An introduction to optimal power flow: Theory, formulation, and examples," *IIE Transactions*, vol. 48, no. 12, pp. 1172–1197, 2016.

[12] P. Wlodarczyk, A. Sumper, and M. Cruz, "Voltage control of distribution grids with multi-microgrids using reactive power management," *Advances in Electrical and Computer Engineering*, vol. 15, no. 1, pp. 83–88, 2015.

[13] K. Baker, J. Guo, G. Hug, and X. Li, "Distributed mpc for efficient coordination of storage and renewable energy sources across control areas," *IEEE Transactions on Smart Grid*, vol. 7, no. 2, pp. 992–1001, 2016.

[14] M. Farina, A. Guagliardi, F. Mariani, C. Sandroni, and R. Scattolini, "Model predictive control of voltage profiles in mv networks with distributed generation," *Control Engineering Practice*, vol. 34, pp. 18–29, 2015.

[15] K. Baker, D. Zhu, G. Hug, and X. Li, "Jacobian singularities in optimal power flow problems caused by intertemporal constraints," in *2013 North American Power Symposium (NAPS)*, Sep. 2013, pp. 1–6. DOI: 10.1109/NAPS.2013.6666876.

[16] I. Moghram and S. Rahman, "Analysis and evaluation of five short-term load forecasting techniques," *IEEE Transactions on power systems*, vol. 4, no. 4, pp. 1484–1491, 1989.

[17] H. S. Hippert, C. E. Pedreira, and R. C. Souza, "Neural networks for short-term load forecasting: A review and evaluation," *IEEE Transactions on Power Systems*, vol. 16, no. 1, pp. 44–55, Feb. 2001, ISSN: 0885-8950. DOI: 10.1109/59.910780.

[18] J. B. Rawlings, D. Q. Mayne, and M. Diehl, *Model Predictive Control: Theory, Computation, and Design*. Nob Hill Publishing, 2017.

[19] A. A. Jalali and V. Nadimi, "A survey on robust model predictive control from 1999-2006," in *2006 International Conference on Computational Inteligence for Modelling Control and Automation and International Conference on Intelligent Agents Web Technologies and International Commerce (CIMCA'06)*, Nov. 2006, pp. 207–207. DOI: 10.1109/CIMCA.2006.29.

[20] D. Bernardini and A. Bemporad, "Stabilizing model predictive control of stochastic constrained linear systems," *IEEE Transactions on Automatic Control*, vol. 57, no. 6, pp. 1468–1480, Jun. 2012, ISSN: 0018-9286. DOI: 10.1109/TAC.2011.2176429.

[21] L. M. R. Scattolini, *Advanced and multivariable control*. 2014.

[22] M. S. Mahmoud and H. M. Khalid, "Model prediction-based approach to fault-tolerant control with applications," *IMA Journal of Mathematical Control and Information*, vol. 31, no. 2, pp. 217–244, 2014.

[23] L. Gan and S. H. Low, "Optimal power flow in direct current networks," *IEEE Transactions on Power Systems*, vol. 29, no. 6, pp. 2892–2904, 2014.

[24] J. W. Simpson-Porco, F. Dörfler, and F. Bullo, "Voltage collapse in complex power grids," *Nature communications*, vol. 7, p. 10 790, 2016.

[25] S. Taheri and V. Kekatos, "Power flow solvers for direct current networks," *arXiv preprint arXiv:1807.03936*, 2018.

[26] W. H. Kersting, "Radial distribution test feeders," in *2001 IEEE Power Engineering Society Winter Meeting. Conference Proceedings (Cat. No.01CH37194)*, vol. 2, Jan. 2001, 908–912 vol.2. DOI: 10.1109/PESW.2001.916993.

[27] J. Lofberg, "Yalmip: A toolbox for modeling and optimization in matlab," in *Computer Aided Control Systems Design, 2004 IEEE International Symposium on*, IEEE, 2004, pp. 284–289.

[28] M. C. Campi and S. Garatti, *Introduction to the Scenario Approach*.

[29] M. C. Campi, S. Garatti, and M. Prandini, "The scenario approach for systems and control design," *Annual Reviews in Control*, vol. 33, no. 2, pp. 149–157, 2009.

[30] G. Schildbach, L. Fagiano, C. Frei, and M. Morari, "The scenario approach for stochastic model predictive control with bounds on closed-loop constraint violations," *Automatica*, vol. 50, no. 12, pp. 3009–3018, 2014.

[31] G. Schildbach, L. Fagiano, and M. Morari, "Randomized solutions to convex programs with multiple chance constraints," *SIAM Journal on Optimization*, vol. 23, no. 4, pp. 2479–2501, 2013. DOI: 10.1137/120878719.

[32] Y. Chen, Y. Wang, D. Kirschen, and B. Zhang, "Model-free renewable scenario generation using generative adversarial networks," *IEEE Transactions on Power Systems*, vol. 33, no. 3, pp. 3265–3275, 2018.

[33] T. Wang, H.-D. Chiang, and R. Tanabe, "Toward a flexible scenario generation tool for stochastic renewable energy analysis," in *2016 Power Systems Computation Conference (PSCC)*, Jun. 2016, pp. 1–7. DOI: 10.1109/PSCC.2016.7540991.

[34] C. A. Hans, P. Sopasakis, A. Bemporad, J. Raisch, and C. Reincke-Collon, "Scenario-based model predictive operation control of islanded microgrids," in *Decision and Control (CDC), 2015 IEEE 54th Annual Conference on*, IEEE, 2015, pp. 3272–3277.

[35] I. Goodfellow, J. Pouget-Abadie, M. Mirza, B. Xu, D. Warde-Farley, S. Ozair, A. Courville, and Y. Bengio, "Generative adversarial nets," in *Advances in neural information processing systems*, 2014, pp. 2672–2680.

Appendix A

Per unit system

Owing to the non-linearity and non-convexity of Power Flow problems, iterative numerical optimization procedures are required and the existence of a global minimum is not guaranteed. In addition, the problem complexity exponentially grows with the size of the grid. The heterogeneity of electric quantities' scales, e.g. from 10^{-1} for SOCs to 10^{6} for powers, leads to significant solver inaccuracy, numerical instability and poor convergence properties.

A common practice in the Power Flow literature [2], [11] is to normalize the electric quantities to the *per unit system* (p.u.). A variable expressed in per unit represents the percentage of its absolute quantity (expressed in SI) with respect to the so-called *per unit base*. Let us therefore denote by v, p, c, z and s respectively any generic voltage, real power, current, impedance and apparent power. Then, denoting base quantities by subscript *base* and absolute quantities b *si*, the normalization is performed as in (A.0.1).

$$v_j = \frac{v_{j,si}}{v_{base}} \qquad p_j = \frac{p_{j,si}}{s_{base}} \qquad c_j = \frac{c_{j,si}}{c_{base}} \qquad z_j = \frac{z_{j,si}}{z_{base}} \tag{A.0.1}$$

Before introducing the choice of base quantities, it should be noted that another strong advantage involved by the adoption of p.u. is that, under the customary assumption of perfectly balanced distribution grid, it allows model a three-phase feeder as a single-phase one simply by adequately defining the base quantities.

Conventionally, for three-phase distribution systems, the base voltage v_{base} matches the primary substation line-to-line voltage, while the three-phase base power[48] s_{base} can be arbitrarily chosen. Once these quantities are fixed, the base current c_{base} and the base impedance z_{base} must be coherently selected as in (A.0.2).

$$c_{base} = \frac{s_{base}}{\sqrt{3}\, v_{base}} \qquad z_{base} = \frac{v_{base}^2}{s_{base}} \tag{A.0.2}$$

In case of a mixed AC-DC grid, a base voltage and power, respectively denoted by v_{base}^{dc} and p_{base}^{dc}, must be selected also for the DC transmission. While the DC base voltage is commonly selected as its nominal value, i.e. the slack nodes' voltage, the choice of the DC base power is paramount to avoid an over-complicated notation throughout the rest of this work. Specifically, p_{base}^{dc} shall be equal to the three-phase base power s_{base}.

[48] The base power is referred to the apparent power, denoted by s_{base}

Appendix B

Benchmark grid parameters

Table B.1: Microgrids generators parameters

Mg #	AC Node	$P^{G,min}$ $[kW]$	$P^{G,max}$ $[kW]$
1	31	30	425
2	37	0	650
3	47	0	1035
4	35	75	828
5	46	75	1500
6	40	0	900
7	10	300	3036
8	8	0	2484

Table B.2: Microgrids batteries parameters

Mg #	$P^{B,min}$ $[kW]$	$P^{B,max}$ $[kW]$	α_i	C_i $[kWh]$	$\zeta(0)$
1	-187.5	187.5	0.001	210	0.5
2	-225	225	0.001	196	0.65
3	-140	140	0.001	252	0.65
4	-180	180	0.001	315	0.6
5	-450	450	0.001	315	0.75
6	-300	300	0.001	476	0.9
7	-225	225	0.001	630	0.85
8	-375	375	0.001	700	0.85

Table B.3: Regulatory limits

v^{min}	v^{max}	δ^{min}	δ^{max}	$v^{dc,min}$	$v^{dc,max}$
$v_j^{nom} - 10\%$	$v_j^{nom} + 10\%$	$-9°$	$9°$	$1 - 10\%$	$1 + 10\%$

Table B.4: MVDC interfaces parameters

Interface #	AC Node	DC Node	P^{max} $[MW]$	Q^{max} $[MVAR]$	η
1	32	1	7500	4000	1
2	35	2	7500	4000	1
3	46	3	7500	4000	1
4	1	4	7500	4000	1

Table B.5: MVDC lines parameters

From	To	Resistance [Ω]	Max current [A]
2	5	1.208	410
1	5	0.215	410
3	5	0.608	410
4	5	2.558	410

Table B.6: AC buses parameters

Bus #	Cluster	V^{nom} [kV]	Shunt susceptance [μS]	Area
1	4	4.16	2.753	2
2	4	4.16	2.774	2
3	4	4.16	0.257	2
4	4	4.16	0.000	2
5	4	4.16	0.412	2
6	4	4.16	0.154	2
7	-	4.16	1.130	2
8	4	4.16	7.340	2
9	4	4.16	2.301	2
10	4	4.16	4.588	2
11	4	4.16	0.565	2
12	4	4.16	10.247	2
13	4	4.16	5.040	1
14	2	4.8	39.615	1
15	2	4.8	74.956	1
16	2	4.8	21.600	1
17	1	4.8	9.811	1
18	2	4.8	5.477	1
19	1	4.8	5.850	1
20	1	4.8	10.270	1
21	3	4.8	6.361	1
22	3	4.8	71.722	1
23	3	4.8	11.411	1
24	3	4.8	6.811	1
25	2	4.8	1.369	1
26	1	4.8	48.760	1
27	1	4.8	3.423	1
28	1	4.8	2.967	1
29	1	4.8	15.171	1
30	1	4.8	0.685	1
31	1	4.8	4.336	1
32	1	4.8	1.597	1
33	2	4.8	3.354	1
34	2	4.8	1.141	1
35	2	4.8	1.597	1
36	2	4.8	69.454	1
37	3	4.8	4.252	1
38	3	4.8	1.826	1
39	3	4.8	6.237	1
40	3	4.8	11.471	1
41	3	4.8	1.141	1
42	3	4.8	7.303	1
43	3	4.8	7.371	1
44	3	4.8	5.670	1
45	3	4.8	1.141	1
46	3	4.8	2.835	1
47	2	4.8	1.826	1
48	2	4.8	4.723	1
49	3	4.8	0.000	1
50	-	4.8	27.994	1

Table B.7: AC branches parameters

From	To	Resistance [Ω]	Reactance [Ω]	Max current [A]
14	15	0.085	0.052	650
15	18	0.159	0.058	650
15	26	1.562	0.793	650
15	16	0.117	0.072	650
16	33	0.095	0.035	650
16	36	0.147	0.075	650
17	27	0.032	0.012	650
17	29	0.196	0.100	650
18	47	0.127	0.046	650
18	25	0.095	0.035	650
19	32	0.111	0.041	650
20	31	0.302	0.110	650
20	30	0.048	0.017	650
21	39	0.079	0.040	650
21	38	0.127	0.046	650
22	37	0.147	0.075	650
21	22	0.079	0.040	650
23	41	0.080	0.029	650
23	42	0.509	0.185	650
24	46	0.098	0.050	650
24	45	0.080	0.029	650
17	26	0.128	0.065	650
27	28	0.207	0.075	650
20	29	0.366	0.133	650
19	29	0.147	0.075	650
33	48	0.069	0.035	650
22	36	2.259	1.147	650
39	40	0.138	0.070	650
40	43	0.157	0.080	650
23	40	0.207	0.075	650
43	44	0.098	0.050	650
24	44	0.098	0.050	650
34	48	0.080	0.029	650
35	48	0.111	0.041	650
22	49	0.002	0.039	650
14	50	0.103	0.069	650
2	5	0.071	0.113	650
2	3	0.071	0.113	650
3	4	0.002	0.039	650
5	6	0.042	0.068	650
2	7	0.129	0.391	650
8	12	0.120	0.065	650
2	9	0.129	0.391	650
9	12	0.042	0.068	650
9	11	0.065	0.196	650
9	13	0.052	0.157	650
1	12	0.045	0.025	650
10	13	0.075	0.041	650

Appendix C

Control system parameters

Table C.1: C-MPC parameters

ω_y	ω_g	ω_δ	ω_b	ω_{dc}	ω_s	ρ
10^2	50	$1 \cdot 10^4$	$5 \cdot 10^{-5}$	10^7	10^6	$7.5 \cdot 10^{-3}$

Table C.2: CS' first stage parameters

φ	γ_1	γ_2	γ_3
30%	2.5	1	10^6

Table C.3: ORPF parameters

κ_1	κ_2	κ_3	κ_4	κ_5
200	120	25	5	1

Appendix D

Generative Adversarial Networks

As mentioned in Chapter 5, in this work the approach proposed in [32] to generate realistic scenarios has been implemented. *Generative Adversarial Networks* (GAN) are a novel research topic first proposed in [35] for image generation purposes, then extended to RES' power profiles generation in [32]. The intuition behind GAN is that, if properly trained, two competitive *Deep Convolutional Neural Networks* (DCNN) can create an output with characteristics similar to the training data out of a random seed.

These two DCNN are called *Generator* and *Discriminator*. The former receives a vector of random numbers as input and generates power profiles, which the latter compares to the training set to determine whether or not they are realistic. During the training of such a neural network, the Generator progressively learns to generate power profiles able to fool the Discriminator, while the latter learns to distinguish the fake power profiles, i.e. the ones produced by the Generator, from the historical ones. The ideal equilibrium is one in which the Generator produces such realistic profiles that the Discriminator is not able to spot the difference.

In figure D.1 the scheme of the GAN proposed in [32] is reported. Although in [32] the mentioned approach is accurately described, it is worth noting few aspects that make it promising and particularly suitable to our needs:

- Owing to the input random seed, all the generated power profiles should be unique.
- The power profiles of multiple PVs or loads can be generated at once, hence it is possible to account for spatial correlation.
- Through conditioned learning, power profiles associated to particular months or weather conditions can be generated.
- With slight adjustments of the publicly available code[49] this method has been extended to loads.

The adopted training sets are the *NREL Solar Integration Dataset*[50] for PV profiles and a dataset provided by RSE S.p.a. for load profiles. It should be noted

[49] `https://github.com/chennnnnyize/Renewables_Scenario_Gen_GAN`
[50] `https://www.nrel.gov/grid/solar-power-data.html`

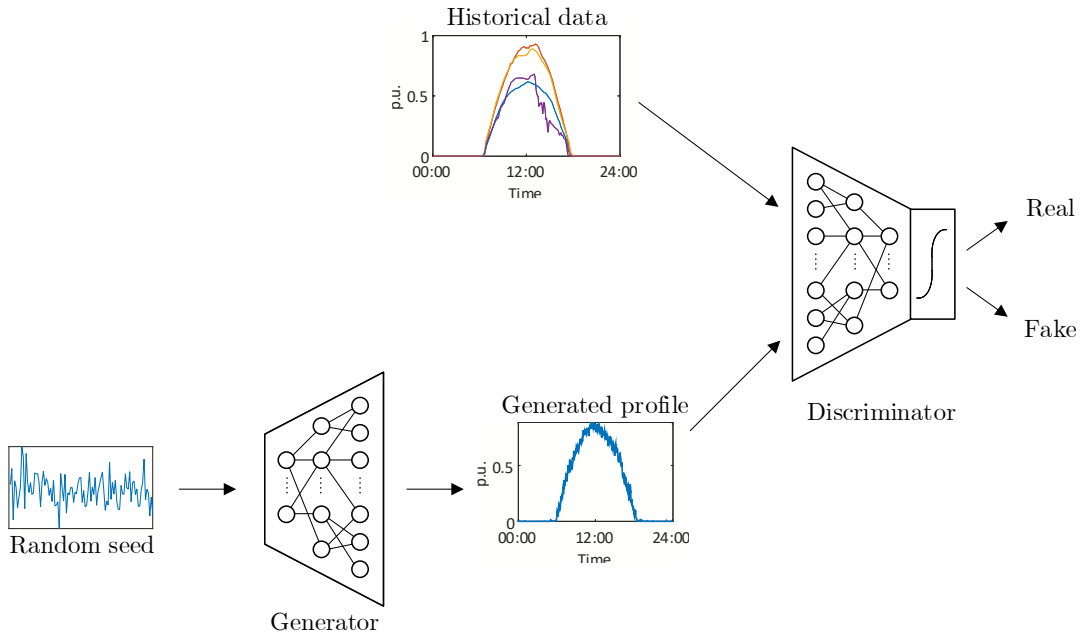

Figure D.1: Scheme of a Generative Adversarial Network for RES' scenario generation

that to achieve a better convergence, differently from [32], in this work the GAN has been trained only with a subset of the mentioned datasets, corresponding to the desired scenarios' month (i.e. October) plus two adjacent months (i.e. September and November), instead of the entire year. Albeit it implies that multiple GAN must be trained, one for each month, this approach provided better results.

The final results, at this stage, are unsatisfactory. Comparing some real PV power profiles, depicted in figure D.2, with generated ones, reported in figure D.3, it can be noted that, although the main trend is captured, the latter are more noisy, due to the random seed from which they are produced. Similar considerations hold also for the loads profiles represented in figures D.4 and D.5. Furthermore, the generated profiles - especially for PV - show unrealistic periodic features, probably associated to the over-fitting of training data.

Despite this approach seems promising, a better tuning of neural network's hyper-parameters is required to generate power profiles effectively resembling the training data.

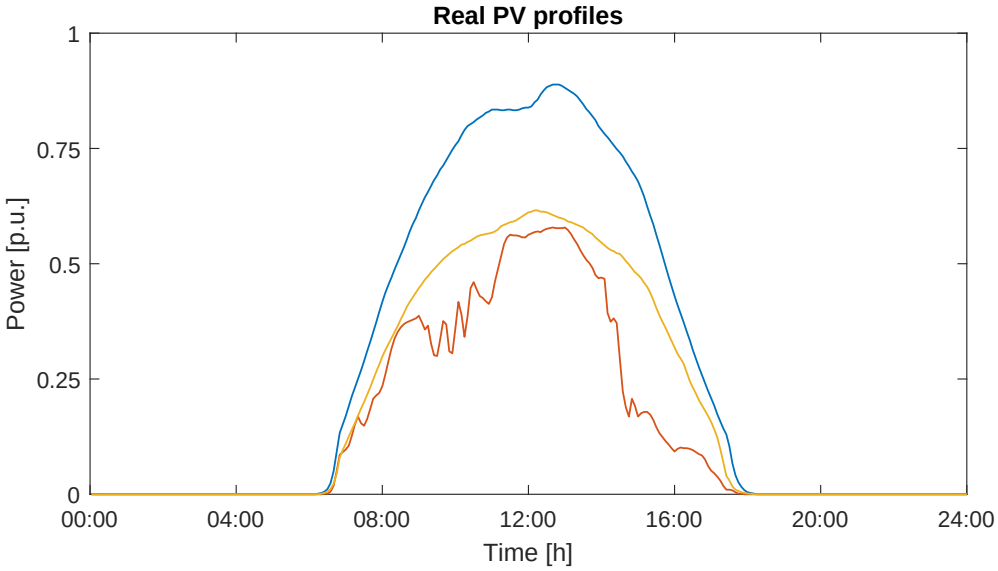

Figure D.2: Three real PV power profiles extracted from NREL Solar Integration Dataset (filtered), October.

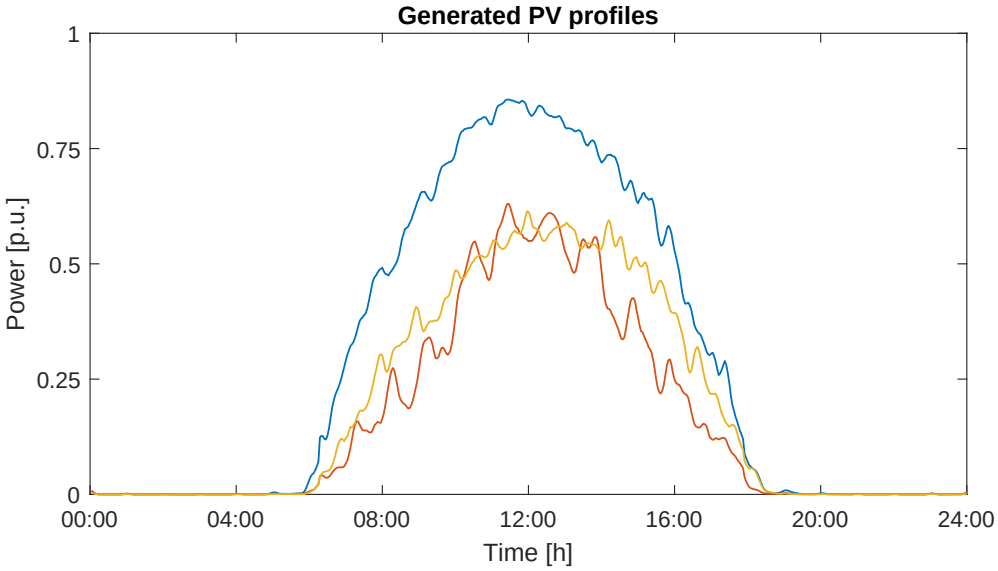

Figure D.3: Three power PV profiles generated by GAN, October.

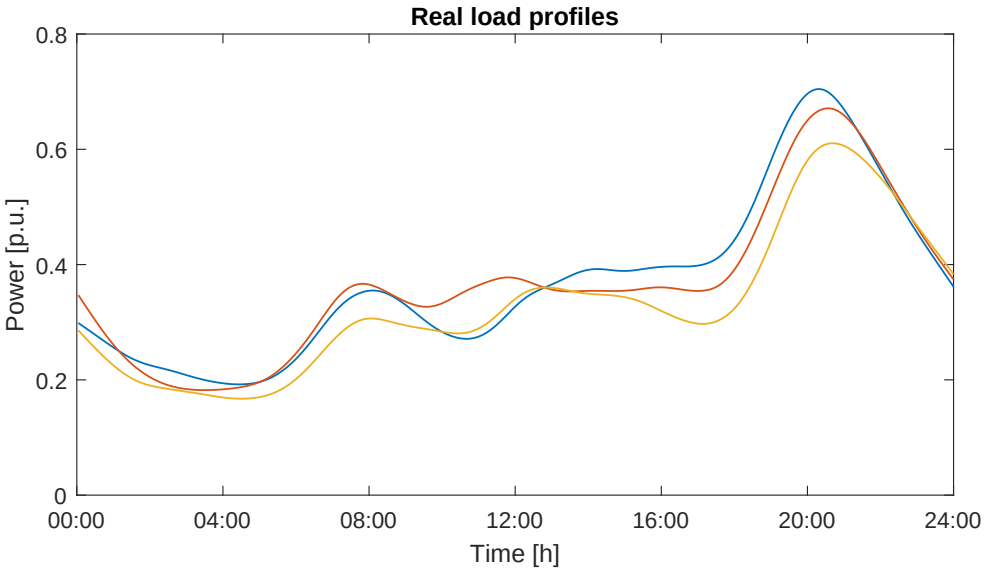

Figure D.4: Three real load power profiles from RSE (filtered), October.

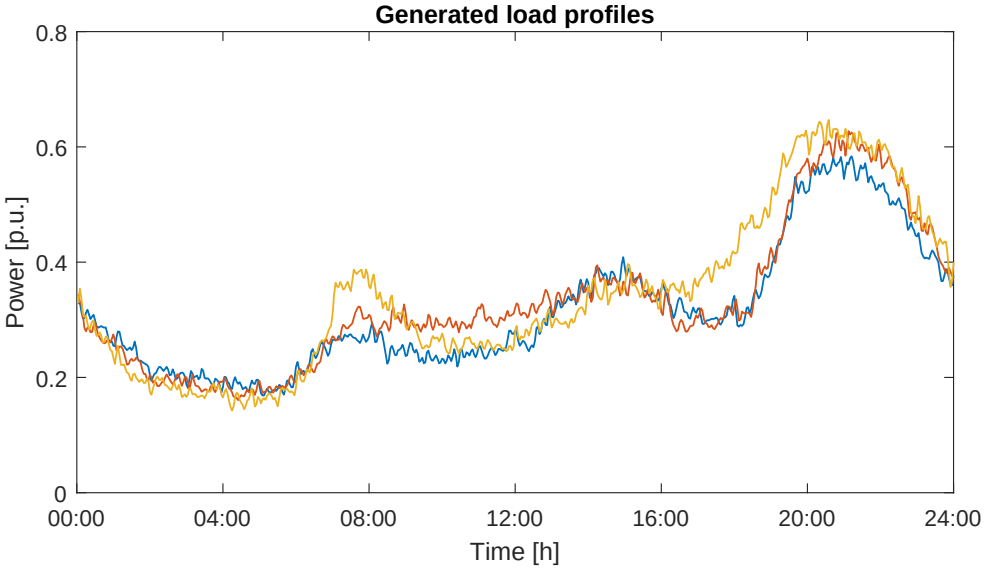

Figure D.5: Three load power profiles generated by GAN, October.

Ringraziamenti

Sono molte le persone che dovrei ringraziare per avermi supportato, direttamente o indirettamente, in questo percorso.

Innanzitutto, sono estremamente grato al Professor Scattolini per avere riposto fiducia in me e per avermi costantemente guidato con professionalità, competenza ed esperienza, lasciandomi al contempo autonomia nel lavoro di ricerca.

Un sincero grazie va anche all' Ing. Alessio La Bella, che con molta pazienza, dedizione e competenza mi ha, sin dal principio, sostenuto e guidato. Oltre a preziosi spunti di riflessione ed idee, infatti, confrontarmi con lui mi ha spinto a superare i miei limiti e a dare del mio meglio.

Ringrazio RSE S.p.a., in particolar modo l'Ing. Carlo Sandroni e l'Ing. Riccardo Lazzari. La loro accoglienza, professionalità e competenza non solo hanno reso possibile questo lavoro, ma mi hanno profondamente arricchito.

Un doveroso grazie va ai miei genitori Giuseppe e Cristina, a mia sorella Simona e a tutta la mia famiglia, che mi ha sostenuto in questo lungo percorso.

Un immenso grazie a Silvia, che negli ultimi anni è entrata nella mia vita, riempiendo le mie giornate di gioia e amore. Le sue parole sono state il miglior antidoto alle mie preoccupazioni e il suo sostegno la più grande forza per affrontare le sfide presenti e future.

Ringrazio i miei più grandi amici, Giulia, Carmelo, Sara, Sabrina, Andrea, Giorgio e Marta, per tutti i momenti di spensieratezza e amicizia che mi hanno donato e mi doneranno.

Ultimi, ma non per importanza, ringrazio dal profondo del cuore Davide, Beppe, Stefano e Diego, con i quali ho condiviso tutti i momenti e le sfide di questi ultimi cinque anni, che la loro amicizia ha reso molto più belli di quanto non avessi mai potuto immaginare.